Chapter 7

Gene Regulatory Networks

> [In the ancestral Indo-European language, the word] *gene* signified beginning, giving birth... [It later] emerged as genus, genius, genital, and generous; then, still holding on to its inner significance, it became "nature" ([from the Latin] *gnasci*).
>
> Lewis Thomas, *Lives of a Cell*

As demonstrated in the previous chapters, all cellular functions are driven by proteins. Protein production occurs through *gene expression*—a process that involves reading information encoded in the DNA. The cellular abundance of each protein is controlled primarily by its production rate; these production rates are, in turn, controlled by specialized proteins called *transcription factors*. A set of genes whose protein products regulate one another's expression rates is referred to as a *gene regulatory network*. In this chapter we will address gene regulatory networks that implement switch-like responses, store memory, generate oscillations, and carry out logical computations and cell-to-cell communication.

Gene expression is a two-step process. The first step, **transcription**, occurs when the coding region of a gene is 're-written' in the form of a complementary RNA strand called a messenger RNA (mRNA). Transcription is carried out by a protein-complex called *RNA polymerase* that binds the promoter region of the gene and then 'walks' along the DNA, catalysing the formation of the mRNA strand from nucleotide precursors.

The second step of gene expression is **translation**, in which the mRNA molecule binds a protein-RNA complex called a ribosome that reads the nucleotide sequence and produces a corresponding polypeptide chain. Translation, like transcription, involves information transfer; the ribosome 'reads along' the mRNA and catalyses the formation of a protein from amino acids building blocks.

Although the organization and behaviour of gene regulatory networks share a number of similarities with metabolic networks and signal transduction pathways, the underlying processes are significantly different. The biochemical interactions in metabolic or signal transduction systems are each decomposable into a handful of elementary chemical events. In contrast, transcription and translation are complex processes that each involve a very large number of biochemical reactions (many of which have not been fully characterized).

We will use a mass-action based formalism to develop models of gene regulatory networks, but we will be applying this rate law in a more abstracted sense than in the previous chapters; our descriptions of gene expression processes will be far more 'coarse-grained' then our earlier models of biochemical networks.

A further complication in modelling genetic systems is that the molecules involved in the regulation of gene expression are often present in very small numbers. Recall from Section 2.1.2 that the continuum hypothesis (which justifies our use of smoothly-varying concentration values) should only be applied when there are large number of molecules present (so that individual reaction events produce near-infinitesimal changes in abundance). Proteins that impact gene expression are often present in small quantities—regularly in the hundreds or less. Moreover, genes themselves are almost always present at very low copy number—rarely more than dozens, and often as few as one or two. Cells typically have a small number of copies of their inherent (chromosomal) genes—typically one or two, in some cases four or more. Genes that are introduced to a bacterial cell from its environment (e.g. in the laboratory) are typically carried on small circular DNA molecules called *plasmids*, which can be maintained at much higher copy numbers—as many as a few hundred.

In addressing the behaviour of systems with low molecule counts, we can justify the mass-action formalism by interpreting differential-equation models as descriptions of the average behavior over a large population of cells. This interpretation is useful when addressing cultures or tissues composed of comparable cells exhibiting similar behaviours.

An alternative modelling framework—one that describes individual reaction events—can be adopted in cases where we seek to truly capture the behaviour of individual cells (for example where single-cell measurements are available). This stochastic framework, which incorporates the probabilistic (i.e. noisy) effects that play a significant role at these small scales, will be taken up in Section 7.6.

7.1 Modelling Gene Expression

7.1.1 Unregulated gene expression

The fundamental processes that constitute gene expression are sketched in Figure 7.1. Transcription and translation involve information transfer from DNA to RNA to protein, while degradation results in turn-over of the RNA and protein pools. Each of these processes relies on a significant amount of background cellular "machinery"—including nucleic acids, RNA polymerases, amino acids, and ribosomes. In developing models of gene expression, we will assume that the activity of these 'housekeeping' elements is fixed.

To simplify our discussion, we will focus on prokaryotic gene expression. Eukaryotic gene regulatory networks are also modelled using the procedure we will develop here, but eukaryotic gene expression involves a number of additional processes that we will not address explicitly (such as splicing of mRNA and transport of mRNA across the nuclear membrane).

Unregulated, or *constitutive*, gene expression involves the four processes shown in Figure 7.1. Applying mass action to arrive at simple rate laws gives

$$\begin{aligned} \frac{d}{dt}m(t) &= k_0 - \delta_m m(t) \\ \frac{d}{dt}p(t) &= k_1 m(t) - \delta_p p(t), \end{aligned} \tag{7.1}$$

where m is the concentration of mRNA molecules and p is the concentration of the gene's protein product. The population-averaged transcription rate k_0 depends on a number of factors, including the gene copy number, the abundance of RNA polymerase, the strength of the gene's promoter (e.g. its affinity for RNA polymerase), and the availability of nucleotide building blocks. Parameter

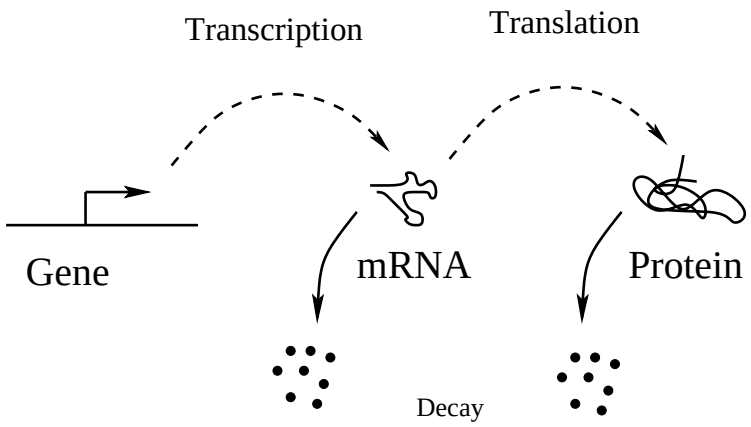

Figure 7.1: Gene expression. Transcription of the gene results in the formation of mRNA molecules, which can then be translated by ribosomes to produce proteins. These production processes are balanced by degradation of mRNA and protein molecules.

k_1, the per-mRNA translation rate, likewise depends on a range of factors, including the availability of ribosomes, the strength of the mRNA's ribosome binding site (i.e. the mRNA's affinity for ribosomes), and the availability of transfer RNAs and free amino acids.

Transcription and translation are balanced by decay of the mRNA and protein pools, characterized by the the degradation rates δ_m and δ_p. Several factors contribute to the decay process. Generally, mRNA and protein molecules may be unstable, and so decay spontaneously (with characteristic half-lives). Additionally, the cell contains ribonucleases and proteases that specifically degrade mRNA and protein molecules.

The parameters δ_m and δ_p can also be used to describe the dilution of mRNA and protein pools caused by cell growth. (Cell volume increases exponentially, causing exponential decrease in concentrations; model (7.1) applies if the cell maintains constant concentrations of the background expression machinery.) In rapidly growing bacterial cells, dilution is often more significant than degradation. In using model (7.1), we will use the parameters δ_m and δ_p as combined degradation/dilution rates.

The steady state concentrations in model (7.1) are easily determined:

$$m^{ss} = \frac{k_0}{\delta_m} \qquad\qquad p^{ss} = \frac{k_1 k_0}{\delta_p \delta_m}.$$

Models of gene expression are often simplified by taking advantage of the fact that mRNA decay is typically much faster than protein decay. (mRNA half-lives are typically measured in minutes, while proteins often have half-lives of hours. In rapidly growing bacterial cells, protein degradation is often negligible, and so the protein decay rate is dictated solely by the cell's growth rate.) This separation of time-scales justifies a quasi-steady state approximation for the mRNA levels. The reduced model is:

$$\frac{d}{dt}p(t) \quad = \quad \frac{k_1 k_0}{\delta_m} - \delta_p p(t). \tag{7.2}$$

The parameter $\alpha = \frac{k_1 k_0}{\delta_m}$ is the *expression rate.*

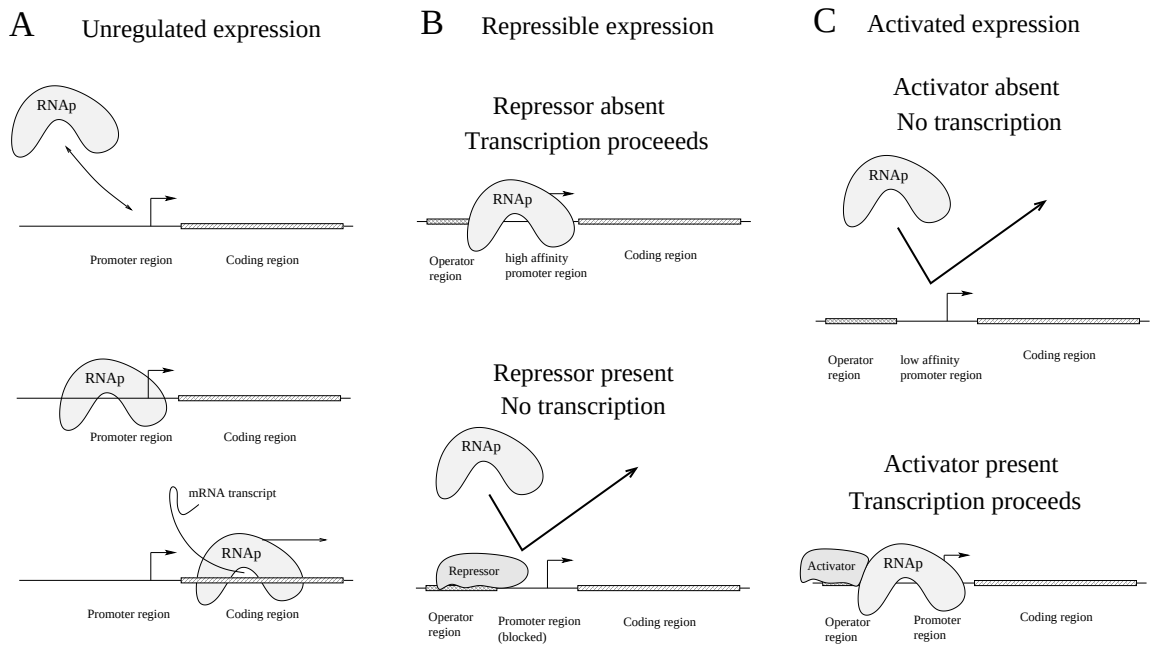

Figure 7.2: Transcriptional regulation. **A.** Unregulated gene expression. RNA polymerase (RNAp) binds the gene's promoter region, then slides along the DNA to the coding region, where it produces the mRNA transcript. **B.** A repressor binds to its operator region and blocks access to the promoter. When the repressor is bound, transcription cannot occur. **C.** An activator enhances transcription. In this case the promoter region has a low affinity for RNA polymerase, and so transcription does not occur from the unregulated gene. Once bound at the operator, the activator binds RNA polymerase and recruits it to the promoter site.

7.1.2 Regulated gene expression

Gene expression can be regulated at many stages, including RNA polymerase binding, elongation of the mRNA strand, translational initiation (i.e. mRNA-ribosome binding), and polypeptide elongation. In addition, mRNA and protein molecules can be specifically targeted for—or protected from—degradation.

Despite this range of control points, the majority of gene regulation occurs through control of the initiation of transcription. In prokaryotes, this is achieved primarily through regulating the association of RNA polymerase with gene promoter regions. Proteins that bind DNA and affect polymerase association are called *transcription factors*. In prokaryotes, transcription-factor binding-sites, called *operator regions*, are typically situated close to the promoter of the affected gene. If a transcription factor increases the rate of RNA polymerase binding it is called an *activator* of gene expression; if it inhibits binding, it is called a *repressor* (Figure 7.2).

Transcription-factor binding

The binding of a transcription factor to an operator site can be described by:

$$O + P \underset{d}{\overset{a}{\rightleftharpoons}} OP$$

where O is the unbound operator, P is the transcription factor protein, and the complex OP is the bound operator. This association/disassociation event occurs on a much faster time-scale than gene

expression, so it can be treated in equilibrium when modelling gene expression. Setting $K = d/a$, we find (compare with equation (3.17)):

$$\begin{aligned} \text{fraction of bound operators} &= \frac{[OP]}{[O]+[OP]} \\ &= \frac{[O][P]/K}{[O]+[O][P]/K} \\ &= \frac{[P]/K}{1+[P]/K} = \frac{[P]}{K+[P]}. \end{aligned} \tag{7.3}$$

Note, K, the dissociation constant of the binding event, is the half-saturating concentration for the transcription factor P.

Equation (7.3) describes the *promoter occupancy*; it represents the fraction of a population of operators that are bound to transcription factor proteins (or, equivalently, the fraction of time that any given operator spends in the protein-bound state).

Rates of transcription from regulated genes

The rate of transcription from a regulated gene depends on the promoter occupancy. If the transcription factor P is an activator, then the rate of gene transcription is proportional to the occupancy:

$$\text{rate of activated transcription} = \alpha \frac{[P]/K}{1+[P]/K}. \tag{7.4}$$

The constant of proportionality, α, is the *maximal transcription rate*. Formula (7.4) suggests that the rate of transcription will be zero when the activator P is absent. Most activated genes are transcribed at a low (so-called *basal*) rate even when the activator is unbound. Incorporating a basal expression rate of α_0 gives:

$$\text{rate of activated transcription} = \alpha_0 + \alpha \frac{[P]/K}{1+[P]/K}. \tag{7.5}$$

In this case, the maximal transcription rate is $\alpha_0 + \alpha$.

When the transcription factor P acts as a repressor, the regulated transcription rate is proportional to the fraction of unbound operators $\frac{1}{1+[P]/K}$. If we allow for a small transcription rate α_0 from the repressed promoter (a 'leak'), we have

$$\text{rate of repressible transcription} = \alpha_0 + \alpha \frac{1}{1+[P]/K}.$$

In many cases this leak is negligible, but absolute repression can never be achieved: thermal fluctuations cause continual unbinding and re-binding at the operator, so there is always some chance that RNA polymerase will find its way to the operator.

Regulation by multiple transcription factors

Genes are commonly regulated by multiple transcription factors, and by multiple copies of each factor. To introduce the general technique for analysing these multiple-regulator schemes, we next provide an analysis of the promoter occupancy for a gene regulated by two transcription factors.

Consider a promoter with two non-overlapping operator sites: O_A binds transcription factor A; O_B binds transcription factor B. The promoter can then be found in four states:

$$\begin{aligned} O: &\quad A \text{ and } B \text{ unbound} \\ OA: &\quad A \text{ bound at } O_A,\ B \text{ unbound} \\ OB: &\quad B \text{ bound at } O_B,\ A \text{ unbound} \\ OAB: &\quad A \text{ at bound } O_A,\ B \text{ bound at } O_B. \end{aligned}$$

If the binding events at O_A and O_B are independent of one another, then the reaction scheme is

$$O + A \underset{d_1}{\overset{a_1}{\rightleftharpoons}} OA \qquad O + B \underset{d_2}{\overset{a_2}{\rightleftharpoons}} OB$$

$$OB + A \underset{d_1}{\overset{a_1}{\rightleftharpoons}} OAB \qquad OA + B \underset{d_2}{\overset{a_2}{\rightleftharpoons}} OAB$$

which results in the following steady state distribution of promoters:

$$\begin{aligned} \text{fraction in state } O: &\quad \frac{1}{1 + \frac{[A]}{K_A} + \frac{[B]}{K_B} + \frac{[A][B]}{K_A K_B}} \\ \text{fraction in state } OA: &\quad \frac{\frac{[A]}{K_A}}{1 + \frac{[A]}{K_A} + \frac{[B]}{K_B} + \frac{[A][B]}{K_A K_B}} \\ \text{fraction in state } OB: &\quad \frac{\frac{[B]}{K_B}}{1 + \frac{[A]}{K_A} + \frac{[B]}{K_B} + \frac{[A][B]}{K_A K_B}} \\ \text{fraction in state } OAB: &\quad \frac{\frac{[A][B]}{K_A K_B}}{1 + \frac{[A]}{K_A} + \frac{[B]}{K_B} + \frac{[A][B]}{K_A K_B}} \end{aligned} \tag{7.6}$$

where $K_A = d_1/a_1$ and $K_B = d_2/a_2$ are the dissociation constants for the two binding events.

Exercise 7.1.1 Derive equations (7.6) by treating the binding events in steady state. □

The rate of transcription from this regulated promoter depends on the nature of the transcription factors A and B. For instance, if both are repressors and the binding of *either* factor blocks polymerase binding, then transcription can only occur from state O; the corresponding transcription rate can be written as

$$\frac{\alpha}{1 + \frac{[A]}{K_A} + \frac{[B]}{K_B} + \frac{[A][B]}{K_A K_B}}$$

Alternatively, the two repressors might inhibit transcription only when *both* are bound, in which case transcription occurs from all states except OAB. The resulting transcription rate takes the form

$$\alpha \frac{1 + \frac{[A]}{K_A} + \frac{[B]}{K_B}}{1 + \frac{[A]}{K_A} + \frac{[B]}{K_B} + \frac{[A][B]}{K_A K_B}}$$

Exercise 7.1.2 Which promoter state(s) would allow transcription if A is an activator of the gene while B is a repressor that completely blocks the RNA polymerase binding site? Suppose that no expression occurs if A is unbound. Formulate a description of the rate of transcription in this case. □

Cooperativity in transcription factor binding

Recall from Section 3.3 that cooperativity occurs when multiple ligands bind a single protein and the association of the first ligand affects the affinity of the other binding sites. Cooperativity also occurs among multiple transcription-factors binding operator-sites along a length of DNA.

Consider the case in which two transcription factors bind at non-overlapping operator sites, and that, when DNA-bound, they also bind one another. Suppose the dissociation rate of the second DNA-binding event is reduced by a factor K_Q. In this case the dissociation constant for A binding to OB is $K_A K_Q$ ($< K_A$), indicating enhanced affinity. (Likewise the dissociation constant for B binding to OA is $K_B K_Q$, which is less than K_B.) The steady state distribution of promoters is then:

$$\begin{aligned}
\text{fraction in state } O: &\quad \frac{1}{1+\frac{[A]}{K_A}+\frac{[B]}{K_B}+\frac{[A][B]}{K_A K_B K_Q}} \\
\text{fraction in state } OA: &\quad \frac{\frac{[A]}{K_A}}{1+\frac{[A]}{K_A}+\frac{[B]}{K_B}+\frac{[A][B]}{K_A K_B K_Q}} \\
\text{fraction in state } OB: &\quad \frac{\frac{[B]}{K_B}}{1+\frac{[A]}{K_A}+\frac{[B]}{K_B}+\frac{[A][B]}{K_A K_B K_Q}} \\
\text{fraction in state } OAB: &\quad \frac{\frac{[A][B]}{K_A K_B K_Q}}{1+\frac{[A]}{K_A}+\frac{[B]}{K_B}+\frac{[A][B]}{K_A K_B K_Q}}.
\end{aligned}$$

If the cooperativity is strong, the second operator site will almost always be occupied when the first binding event has occurred. Consequently, the states OA and OB will be negligible. This case corresponds to $K_Q \ll 1$, which allows the approximation

$$1+\frac{[A]}{K_A}+\frac{[B]}{K_B}+\frac{[A][B]}{K_A K_B K_Q} \approx 1+\frac{[A][B]}{K_A K_B K_Q}.$$

The distribution of promoter states is then:

$$\begin{aligned}
\text{fraction in state } O: &\quad \frac{1}{1+\frac{[A][B]}{K_A K_B K_Q}} \\
\text{fraction in state } OAB: &\quad \frac{\frac{[A][B]}{K_A K_B K_Q}}{1+\frac{[A][B]}{K_A K_B K_Q}}.
\end{aligned}$$

In the particular case that the two transcription factors are identical ($A = B = P$) the distribution becomes:

$$\begin{aligned}
\text{fraction in state } O: &\quad \frac{1}{1+\frac{[P]^2}{K_P^2 K_Q}} \\
\text{fraction in state } OAB: &\quad \frac{\frac{[P]^2}{K_P^2 K_Q}}{1+\frac{[P]^2}{K_P^2 K_Q}}.
\end{aligned}$$

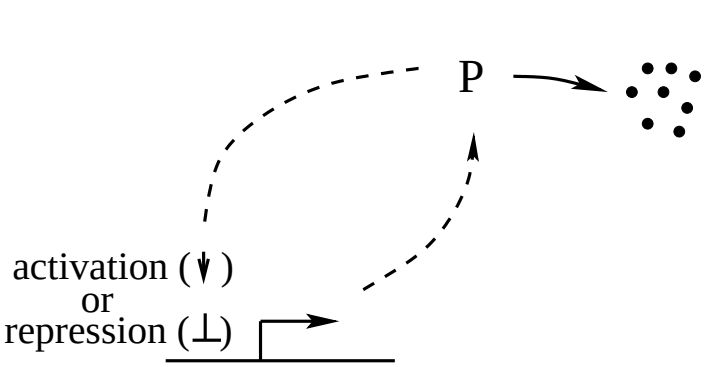

Figure 7.3: Autoregulatory gene circuit. The protein product of the gene regulates its own expression by acting as an activator or as an inhibitor.

The fractional occupancy thus takes the familiar form of a Hill function (as introduced in Section 3.3).

When N transcription factors bind with strong cooperativity, promoter occupancy can be written as

$$\frac{\left(\frac{[P]}{K}\right)^N}{1+\left(\frac{[P]}{K}\right)^N} = \frac{[P]^N}{K^N+[P]^N}, \tag{7.7}$$

where K is the half-saturating concentration. This functional form is often used as an empirical fit when the details of transcription factor binding are unknown.

Transcription factors commonly bind DNA as multimers (e.g. dimers or tetramers). Formula (7.7) can sometimes be used to describe occupancy by a multimer. However, because the multimerization process occurs in the cytosol—rather than at the operator site—the analysis in this section does not apply directly. See Problem 7.8.4 for details.

7.1.3 Gene regulatory networks

A gene regulatory network, also called a *genetic circuit*, is a group of genes whose protein products regulate one another's expression. The simplest genetic circuit consists of a single gene that regulates its own activity (Figure 7.3). If the gene's protein product enhances expression, the gene is called as *autoactivator*; if the product inhibits expression, the gene is an *autoinhibitor*.

Autoinhibition

To construct a simple model of an autoinhibitor, we treat mRNA in quasi-steady state and presume that the transcription factor P binds to a single operator site. The resulting model is

$$\frac{d}{dt}p(t) \quad = \quad \alpha\frac{1}{1+p(t)/K} - \delta_p p(t), \tag{7.8}$$

where $p = [P]$.

Many genes are autoinhibitory. One advantage of this regulatory scheme is reduction of sensitivity to certain perturbations: autoinhibition decreases the sensitivity to variation in the maximal

expression rate α (Problem 7.8.2). Because α depends on a host of background processes, this increased robustness can provide a significant advantage over unregulated expression.

Another advantage of autoinhibition is a fast response to changes in demand for protein product. Consider an unregulated gene whose product attains a particular concentration. If an autoinhibitory gene is to generate an equivalent abundance of protein, it must have a higher maximal expression rate α, and will consequently respond more quickly when changes in protein level are required (Problem 7.8.1).

Autoactivation

The behaviour of an autoactivating gene circuit can be modelled as

$$\frac{d}{dt}p(t) = \alpha\frac{p(t)/K}{1+p(t)/K} - \delta_p p(t). \tag{7.9}$$

Positive feedback of this sort can lead to run-away behaviour. However, because the expression rate cannot rise above α, autoactivation typically results in quick convergence to a state in which the gene is expressing at a high rate—an ON state. (This simple model also exhibits a steady OFF state, at $p = 0$.)

Exercise 7.1.3 Derive a formula for the non-zero steady-state solution of model (7.9). Confirm that this steady state does not occur when $\alpha < K\delta_p$. Verify that when the non-zero steady state exists, it is stable and the zero steady-state is unstable. □

An autoactivator P that binds cooperatively at multiple operator sites can be described by:

$$\frac{d}{dt}p(t) = \alpha\frac{(p(t)/K)^N}{1+(p(t)/K)^N} - \delta_p p(t). \tag{7.10}$$

This nonlinear model can exhibit bistability, in which the OFF state ($p = 0$) and the high-expressing ON state are both stable. The basin of attraction of the OFF state tends to be small, meaning that once turned ON, it takes a significant effect to transition to the OFF state. In the next section, we will consider genetic switches that exhibit more balanced behaviours.

Exercise 7.1.4 Verify that when $N = 2$, the system in equation (7.10) exhibits three non-negative steady states provided that $\alpha > 2K\delta_p$. □

7.2 Genetic Switches

7.2.1 The *lac* operon

One of the best understood gene circuits involves a set of genes found in *E. coli* whose products allow the bacterium to metabolize lactose (milk sugar). This set of genes is contained in an *operon*—a single promoter region followed by a set of coding regions, one for each protein product (Figure 7.4). The genes in an operon are expressed simultaneously, and are co-ordinately regulated via the shared promoter.

The *lac* operon contains coding regions for three proteins:

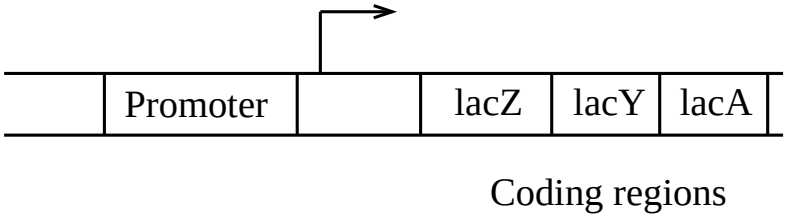

Figure 7.4: The *lac* operon. The coding regions for the three *lac* genes—*lacZ*, *lacY* and *lacA*—follow one another on the DNA. Transcription of these coding regions begins at a shared promoter, so the genes are transcribed together.

- β-galactosidase – coded by the gene *lacZ*
- β-galactoside permease – coded by the gene *lacY*
- β-galactoside transacetylase – coded by the gene *lacA*.

Together, these proteins allow *E. coli* to metabolize lactose. In its natural environment (the mammalian gut), lactose is typically far less abundant than other sugars, and so the cell represses expression from the *lac* operon, in order to conserve resources. This repression is caused by a transcription factor called LacI (or simply *lac* repressor), which binds to an operator region near the operon's promoter and blocks expression (Figure 7.5A).

The *lac* repressor is constitutively expressed; when lactose is scarce the repression is almost complete—leaked expression maintains only a few copies of each of the *lac* protein products in the cell. When lactose is abundant, it is converted to *allolactose*, which binds lac repressor, reducing its affinity for the operator site (by about a thousandfold). Thus, expression from the operon is triggered by the presence of lactose, with allolactose as the *inducer* (Figure 7.5B).

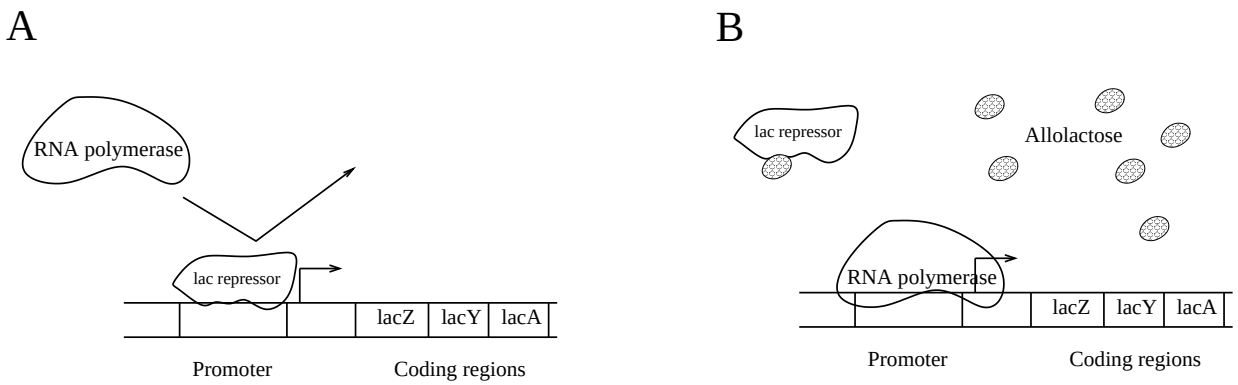

Figure 7.5: The *lac* repressor, LacI. **A.** The *lac* repressor binds at the *lac* promoter, interfering with RNA polymerase binding. **B.** When bound to allolactose, the *lac* repressor is unable to bind DNA. RNA polymerase is then free to bind the *lac* promoter and transcription proceeds.

In addition to the direct induction by allolactose, the presence of lactose sets off a positive feedback that leads to rapid expression of the *lac* genes. This feedback is implemented by the *lac* proteins themselves: β-galactoside permease is a transmembrane protein that transports lactose into the cell; β-galactosidase is an enzyme that catalyses the conversion of lactose to allolactose.

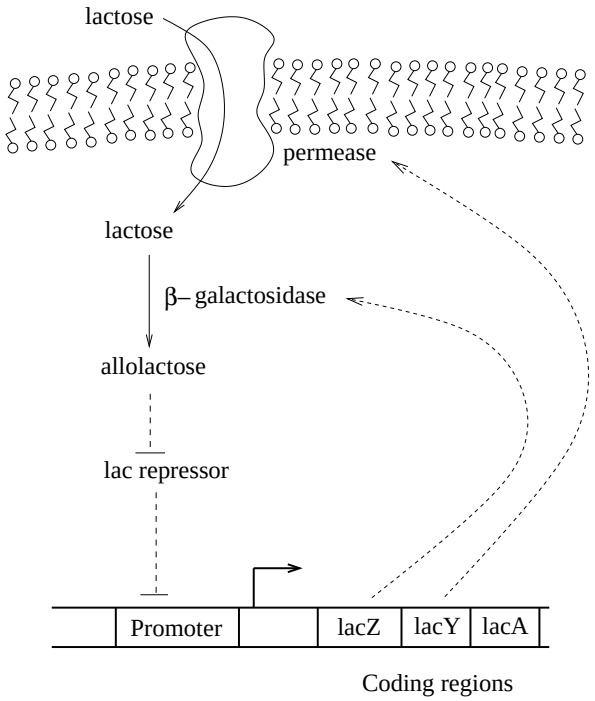

Figure 7.6: Feedback in the *lac* operon. The protein products of the operon—permease and β-galactosidase—bring lactose into the cell and convert it to allolactose. Allolactose activates gene expression by de-repression (inactivation of the *lac* repressor).

β-galactosidase also catalyses the metabolism of lactose. (The third protein in the operon, β-galactoside transacetylase, chemically modifies β-galactosidase, but its role in lactose metabolism is currently unclear.) These *lac* proteins, as mentioned, are present at very low levels when lactose is absent. When lactose is introduced to the environment, the action of this handful of *lac* protein molecules leads to a small amount of allolactose being present in the cell, and the repression of the *lac* operon weakens. This weakened repression leads to increased expression from the operon, resulting in increased levels of allolactose, and further increases in expression, as in Figure 7.6. (This is not the whole story: transcription from the *lac* operon requires the presence of an activator called catabolic gene activating protein (CAP), which is only active when glucose is absent from the environment. Glucose is the preferred energy and carbon source for these cells. The CAP mechanism ensures that when glucose is present the *lac* genes are not expressed, regardless of the availability of lactose.)

A model of the *lac* operon

In 2007, Moisés Santillán, Michael Mackey and Eduardo Zeron published a model of *lac* operon activity (Santillán *et al.*, 2007). We will address a simplified version of their model.

To begin, we describe binding of the *lac* repressor (R) to the operon's operator site by

$$O + R \underset{k_{-1}}{\overset{k_1}{\rightleftharpoons}} OR.$$

where O is the unbound operator and OR is the repressor-bound operator. (In fact, the repressor

binds at three distinct operator sites; we'll ignore that complication in this simple model.) Treating the repressor binding event in steady state, the fraction of un-repressed genes can be written as

$$\frac{1}{1+r(t)/K_1},$$

where r is the concentration of *lac* repressor and $K_1 = \frac{k_{-1}}{k_1}$ is the dissociation constant. Letting m denote the concentration of operon mRNA, we can write

$$\frac{d}{dt}m(t) = a_1 \frac{1}{1+r(t)/K_1} - \delta_M\, m(t) \tag{7.11}$$

where a_1 is the maximal rate of transcription and δ_M is the mRNA degradation/dilution rate.

We next consider the permease (coded by *lacY*). Letting y denote its concentration, we have

$$\frac{d}{dt}y(t) \quad = \quad c_1 m(t) - \delta_Y y(t) \tag{7.12}$$

where c_1 is the rate of translation and δ_Y is the protein's degradation/dilution rate.

Because the operon's protein products are translated from the same mRNA transcript, these proteins are translated at comparable rates. Supposing that β-galactosidase and permease also share the same degradation/dilution rate, the model for β-galactosidase is identical to equation (7.12). However, the β-galactosidase protein is a tetramer, while permease is a monomer. Ignoring the dynamics of tetramer formation, we can write the β-galactosidase tetramer concentration, denoted b, as one fourth that of the permease

$$b(t) = \frac{y(t)}{4}. \tag{7.13}$$

Lactose uptake is mediated by the permease. Assuming Michaelis-Menten kinetics for the transport event gives

$$\text{lactose uptake} = \frac{k_L\, y(t) L_e}{K_{ML} + L_e}$$

where k_L is the maximal (per permease) transport rate, L_e is the external lactose concentration, and K_{ML} is the Michaelis constant. Once it has been transported across the membrane, lactose is either converted to allolactose or is metabolized (into the simpler sugars glucose and galactose); both reactions are catalysed by β-galactosidase. Denoting the intracellular concentration of lactose by L, we write

$$\frac{d}{dt}L(t) = \frac{k_L\, y(t) L_e}{K_{ML} + L_e} - \frac{k_g\, b(t) L(t)}{K_{Mg} + L(t)} - \frac{k_a\, b(t) L(t)}{K_{Ma} + L(t)} - \delta_L\, L(t),$$

where δ_L is the dilution rate. The parameters k_g and k_a are the maximal (per β-galactosidase) rates at which lactose can be metabolized or converted to allolactose, respectively; K_{Mg} and K_{Ma} are the corresponding Michaelis constants.

Making the assumption that the two reactions catalysed by β-galactosidase have identical kinetics (i.e. $k_g = k_a$, $K_{Mg} = K_{Ma}$) we arrive at a simplified description of the lactose dynamics:

$$\frac{d}{dt}L(t) = \frac{k_L\, y(t) L_e}{K_{ML} + L_e} - 2\frac{k_g\, b(t) L(t)}{K_{Mg} + L(t)} - \delta_L\, L(t). \tag{7.14}$$

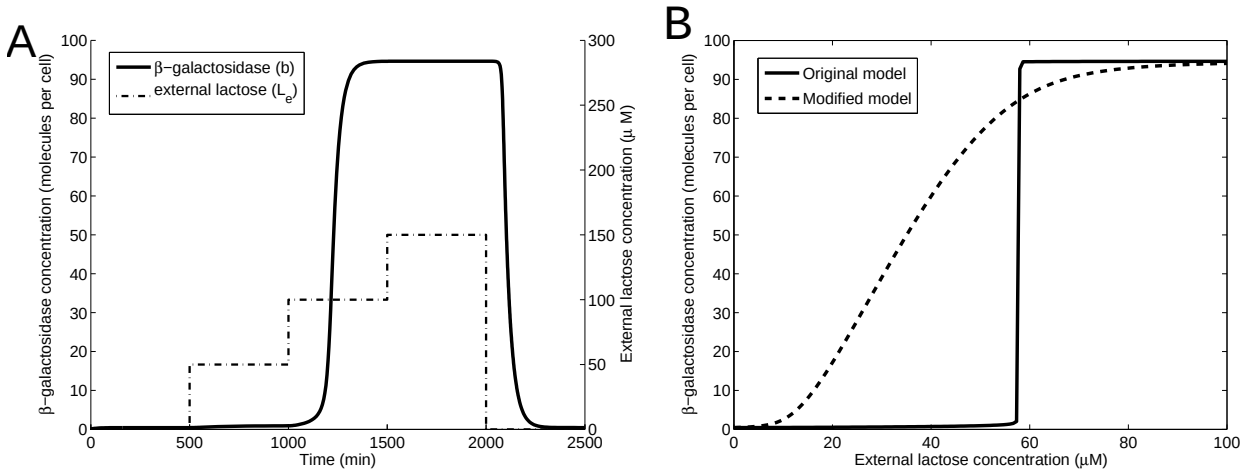

Figure 7.7: Switching behavior in the *lac* operon. **A.** Dynamic response. A series of steps in the external lactose concentration (L_e) lead to changes in the activity of the *lac* operon, reflected in the abundance of β-galactosidase. The initial increase from 0 to 50 μM (at time 500 minutes) causes a negligible rise in activity. A later increase to 100 μM (at 1000 min) has a significant impact: the system shifts abruptly to its 'on' state. A further increase to 150 μM (at 1500 min) elicits no response—the system is already fully active. Finally, at time 2000 min the external lactose is removed. Once the internal lactose level drops, the system rapidly switches to the 'off' state. **B.** Dose-response. The solid line shows the behaviour of the *lac* operon model. The steady-state level of operon activity (indicated by β-galactosidase abundance) switches abruptly at a threshold lactose concentration. The dashed dose-response curve corresponds to a hypothetical model in which the positive feedback loop has been cut (details in Problem 7.8.5). The resulting graded response contrasts sharply with the switch-like behaviour of the true *lac* model. Parameter values: $\delta_M = 0.48$ min^{-1}, $\delta_Y = 0.03$ min^{-1}, $\delta_L = 0.02$ min^{-1}, $a_1 = 0.29$ molecules min^{-1}, $K_2 = 2.92 \times 10^6$ molecules, $K_1 R_T = 213.2$, $c_1 = 18.8$ min^{-1}, $k_L = 6.0 \times 10^4$ min^{-1}, $K_{ML} = 680$ μM, $k_g = 3.6 \times 10^3$ min^{-1}, $K_{Mg} = 7.0 \times 10^5$ molecules.

Santillán and his colleagues made the further simplifying assumption that the concentration of allolactose, denoted A, is equivalent to the concentration of lactose (justified in Exercise 7.2.1), so

$$A(t) = L(t). \tag{7.15}$$

Finally, we address inactivation of *lac* repressor by allolactose. The repressor is a homotetramer (i.e. a complex of four identical monomers). It is inactivated by the binding of an allolactose molecule to any of its four monomers. Taking these binding events as independent, the fraction of unbound monomers is

$$\text{fraction of unbound monomers} = \frac{K_2}{K_2 + A(t)}, \tag{7.16}$$

where K_2 is the dissociation constant. The concentration of active repressor tetramers (in which all four monomers are unbound) is then

$$r(t) = R_T \left(\frac{K_2}{K_2 + A(t)} \right)^4, \tag{7.17}$$

where R_T is the total concentration of repressor protein (presumed constant).

Equations (7.11-7.17) comprise a model with three independent state variables: m, y, and L. Figure 7.7 illustrates the model's response to changes in the external lactose level, L_e. Panel A shows the time-varying response to a series of increases in the external lactose level. When L_e rises from 0 to 50 μM, there is a negligible response in system activity, as evidenced by the minor increase in β-galactosidase abundance. When the lactose level doubles to 100 μM, a dramatic increase in enzyme level is triggered. A further step in the lactose level to ($Le = 150$ μM) elicits no response—the system has already switched to its fully 'on' state. When the external lactose is removed, the system abruptly returns to its 'off' state of low activity.

The dose-response curve in Panel B shows the switch-like nature of the system's response. The solid curve shows that the model's transition from low activity to high activity occurs at a threshold lactose concentration. This 'all-or-nothing' response results in a binary (yes/no) response to the lactose input. Panel B also shows the behaviour of a modified model in which the positive feedback loop has been cut (details in Problem 7.8.5). The dashed dose-response curve for this hypothetical model shows a graded response to lactose availability, in contrast to the switch-like behaviour of the true *lac* system.

The *lac* operon is a sensory gene regulatory network. Its function is to provide the cell with an appropriate response to a the current environmental condition. When conditions change, the response changes as well; in this case, the switch turns 'on' when lactose is present, and 'off' when lactose is absent. In the next section, we consider a system in which a yes/no decision must persist after the activating stimulus has been removed.

Exercise 7.2.1 The rate of allolactose production is given in equation (7.14) as $\frac{k_g\, b(t)L(t)}{K_{Mg}}$. Allolactose is almost identical to lactose in structure, and so is metabolized by β-galactosidase in the same manner as lactose (and consequently with the same kinetics). Denoting the concentration of allolactose by A, and allowing for dilution, this gives

$$\frac{d}{dt}A(t) = \frac{k_g b(t)L(t)}{K_{Mg} + L(t)} - \frac{k_a b(t)A(t)}{K_{Ma} + A(t)} - \delta_L A(t).$$

Taking $k_g = k_a$ and $K_{Mg} = K_{Ma}$ (as above), Santillán and colleagues made the assumptions that (i) dilution of allolactose is negligible; and (ii) allolactose is in quasi-steady state. Verify that these assumption lead to the equivalence

$$A^{qss}(t) = L(t).$$

□

Exercise 7.2.2 Experimental studies of the *lac* operon often make use of IPTG (isopropyl β-D-1-thiogalactopyranoside), which is a molecular mimic of allolactose, but is not metabolized in the cell. Extend the model to include the effect of IPTG. For simplicity, suppose that IPTG is present at a fixed intracellular concentration. □

7.2.2 The phage lambda decision switch

Developmental gene regulatory networks are responsible for guiding the differentiation processes that occur as a single fertilized egg cell develops into a multi-cellular organism. Many of the decisions made during development require discrete (yes/no) responses to environmental conditions.

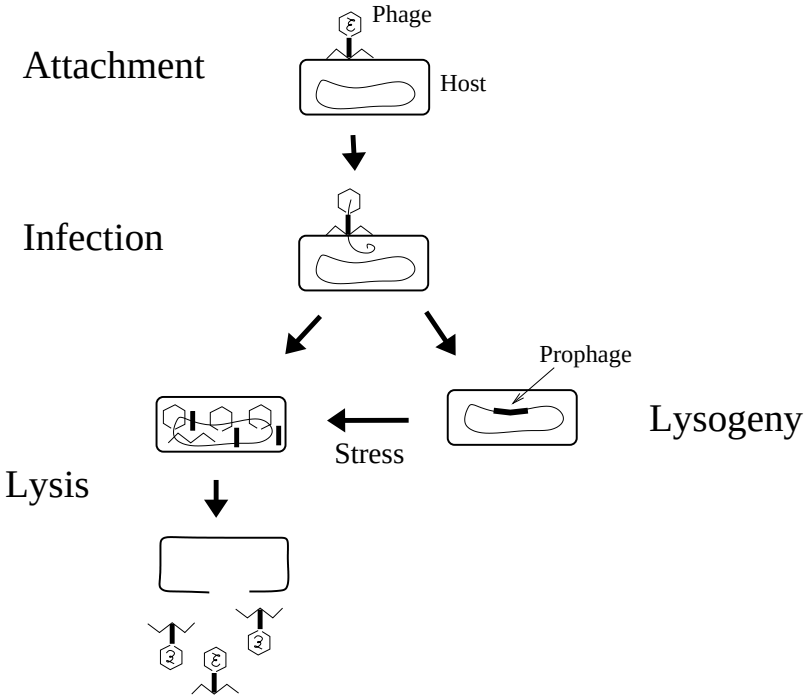

Figure 7.8: Phage lambda infection. Upon attaching to a host cell, the phage injects its genome and then follows one of two infection processes. If the host is healthy, the phage genome is incorporated into the host's DNA, as a so-called prophage. The prophage is copied when the cell divides, so all the host's progeny are dormantly infected. Alternatively, if the host cell is under stress, expression of phage genes leads to the production of new phage particles. The cell wall is then ruptured (lysed), releasing the phage particles to infect new hosts. Adapted from Figure 1.2 of (Ptashne, 2004).

Moreover, because the triggering signals do not continue indefinitely, these responses need to be persistent.

In this section, we will address the lysis/lysogeny decision-switch in phage lambda. This genetic circuit that has a binary (on/off) character and retains a memory of past stimuli. This is a viral response process occurs in host bacterial cells. Nevertheless, it serves as a biological model of more complex differentiation processes in multicellular organisms.

Phage lambda is a bacteriophage—a virus that infects bacterial cells. Phage particles, like all viruses, consist of a small genome encased in a protein shell. Upon penetrating the membrane of an *E. coli* host cell, the phage follows one of two infection processes (Figure 7.8):

- **lytic growth:** the host's genetic machinery is employed to produce about a hundred new phages, which then lyse (burst) the host cell.

- **lysogenic growth:** the phage's genetic material is integrated into the host cell's genome. (The viral genome is then called a *prophage*.) When the lysogenized host divides, it makes a copy of the prophage along with its own DNA. The phage thus dormantly infects all progeny of the host cell.

The phage senses the host's condition and chooses the appropriate infection mechanism: if the host is growing well, the phage integrates and multiplies lysogenically along with the host and

its progeny; if the host cell is starving or damaged, the phage grows lytically—an 'abandon ship' response. This decision is based on a genetic switch.

The decision switch

We will not address the initial infection process, which involves several phage genes. Instead, we will model the simpler situation in which a prophage 'chooses' whether to continue to grow lysogenically or to begin the lytic process. This decision switch can be described in terms of two genes and their protein products:

- gene *cI* codes for protein cI, also called repressor;
- gene *cro* codes for protein cro (an acronym for **c**ontrol of **r**epressor and **o**thers).

These two genes are adjacent to one another on the phage DNA. They lie on opposite strands of the double helix, and are consequently transcribed in opposite directions. Their promoters lie back-to-back, as shown in Figure 7.9.

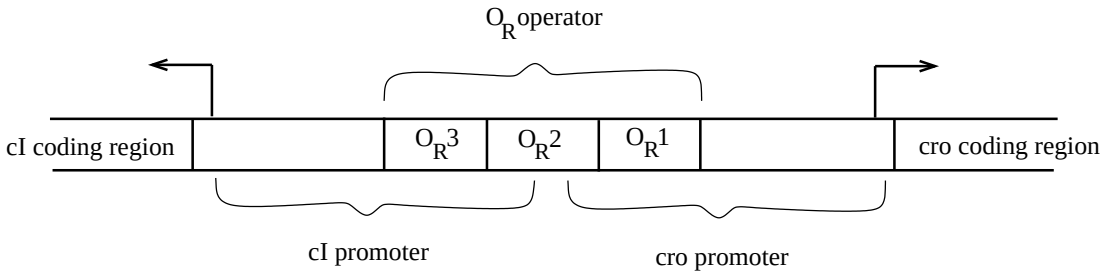

Figure 7.9: Phage lambda decision genes. The *cI* and *cro* genes lie on opposite strands of the DNA double helix and so are transcribed in opposite directions. Their promoter regions lie back-to-back. The shared operator, called O_R, overlaps both promoters; it contains three sites at which both cI and cro bind.

Both the cI and cro proteins regulate their own and each other's expression. This regulation occurs through the binding of these proteins to an operator region that overlaps both the *cI* and *cro* promoters. This operator region is called O_R. The O_R region contains three binding sites called O_R1, O_R2, and O_R3. Both cI and cro bind to all three of these regions, but in different manners and with opposing effects, as we next describe.

Regulation by cI

The cI protein is a homodimer. These dimers bind strongly to O_R1, and weakly (with about 10 times less affinity) to O_R2 and O_R3. However, a cI dimer bound to O_R1 interacts with another at O_R2. This cooperativity greatly increases the affinity of cI dimers for O_R2. Consequently, at low concentrations, cI dimers are found bound to O_R1 and O_R2, while at high concentrations, cI dimers will be bound to all three operator sites.

The effects of cI binding are as follows (Figure 7.10A):

- When no proteins are bound at the operator site, there is strong expression of cro. The cI promoter has only weak affinity for RNA polymerase, so there is minimal expression of cI in this case.

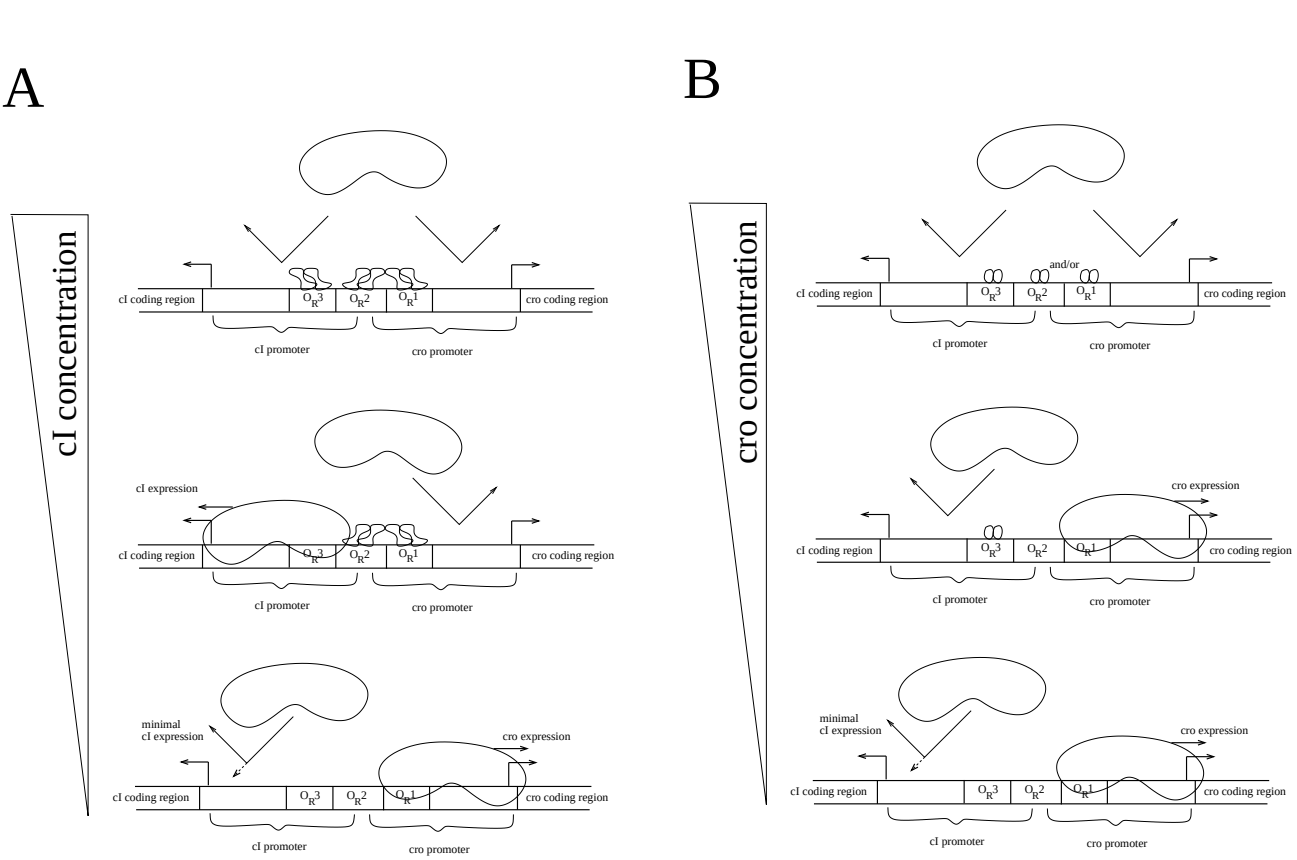

Figure 7.10: Regulation by cI and cro. **A.** Dimers of cI bind to O_R1 and O_R2 at low concentration, and at O_R3 at higher concentration. Basal expression of cI is weak, but polymerase binding is enhanced by a cI dimer bound at O_R2. When bound to O_R1, cI blocks cro expression. When cI binds O_R3, it blocks expression from the *cI* gene. **B.** Dimers of cro bind strongly to O_R3, and weakly to O_R2 and O_R1. When bound to O_R3, cro blocks expression of cI. When bound to O_R2 or O_R1, cro blocks its own expression.

- When cI dimer is bound to O_R1, it inhibits cro expression by blocking access to the cro promoter.
- When cI dimer is bound to O_R2, it upregulates its own expression (about ten-fold) by binding to RNA polymerase at the cI promoter, effectively increasing the affinity of the docking site. Thus cI is an autoactivator.
- When cI dimer is bound to O_R3, it blocks access to the cI promoter, and thus represses its own expression. Thus, at high concentrations, cI is an autoinhibitor.

The interplay of autoactivation at low levels and autoinhibition at high levels results in tight regulation of the cI concentration.

Regulation by cro

The cro protein is also a homodimer. These dimers bind to all three operator sites, with affinity opposite to that of cI, and with no cooperative effects. The cro dimer has a high affinity for O_R3, and so binds there at low concentrations; it has lower affinity for O_R2 and O_R1 (roughly equal), and so is found at these sites only at higher concentrations.

The effects of cro binding are as follows (Figure 7.10B):

- As described above, when no proteins are bound at the operator site, cro is expressed strongly while only weak expression of cI occurs.
- When cro dimer is bound to O_R3, it blocks the cI promoter. Hence cro inhibits expression of cI.
- When cro dimer is bound to O_R2 or O_R1, it inhibits its own expression by blocking access to the cro promoter. Thus, at high concentrations, cro is an autoinhibitor.

Bistability

The *cI* and *cro* genes are antagonists—each represses the other. Consequently, we expect the system to exhibit two steady states: either cI will be abundant, repressing cro; or cro will be abundant, repressing cI. These two states characterize the two pathways of infection.

- In the lysogenic state, the cI concentration is high, and the cro concentration is low.
- Lysis begins when the cI concentration is low and the cro concentration is high.

The system is bistable. The lysogenic state is stable on a long time-scale; it can be maintained for generations of hosts. In contrast, the lytic state is necessarily transient—it leads to the host cell's death. Nevertheless, we are justified in calling the lytic condition a steady state on the relatively short timescale of the decision switch itself.

Flipping the switch

Once it has integrated into the host's genome, the prophage continuously monitors the state of the cell. When it senses that the host cell is in jeopardy, it 'flips the switch' to begin lytic growth. There is no mechanism for a switch in the opposite direction—lytic growth is an irreversible process.

The switch to lysis occurs when the host cell is under stress (e.g. is injured or starving). In the laboratory, the simplest way to induce lysis is by exposing the cells to ultraviolet light, which causes DNA damage. Cells responds to this damage by invoking expression of a number of repair proteins—this is called the *SOS response*. A key component of the SOS response is the bacterial protein RecA, which is triggers expression of DNA repair genes. The phage protein cI interacts with activate RecA, resulting in cleavage of cI. Once cleaved, cI cannot bind the O_R sites, and so can no longer regulate gene expression. This frees *cro* from repression, leading to lytic phage growth.

Modelling the switch

We present here a simple model that captures the bistable nature of the system with minimal detail. (A detailed model that incorporates descriptions of DNA-binding and expression processes can be found in (Reinitz and Vaisnys, 1990).

We will neglect mRNA dynamics and incorporate only two state variables: the concentrations of cI and cro protein. Because cI is also called repressor, we will write $r = [\text{cI}]$ and $c = [\text{cro}]$. The

model takes the form

$$\begin{aligned} \frac{d}{dt}r(t) &= f_r(r(t),c(t)) - \delta_r r(t) \\ \frac{d}{dt}c(t) &= f_c(r(t),c(t)) - \delta_c c(t), \end{aligned} \tag{7.18}$$

where δ_r and δ_c account for dilution and degradation, and f_r and f_c describe the rates of expression from the cI and cro promoters, respectively.

To characterize the operator occupancy function, we begin by making the following simplifying assumptions: (i) cro and cI will never bind the operator simultaneously; (ii) strong cooperativity causes the binding of cI at O_R2 to happen concurrently with cI binding to O_R1; and (iii) states in which cro dimer is bound to O_R1 or O_R2 can be lumped together. These assumptions result in five distinct DNA-binding states (Figure 7.10), as summarized in the following table, which indicates the rates of expression of cI and cro from each state. (The parameters a and b are the expression rates from the unregulated genes.)

State	Notation	rate of cI expression	rate of cro expression
unbound operator	O	a	b
cI at O_R1 and O_R2	$O(cI_2)_2$	$10a$	0
cI at O_R1, O_R2, and O_R3	$O(cI_2)_3$	0	0
cro at O_R3	$O(cro_2)$	0	b
cro at O_R3 and O_R1 and/or O_R2	$O(cro_2)_{2+}$	0	0

We have assumed that there is no expression from the repressed states (i.e. leakage is negligible). Next, we consider the occupancy functions for these binding states. For simplicity, we assume that all cI and cro protein is in the dimer form, so that

$$[cI_2] = \frac{r(t)}{2} \qquad \text{and} \qquad [cro_2] = \frac{c(t)}{2}.$$

Treating the corresponding DNA-binding events in quasi-steady state we arrive at expression rates for cI and cro (Exercise 7.2.3):

$$\begin{aligned} \text{cI expression rate}: \quad f_r(r,c) &= \frac{a + 10aK_1(r/2)^2}{1 + K_1(r/2)^2 + K_2K_1(r/2)^3 + K_3(c/2) + K_4K_3(c/2)^2} \\ \text{cro expression rate}: \quad f_c(r,c) &= \frac{b + bK_3(c/2)}{1 + K_1(r/2)^2 + K_2K_1(r/2)^3 + K_3(c/2) + K_4K_3(c/2)^2} \end{aligned} \tag{7.19}$$

The model behaviour is illustrated in Figure 7.11. The phase portrait in Panel A reveals the bistable nature of the system. Both stable states exhibit near-zero levels of the repressed protein. The lytic state has a small basin of attraction; only initial conditions with overwhelmingly large concentrations of cro will end up in this high-cro, low-cI condition. Panel B shows the system behaviour when RecA is active (simulated by a tenfold increase in δ_r). This parameter change shifts the r-nullcline so that the system is monostable—only the lytic steady state (high-cro, low-cI) remains.

The lambda decision network fulfills the two requirements of a developmental switch: a threshold transition from one condition to another, and a persistent memory. This response is consistent with Lewis Wolpert's 'French Flag' developmental model, in which a nascent tissue is exposed to

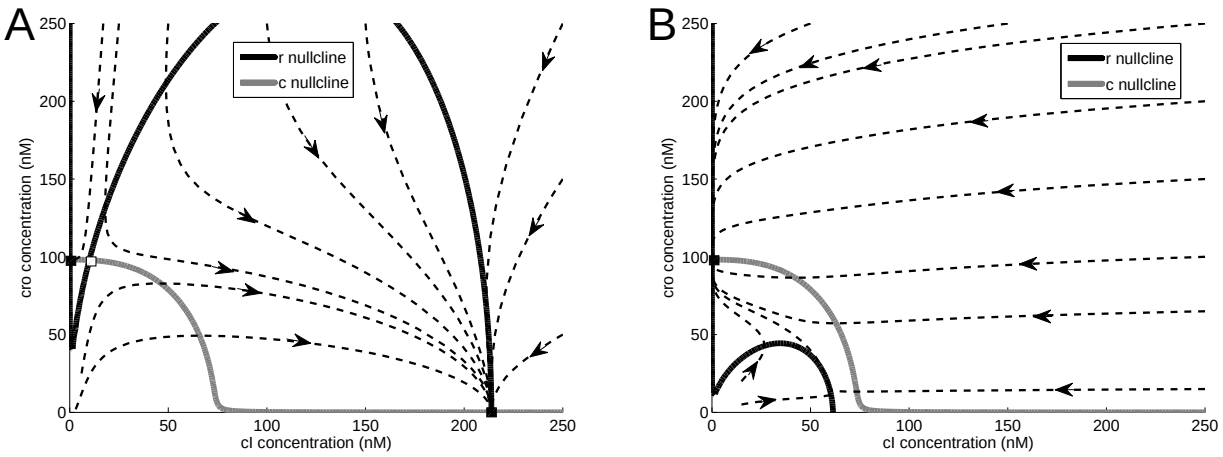

Figure 7.11: Behaviour of the decision switch model. **A.** This phase portrait shows the bistable nature of the system. The nullclines intersect three times (boxes). The two steady states are found close to the axes; in each case the repressed protein is virtually absent. **B.** When RecA activity is included (by increasing δ_r tenfold), the system becomes monostable—all trajectories are attracted to the lytic (high-cro, low-cI) state. Parameter values: $a = 5$ min^{-1}, $b = 50$ min^{-1}, $K_1 = 1$ nM^{-2}, $K_2 = 0.1$ nM^{-1}, $K_3 = 5$ nM^{-1}, $K_4 = 0.5$ nM^{-1}, $\delta_r = 0.02$ min^{-1} (0.2 in panel B), $\delta_c = 0.02$ min^{-1}.

a gradient of a chemical signal—called a morphogen—that induces differentiation into different cell types. The signal strength varies continuously over the tissue domain, and does not persist indefinitely. In response, each cell makes a discrete decision (as to how to differentiate), and internalizes that decision so that the effect persists after the signal is removed.

The phage lambda decision circuit is a valuable model of developmental gene circuits. However, because it is irreversible, it cannot serve as an example of a generic on/off switch that could be employed as part of a larger decision-making circuit. In the next section, we consider a genetic switch that was designed to be reversible.

Exercise 7.2.3 Derive the expression rates in equation (7.19) as follows. Note that the DNA-binding events are:

$$\mathrm{O} + \mathrm{cI}_2 + \mathrm{cI}_2 \underset{k_{-1}}{\overset{k_1}{\rightleftharpoons}} \mathrm{O(cI}_2)_2 \qquad \mathrm{O(cI}_2)_2 + \mathrm{cI}_2 \underset{k_{-2}}{\overset{k_2}{\rightleftharpoons}} \mathrm{O(cI}_2)_3$$

$$\mathrm{O} + \mathrm{cro}_2 \underset{k_{-3}}{\overset{k_3}{\rightleftharpoons}} \mathrm{O(cro}_2) \qquad \mathrm{O(cro}_2) + \mathrm{cro}_2 \underset{k_{-4}}{\overset{k_4}{\rightleftharpoons}} \mathrm{O(cro}_2)_{2+}$$

For $i = 1, 2, 3, 4$, define the association constants $K_i = k_i/k_{-i}$, and determine the equilibrium conditions for each binding event. Next, use these equilibrium equations, along with conservation of operator sites:

$$[\mathrm{O}] + [\mathrm{O(cI}_2)_2] + [\mathrm{O(cI}_2)_3] + [\mathrm{O(cro}_2)] + [\mathrm{O(cro}_2)_{2+}] = \mathrm{O}_T,$$

to determine the occupancy function for each of the five states. Finally, use the expression rates for each state (in the table above) to derive the expression rates in equation (7.19). □

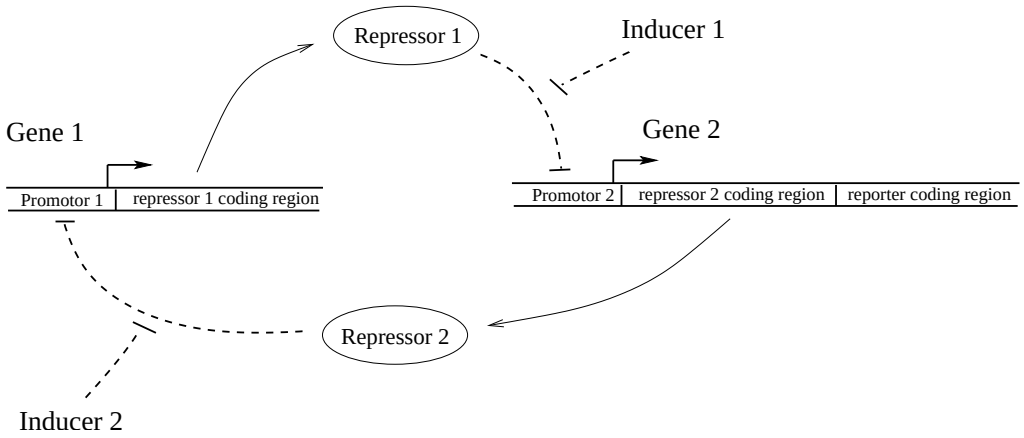

Figure 7.12: Collins toggle switch. Two genes repress one another's expression, leading to a bistable system. Each transcription factor was chosen so that it could be deactivated by an experimental intervention.

7.2.3 The Collins toggle switch

As discussed in Chapter 1, in the year 2000, Timothy Gardner, Charles Cantor and Jim Collins designed and constructed a genetic toggle switch by re-wiring the components of existing gene regulatory networks (Gardner *et al.*, 2000).

Their engineered circuit (Figure 7.12) employs the same mutual repression scheme that we saw in the phage lambda decision switch. However, the toggle switch can be 'flipped' in both directions: the transcription factors were chosen so that each could be inhibited by an appropriate intervention.

The toggle switch design includes a *reporter* gene, which allows for direct observation of the system's activity. The reporter is *green fluorescent protein* (GFP), which fluoresces green when exposed to blue light. The coding region for the GFP reporter was attached downstream of the coding region for one of the two repressors, creating an operon. The concentration of GFP—and intensity of fluorescence—is then correlated with the concentration of that repressor.

Gardner and his colleagues constructed multiple instances of the toggle switch network. They used only genes and promoters whose behaviour had been well characterized: the Lac repressor and the Tet repressor from *E. coli*, and cI from phage lambda. (The Tet repressor inhibits expression from the *tet* genes that are responsible for protection from tetracycline, an antibiotic.) The target of cI repression was not the cro promoter studied in the previous section, but another phage promoter, P_L, whose repression mechanism is simpler. For each of these transcription factors, expression from the target gene could be induced by inactivating the repression. (The lac repressor is inactivated by isopropyl β-D-1-thiogalactopyranoside (IPTG)—a non-metabolizable analogue of allolactose. Likewise, Tet repressor can be inactivated by anhydrotetracycline (aTc)—a non-toxic analogue of its usual inactivator tetracycline. The phage protein cI does not have a native inactivation mechanism. Gardner and colleagues made use of a mutated form of cI that is temperature-sensitive: it functions normally at 30°C, but is non-functional when the temperature is raised to 42°C.)

Gardner and his colleagues developed a simple model in order to explore the behavior of the switch circuit. The model was not meant to accurately reflect the specifics of their proposed construction, but was used to investigate the nature of bistability in such a device.

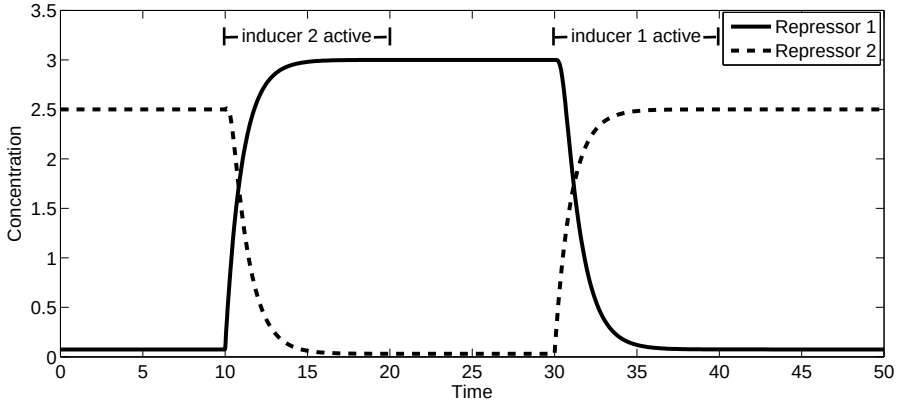

Figure 7.13: Behaviour of the toggle switch model. Repressor 2 is abundant in the initial condition. At time $t = 10$, inducer 2 is introduced, rendering repressor 2 inactive, and so inducing expression of repressor 1. Repressor 1 is then able to repress expression of repressor 2. The high level of repressor 1 is maintained after the inducer is removed at $t = 20$. The opposite effect occurs on introduction of inducer 1 (at $t = 30$, removal at $t = 40$). Parameter values: $\alpha_1 = 3$ (concentration/time), $\alpha_2 = 2.5$ (concentration/time), $\beta = 4$ and $\gamma = 4$. Inducer activity is simulated by increasing i_1 or i_2 from 0 to 10 in each case. Units are arbitrary.

Neglecting mRNA dynamics, the model can be written

$$\frac{d}{dt}p_1(t) = \frac{\alpha_1}{1+\left(\frac{p_2(t)}{1+i_2}\right)^{\beta}} - p_1(t) \tag{7.20}$$

$$\frac{d}{dt}p_2(t) = \frac{\alpha_2}{1+\left(\frac{p_1(t)}{1+i_1}\right)^{\gamma}} - p_2(t) \tag{7.21}$$

where p_1 and p_2 are the concentrations of the two proteins, α_1 and α_2 are their maximal expression rates, β and γ indicate the degree of nonlinearity (i.e. cooperativity) in the repression mechanisms, and i_1, i_2 characterize the two inducers. Dilution is considered to be dominant over degradation, so the decay rates are identical. Gardner and colleagues scaled the time and concentration units to reduce the number of parameters in the model (Exercise 7.2.4).

Figure 7.13 shows the model behaviour. The two inducers have the desired effect of causing transitions between the stable steady states. Figure 7.14A shows a phase portrait for the un-induced (bistable) system. The portrait in Panel B shows the monostable system that occurs when inducer 2 is present.

Gardner and his colleagues used their model to predict features of the circuit that would result in bistability. The two-dimensional bifurcation plot in Figure 7.15 shows the results of such an analysis. This plot subdivides the α_1-α_2 parameter space into regions in which the system is monostable or bistable, for various values of β and γ. As expected, when $\alpha_1 = \alpha_2$, the system is perfectly balanced and so is bistable, provided that the maximal expression rates are sufficiently large (otherwise a single balanced steady state occurs). When the two expression rates are not balanced, bistability may be lost as one gene dominates the other. The degree of imbalance that is allowed within the bistability domain depends strongly on γ and β, which reflect the degree of nonlinearity in repressor-DNA binding. The greater the nonlinearity, the more allowance the switch has for unequal expression rates. These observations suggest that (i) bistability is favored by stronger promoters

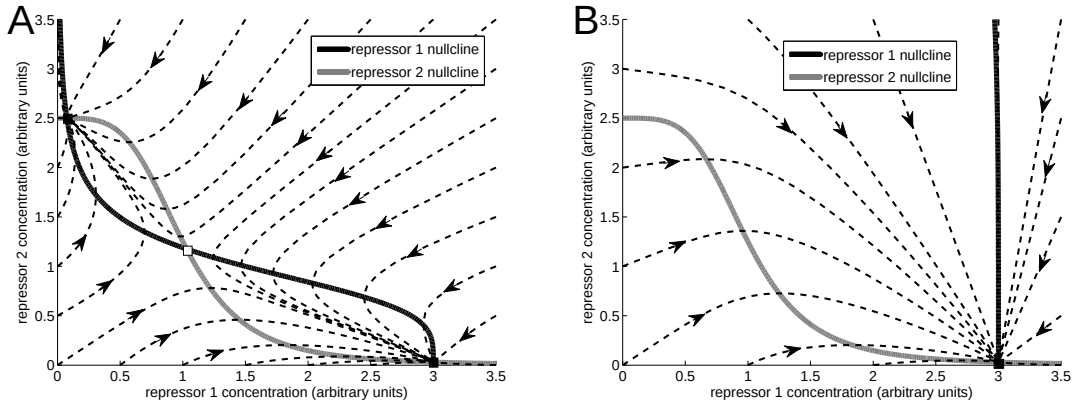

Figure 7.14: Phase portraits for the toggle switch. **A.** The un-induced switch ($i_1 = i_2 = 0$). The nullclines intersect three times: at two stable steady states and one intermediate unstable steady state. **B.** Under the influence of inducer 2 ($i_2 = 10$), the nullcline for repressor 1 has shifted so there is a single steady state, to which all trajectories converge. Parameter values as in Figure 7.13. Adapted from Figure 2 of (Gardner *et al.*, 2000).

and ribosome binding sites; and (ii) the more cooperativity involved in repressor-DNA binding, the more robust the switch's bistability will be to asymmetry between the two component genes. Gardiner and colleagues used these principles to construct multiple functioning instances of the genetic switch (implemented in *E. coli* cells). They successfully confirmed the bistable behaviour of the device by monitoring the GFP read-out in the lab.

Exercise 7.2.4 When constructing a generic model, rescaling of units can absorb parameters into the definition of time- or concentration-scales, thus reducing the number of free parameters. For instance, the concentration profile $s(t) = e^{-t/60}$ nM, where t is measured in seconds, can be written as $s(\tau) = e^{-\tau}$ nM, where τ is measured in minutes (i.e. in time-units of 60 seconds).

Consider a model of gene expression:

$$\frac{d}{dt}p(t) = \frac{\alpha}{K + p(t)} - \delta p(t).$$

Describe the re-scaling of time and concentration units in which the model can be written as

$$\frac{d}{d\tau}\tilde{p}(\tau) = \frac{\tilde{\alpha}}{1 + \tilde{p}(\tau)} - \tilde{p}(\tau).$$

□

Exercise 7.2.5 In the simple case of $\beta = \gamma = 1$, the results in Figure 7.15 can be derived analytically. Verify that in this case the system is monostable (it exhibits a single steady state) whenever $\alpha_1 = \alpha_2$. (Take $i_1 = i_2 = 0$.) □

7.3 Oscillatory Gene Networks

We next consider examples of gene regulatory networks that generate persistent oscillations. These networks allow cells to maintain internal clocks that can be used to predict periodic changes in conditions (such as the night-day cycle).

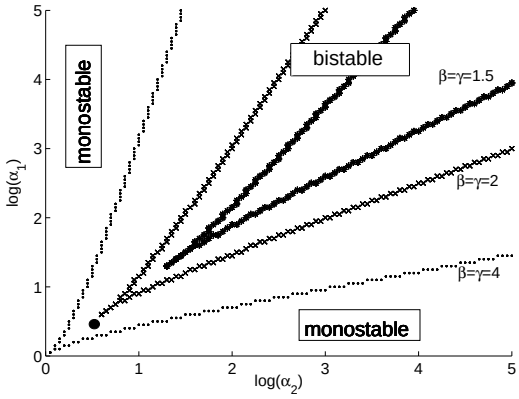

Figure 7.15: Dependence of bistability on parameter values. For each value of β and γ, the α_1-α_2 parameter space is divided into regions in which the system is monostable or bistable ($i_1 = i_2 = 0$). As the degree of nonlinearity (i.e. β and γ) increases, the bistable region grows, indicating that bistability is preserved despite asymmetry between the two components of the switch. The parameter set for the simulation in Figure 7.13 is indicated by the dot near the bottom left-hand corner. Adapted from Figure 2 of (Gardner *et al.*, 2000).

7.3.1 The Goodwin oscillator

In 1965, Brian Goodwin proposed a generic model of an oscillatory genetic circuit (Goodwin, 1965). The model, sketched in Figure 7.16, involves a single gene. The mRNA, X, is translated into enzyme Y, which catalyses production of metabolite Z, which causes inhibition of expression (by activating an unmodelled repressor). Neglecting the specifics of catalysis and inhibition, Goodwin formulated the model in terms of concentrations x, y and z as:

$$\begin{aligned} \frac{d}{dt}x(t) &= \frac{a}{k^n + (z(t))^n} - bx(t) \\ \frac{d}{dt}y(t) &= \alpha x(t) - \beta y(t) \\ \frac{d}{dt}z(t) &= \gamma y(t) - \delta z(t). \end{aligned} \tag{7.22}$$

The model was not meant to describe a particular system; it was constructed to demonstrate how persistent oscillations could be generated by an autoinhibitory gene circuit.

Goodwin included three states in the model to impose sufficient delay in the negative feedback loop. As discussed in Section 4.3, oscillations can arise from negative feedback if the effect of the feedback is delayed and if there is sufficient nonlinearity in the loop. Indeed, a two-state model that arises from applying the quasi-steady state assumption to the Goodwin model cannot exhibit sustained oscillations, as verified by J. S. Griffith (Griffith, 1968).

Even with three steps providing a lag in the feedback, a high degree of nonlinearity is required to generate limit-cycle oscillations in this model. In his paper, Griffith showed that the system will only exhibit damped oscillations if the Hill coefficient n is less than eight, and even for $n > 8$, oscillations only occur for certain values of the other parameters (Problem 7.8.8).

The system's oscillatory behaviour is shown in Figure 7.17. The mechanism of oscillations is apparent in Panel A. In each cycle, the mRNA concentration rises, followed by a rise in enzyme concentration, and then a rise in metabolite concentration. The rise in z causes a crash in x, which

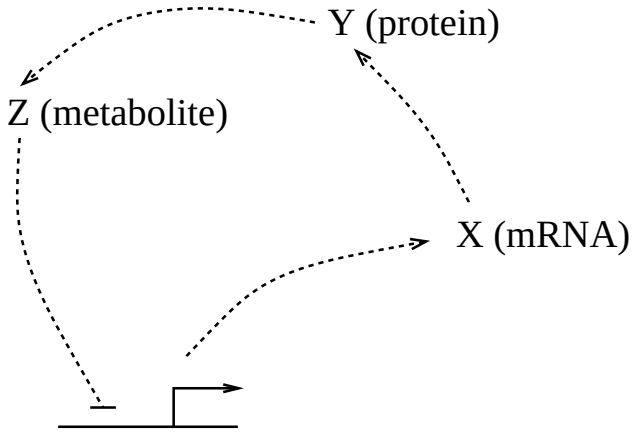

Figure 7.16: The Goodwin oscillator. The mRNA (X) is translated into an enzyme (Y), which catalyses production of a metabolite (Z), which (indirectly) represses gene expression. This negative feedback, coupled with the delay inherent in the three-step loop, can result in oscillatory behavior.

causes y and z to drop, allowing x to rise again. Panel B shows a three-dimensional phase portrait, confirming that the system trajectories all settle to a periodic (limit cycle) behaviour.

Exercise 7.3.1 Goodwin offered multiple interpretations of his model. In addition to the description given here (X is mRNA, Y is enzyme, Z is metabolite), he also suggested that the model could be used to describe the following feedback loops:
a) X is nuclear mRNA, Y is cytoplasmic mRNA, Z is protein product;
b) X is mRNA, Y is inactive protein product, Z is active protein product;
Under what assumptions can the model apply to each of these cases? □

7.3.2 Circadian rhythms

The Goodwin model demonstrates that an autoinhibitory gene can generate persistent oscillations. A specific instance of this behavior is provided the circadian rhythm generator in the fruit fly *Drosophila melanogaster*.

We are familiar with the circadian rhythms of our own bodies; they regulate our sleep-wake cycles and are disrupted by jet-lag when we travel across time zones. Because they allow prediction of periodic changes in temperature and light, these internal rhythms are an important aspect of many organisms' biology.

Behavioral studies of these internal clocks have shown them to have a free-running period of roughly 24 hours (i.e. in the absence of external cues). Moreover, these rhythms are readily entrained to light and temperature cues and are remarkably robust to changes in ambient temperature.

In mammals, the primary circadian pacemaker has been identified as a group of about 8000 neurons in the suprachiasmatic nucleus (located in the hypothalamus), which have a direct connection to the retina (in the eye). A model of the gene network responsible for generation of circadian rhythms in mammals is provided in (LeLoup and Goldbeter, 2003).

Here, we consider the first dynamical mathematical model that was proposed for a circadian oscillator: Albert Goldbeter's model of circadian rhythms in *Drosophila* (reviewed in (Goldbeter, 1996)).

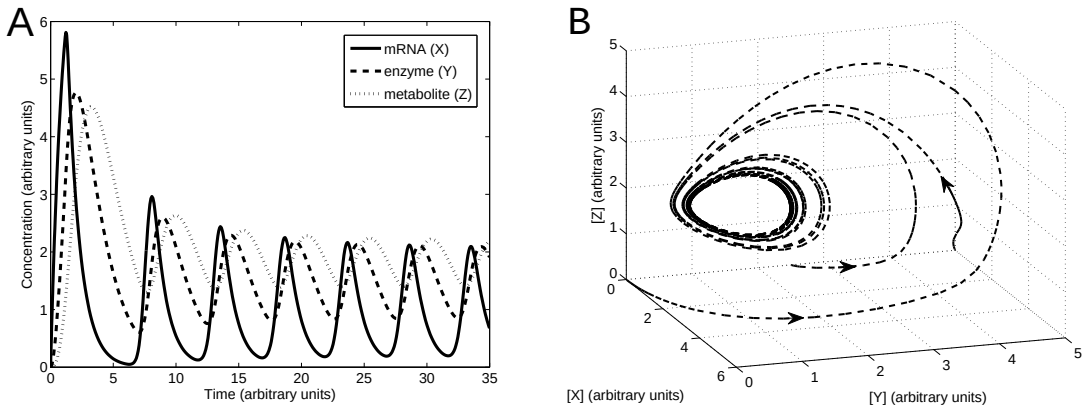

Figure 7.17: The Goodwin oscillator. **A.** This simulation shows relaxation to sustained (limit cycle) oscillations. **B.** A phase portrait showing convergence to a limit cycle in the three-dimensional phase space. Parameter values are $a = 360$ (concentration $\cdot$ time^{-1}), $k = 1.368$ (concentration), $b = 1$ (time^{-1}), $\alpha = 1$ (time^{-1}), $\beta = 0.6$ (time^{-1}), $\gamma = 1$ (time^{-1}), $\delta = 0.8$ (time^{-1}), $n = 12$. Units are arbitrary.

Studies of *Drosophila* have yielded many advances in genetics. In 1971, Ronald Konopka and Seymour Benzer published a study in which they identified flies with mutations that caused changes in the period of the free-running circadian rhythm (Konopka and Benzer, 1971). These mutations occurred in a gene named *per* (for period); the protein product is called PER. In contrast to wild-type (i.e. non-mutant) flies, whose rest/activity patterns demonstrated a roughly 24 hour free-running period, they reported on three mutations:

- an arrhythmic mutant that exhibits no discernible rhythm in its activity;
- a short-period mutant with a period of about 19 hours;
- a long-period mutant with a period of about 28 hours.

Additional molecular analysis provided clues to the dynamic behaviour of *per* gene expression. Observations of wild-type flies revealed that total PER protein levels, *per* mRNA levels, and levels of phosphorylated PER protein all oscillate with the same 24-hour period, with the peak in mRNA preceding the peak in total protein by about 4 hours. Moreover, it was shown that when the import of PER protein into the nucleus was blocked, the oscillations did not occur. Based on these observations, Goldbeter constructed a model of an autoinhibitory *per* circuit.

Goldbeter's model, sketched in Figure 7.18, has the same basic structure as the Goodwin model: a gene codes for a product that, after a delay, represses its own expression. In this case the delay is caused by transport across the nuclear membrane and a two-step activation process (by phosphorylation).

The feedback loop begins with the production of *per* mRNA (M), which is exported from the nucleus to the cytosol. In the cytosol, the mRNA is translated into protein, and is subject to degradation. Newly-translated PER protein (P_0) is inactive. It undergoes two rounds of phosphorylation to become active PER (P_2), which is reversibly transported across the nuclear membrane. Once in the nucleus (P_N), PER represses transcription of the *per* gene. Degradation of PER is assumed to occur only in the cytosol, and degradation of inactive PER is assumed negligible.

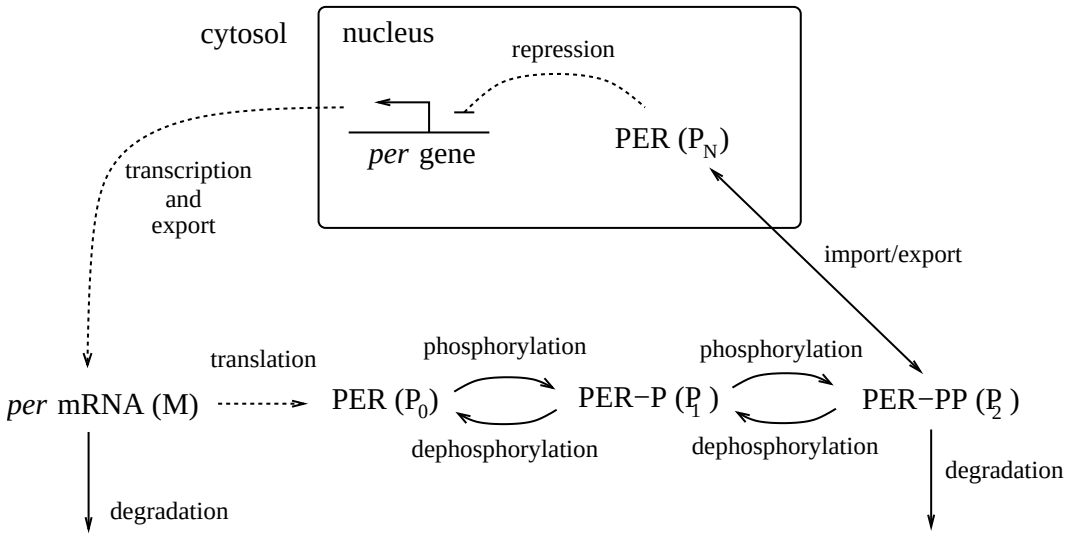

Figure 7.18: Goldbeter's circadian oscillator model. The *per* gene is transcribed in the nucleus; *per* mRNA (M) is exported to the cytosol, where is it translated and is subject to degradation. PER protein (P_0) is activated by two reversible rounds of phosphorylation. Active PER (P_2) is subject to degradation, and can cross the nuclear membrane. Once in the nucleus, PER (P_N) represses transcription of the *per* gene. Delay oscillations arise from the combination of autoinhibitory feedback, nonlinear repression kinetics, and delay (caused by expression, activation, and transport). Adapted from Figure 11.6 of (Goldbeter, 1996).

Goldbeter's model takes the form

$$\begin{aligned}
\frac{d}{dt}m(t) &= \frac{v_s}{1+(p_N(t)/K_I)^n} - \frac{v_m m(t)}{K_{m1}+m(t)} \\
\frac{d}{dt}p_0(t) &= k_s m(t) - \frac{V_1 p_0(t)}{K_1+p_0(t)} + \frac{V_2 p_1(t)}{K_2+p_1(t)} \\
\frac{d}{dt}p_1(t) &= \frac{V_1 p_0(t)}{K_1+p_0(t)} - \frac{V_2 p_1(t)}{K_2+p_1(t)} - \frac{V_3 p_1(t)}{K_3+p_1(t)} + \frac{V_4 p_2(t)}{K_4+p_2(t)} \\
\frac{d}{dt}p_2(t) &= \frac{V_3 p_1(t)}{K_3+p_1(t)} - \frac{V_4 p_2(t)}{K_4+p_2(t)} - k_1 p_2(t) + k_2 p_N(t) - \frac{v_d p_2(t)}{K_d+p_2(t)} \\
\frac{d}{dt}p_N(t) &= k_1 p_2(t) - k_2 p_N(t).
\end{aligned}$$

The model is based on first-order kinetics for transport across the nuclear membrane, and Michaelis-Menten kinetics for the degradation and phosphorylation/dephosphorylation processes. Transcription and export of mRNA are lumped into a single process, which is cooperatively repressed by P_N with Hill coefficient n. As with the Goodwin model, this model only exhibits oscillatory behaviour if the repression kinetics is sufficiently nonlinear. Goldbeter carried out his analysis with $n = 4$; he found that the model can exhibit oscillations with $n = 2$ or even $n = 1$, but only under restrictive conditions on the other parameter values.

The oscillatory behaviour of the model is illustrated in Figure 7.19. Panel A shows the periodic behaviour of *per* mRNA, total PER protein, and nuclear PER protein. The period is roughly 24 hours, and the mRNA peak precedes the total PER peak by about 4 hours. This behaviour is consistent with experimental observation, but does not provide direct validation of the model,

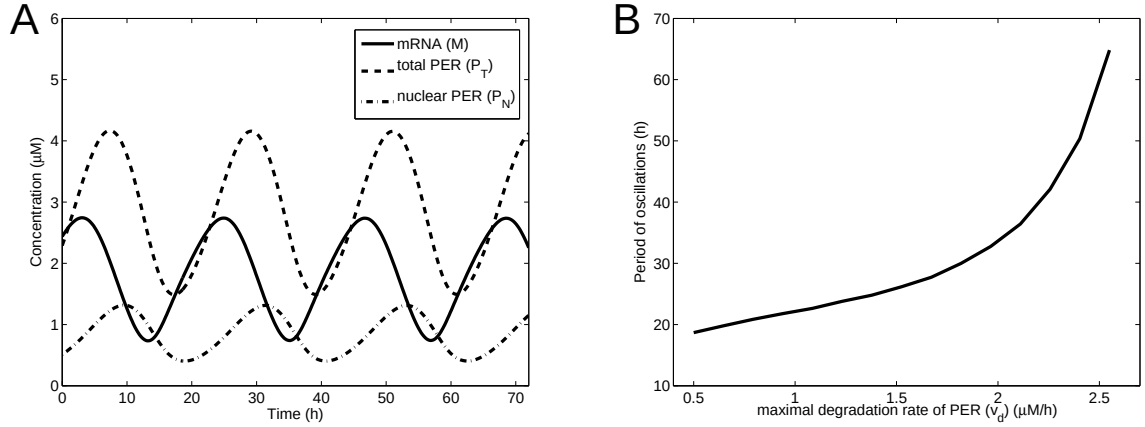

Figure 7.19: Behaviour of the Goldbeter circadian oscillator model. **A.** The simulated concentrations of mRNA (m), total PER protein ($p_T = p_0 + p_1 + p_2 + p_N$), and nuclear PER protein (p_N). The period of the oscillation is about 24 hours, with a lag of about 4 hours between the peak in mRNA and protein levels. **B.** This continuation diagram shows the effect of changes in the maximal PER degradation rate (v_d) on the oscillation period. Within the range over which oscillations occur, the period ranges from about 20 to more than 60 hours. Parameter values are $v_s = 0.76$ μM/h, $v_m = 0.65$ μM/h, $v_d = 0.95$ μM/h (Panel A) , $k_s = 0.38$ h^{-1}, $k_1 = 1.9$ h^{-1}, $k_2 = 1.3$ h^{-1}, $V_1 = 3.2$ μM/h, $V_2 = 1.58$ μM/h, $V_3 = 5$ μM/h, $V_4 = 2.5$ μM/h, $K_1 = K_2 = K_3 = K_4 = 1$ μM, $K_I = 1$ μM, $K_{m1} = 0.5$ μM, $K_d = 0.2$ μM, $n = 4$. Adapted from Figures 11.7 and 11.9 of (Goldbeter, 1996).

because Goldbeter chose parameter values to arrive at this behaviour. Nevertheless, the model represented a valuable hypothesis as to how circadian rhythms could be generated by the activity of the *per* gene.

Goldbeter used the model to explore possible mechanisms for the effects of the short- and long-period *per* mutations. To explore the hypothesis that these mutations affect the rate of PER degradation, he determined the effect of changes in the maximal PER degradation rate (v_d) on the oscillation period. His findings, reproduced in Figure 7.19B, show that as v_d varies (between 0.45 and 2.6 μM/hr), the period ranges between 20 and 62 hours (beyond this range the oscillations are lost). The mutant periods fall roughly into this range, indicating that alterations in the protein degradation rate could be the cause of the observed changes.

In the years since Goldbeter's model was published, additional experiments have led to a better understanding of the circadian clock in *Drosophila*. A model that incorporate more recent findings is explored in Problem 7.8.10.

7.3.3 Synthetic oscillatory gene networks

In this section we address two gene circuits that were engineered to display oscillatory behaviour.

A synthetic delay oscillator: the repressilator

In the year 2000, Michael Elowitz and Stanislas Leibler announced the construction of an oscillatory synthetic circuit (Elowitz and Leibler, 2000). Elowitz and Leibler called their device the *repressilator*, in homage to the theoretical oscillating chemical system known as the *Brusselator*

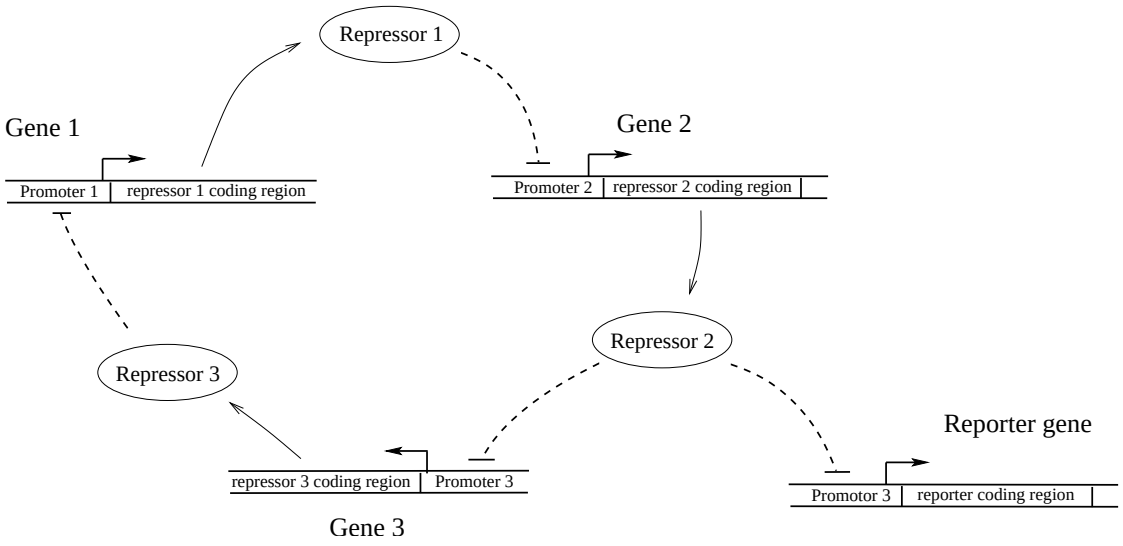

Figure 7.20: Repressilator gene network. Three genes each repress expression of the next around a loop. This network architecture can give rise to sustained oscillations—the protein levels rise and fall in succession. The reporter gene, GFP, is under the control of a separate copy of promoter 3.

(Exercise 4.3.1).

The repressilator design, like the Collins toggle switch, involves stringing together promoter-repressor pairs; in this case there are three genes in the loop (Figure 7.20). This three-repressor loop does not lend itself to steady-state behaviour. When any one protein dominates over the others, it leads to its own repression—the dominant protein de-represses its own repressor, which then becomes dominant. When this process continues around the loop, the result is sustained oscillations in the protein concentrations. This is a delay oscillator—each protein inhibits its own expression through the chain of three inhibitions.

Elowitz and Leibler constructed a simple model of the network as part of the design process. Because they needed to capture the network's time-varying behaviour, they included mRNA dynamics explicitly. Assuming that all three genes have identical characteristics, they arrived at the following model:

$$\frac{d}{dt}m_1(t) = \alpha_0 + \frac{\alpha}{1+[p_3(t)]^n} - m_1(t) \qquad \frac{d}{dt}p_1(t) = \beta m_1(t) - \beta p_1(t)$$
$$\frac{d}{dt}m_2(t) = \alpha_0 + \frac{\alpha}{1+[p_1(t)]^n} - m_2(t) \qquad \frac{d}{dt}p_2(t) = \beta m_2(t) - \beta p_2(t)$$
$$\frac{d}{dt}m_3(t) = \alpha_0 + \frac{\alpha}{1+[p_2(t)]^n} - m_3(t) \qquad \frac{d}{dt}p_3(t) = \beta m_3(t) - \beta p_3(t).$$

The six state-variables are the mRNA concentrations (m_1, m_2, m_3) and the protein concentrations (p_1, p_2, p_3). The parameter α_0 represents the rate of 'leaky' transcription from the fully repressed promoter, while $\alpha_0 + \alpha$ is the maximal expression rate (achieved in the absence of repression). The degree of cooperativity in repressor-DNA binding is characterized by the Hill coefficient n. Parameter β is the decay rate for the proteins. Additional parameters were eliminated by scaling of the time and concentration units.

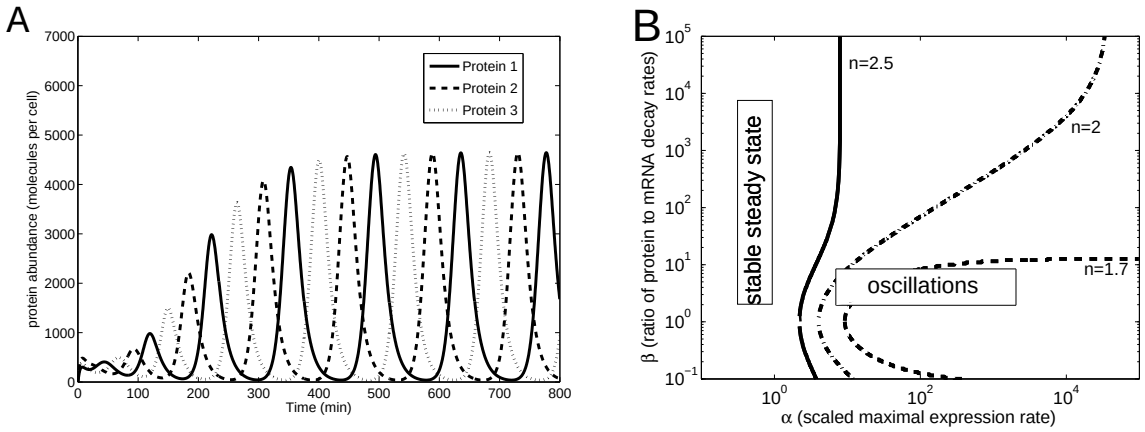

Figure 7.21: Behaviour of the repressilator model. **A.** Simulation of the model. The peaks in protein concentration are about 50 minutes apart, giving an overall period of about 150 minutes. Parameter values: $\alpha_0 = 0.03$ (molecules per cell $\cdot \min^{-1}$), $\alpha = 298.2$ (molecules per cell $\cdot \min^{-1}$), $\beta = 0.2$ ($\min^{-1}$), $n = 2$. The model outputs are scaled as follows: protein concentration = 40 $p_i(t)$ (corresponding to a half-saturating constant of 40 molecules per cell); time = t/0.3485 (corresponding to a mRNA half life of 2 minutes). **B.** A set of two-dimensional bifurcation plots showing the range of α and β values for which the model exhibits sustained oscillations. Oscillations are favored by β near one, and α and n large. Adapted from Figure 1 of (Elowitz and Leibler, 2000).

A simulation of the model is shown in Figure 7.21A. The symmetric nature of the model is apparent; all three protein profiles follow identical cycles. The parameters have been chosen so that the period is about 150 minutes.

Figure 7.21B shows a set of two-dimensional bifurcation plots demonstrating the system behaviour. As expected, oscillatory behaviour is favored by stronger cooperativity in the repression kinetics (i.e. increased nonlinearity n). Moreover, stronger expression (α) results in a more robust oscillator. The plot also shows that the value of β (the ratio of protein decay rate to mRNA decay rate) has a significant impact on the behaviour of the system. Oscillatory behaviour is easier to attain when this ratio is close to one. This finding is consistent with the need for a significant delay in the loop; if mRNA dynamics are very fast, they will not contribute to the overall delay. A similar analysis shows that low leakiness (α_0) favors oscillations (Problem 7.8.12).

Elowitz and Leibler made used model-based observations in their design process. Firstly, they only chose promoters that were known to be cooperatively repressed (high n values), and selected strong versions of those promoters (high α) with tight repression (low α_0). Secondly, to bring the protein decay rate closer to the (typically much faster) mRNA decay rate, they added a 'degradation tag' to the proteins in the network, reducing their half lives by as much as 15-fold.

Elowitz and Leibler constructed their circuit from the same promoter-repressor pairs that were employed in the Collin's toggle switch: *LacI* and *tetR* from *E. coli*, and *cI* from phage lambda. They were able to synchronize a population of *E. coli* cells hosting the network by exposing them to a pulse of IPTG (which inhibits *LacI*), and successfully demonstrated oscillations. The period of the oscillations (about 150 minutes) was considerably longer than the doubling time of the cells (about 30 minutes); the state of the oscillations was passed from mother to daughter cells after division.

Although the repressilator design resulted in oscillatory behaviour, the oscillations themselves

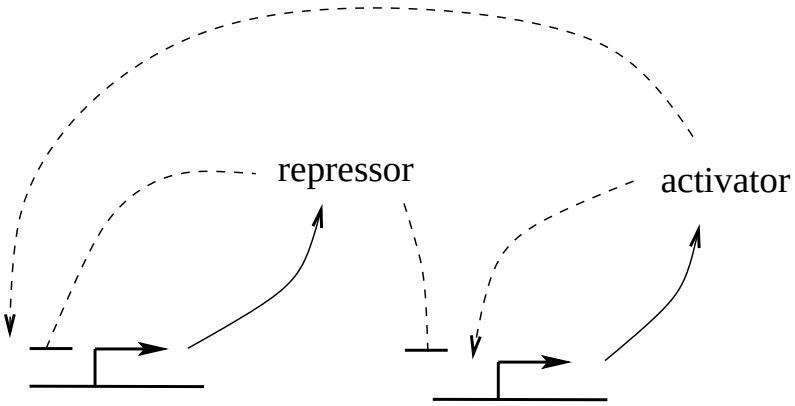

Figure 7.22: Genetic relaxation oscillator network. Identical promoters drive expression of the activator and the repressor. The interplay between positive and negative feedback can lead to sustained oscillations (characterized by bursts of expression followed by periods of repression).

were irregular; the cells exhibited significant variation in amplitude, period, and phase. We next consider an engineered gene network that acts as a relaxation oscillator, and consequently exhibits less variability in its periodic behaviour.

A synthetic relaxation oscillator

Relaxation oscillators typically exhibit more robust behaviour than delay oscillators. To implement an oscillator with robust periodic behaviour, Jesse Stricker and colleagues designed and constructed a relaxation oscillator involving two genes: an activator and a repressor (Stricker *et al.*, 2008). They employed a promoter that is regulated by both of these transcription factors. The network, sketched in Figure 7.22 incorporates two identical copies of this promoter, separately driving expression of the repressor and activator.

Stricker and co-workers used both deterministic (differential equation-based) and stochastic models in designing the system. A preliminary model, published earlier by Jeff Hasty and colleagues (Hasty *et al.*, 2002), takes the form (details in Exercise 7.3.2):

$$\begin{aligned} \frac{d}{dt}x(t) &= \frac{1+x(t)^2+\alpha\sigma x(t)^4}{(1+x(t)^2+\sigma x(t)^4)(1+y(t)^4)} - \gamma_x x(t) \\ \frac{d}{dt}y(t) &= a_y\frac{1+x(t)^2+\alpha\sigma x(t)^4}{(1+x(t)^2+\sigma x(t)^4)(1+y(t)^4)} - \gamma_y y(t), \end{aligned} \tag{7.23}$$

where x and y are the concentrations of the activator, X, and repressor, Y.

The model's behaviour is shown in Figure 7.23. Panel A shows the persistent oscillations exhibited by the system: the activator X and repressor Y are expressed together. Their concentrations grow until the repressor cuts off expression. Concentrations then fall until repression is relieved and the next burst of expression begins. The oscillations exhibit sharp peaks—particularly for X. This relaxation behaviour is displayed in panel B, which shows the limit cycle trajectory in the phase plane, along with the nullclines. The horizontal motions are rapid—the trajectory spends most of its time following the x nullcline at low X concentration (in the repressed state). Because this behaviour is dependent on positive feedback (autoactivation), it is relatively robust to parameter variation.

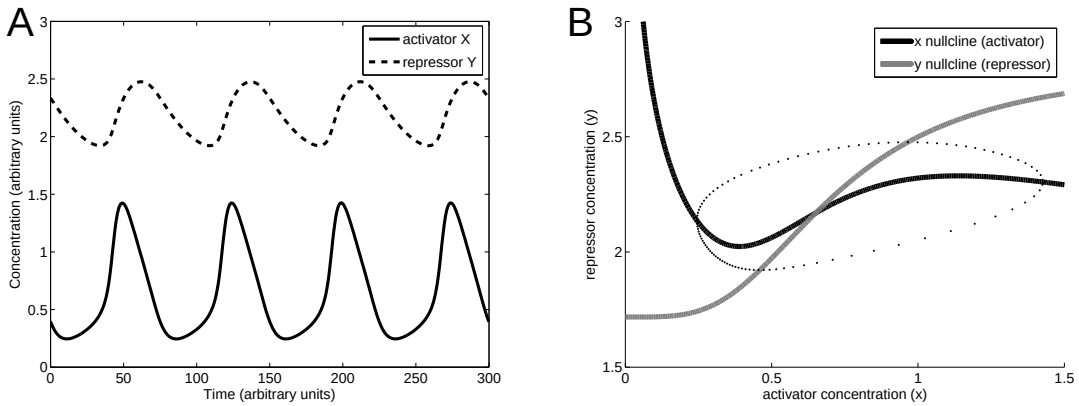

Figure 7.23: The Hasty relaxation oscillator model. **A.** This simulation of the system's periodic behaviour shows concentrations of the activator X and the repressor Y rising and falling in near unison. Sharp peaks in the concentration of X indicate that this is a relaxation oscillator. **B.** This phase portrait shows the nullclines along with the limit cycle trajectory. The points are plotted along a single period, and are spaced equally in time. The trajectory transits rapidly around the cycle, but moves slowly in the repressed (low $[X]$) condition. Parameter values: $\alpha = 11$, $\sigma = 2$, $\gamma_x = 0.2$ (time^{-1}), $\gamma_y = 0.06$ (time^{-1}), $a_y = 0.2$ (concentration $\cdot$ time^{-1}). Units are arbitrary.

Stricker and colleagues successfully implemented their relaxation oscillator design using *LacI* and an activator called *araC*. They used a microfluidic platform to observe individual cells and saw steady, persistent oscillations over several periods. They also found that they could tune the period of the oscillator through partial inactivation of *LacI*.

Both the repressilator and the Stricker oscillator successfully generate single-cell oscillations. However, when implemented in a population, deviations in phase between individual cells tend to cancel out the population-averaged oscillatory signal. In the next section, we will address gene networks that involve cell-to-cell communication, providing a mechanism to synchronize populations of cellular oscillators.

Exercise 7.3.2 Derive the expression rates in the model (7.23). The repressor is assumed to bind with strong cooperativity at four sites. The activator X binds with strong cooperativity at each of two distinct pairs of sites. Assume that the activator and repressor binding events are independent of one another. Expression, which is completely blocked by Y binding, occurs at a basal rate unless all four X sites are occupied. Rescale the concentration units so that the half-saturating constants for DNA-binding of the first two X molecules and of the four Y molecules are both one. Rescale the time units so that the basal expression rate for X is one. The parameter α is the degree to which the expression rate increases when the second activator pair is bound, while σ is the ratio of the binding affinities at the two pairs of activator sites. □

7.4 Cell-to-Cell Communication

Gene networks operating in individual cells can communicate their states to one another by producing a signalling molecule that can pass from one cell to another—providing an *intercellular* connection. In this section we will consider two examples of cell-to-cell communication in engineered gene

circuits: the passing of signals between two distinct populations of cells, and the synchronization of an identical population of cellular oscillators. These circuits are based on bacterial quorum sensing mechanisms, which we introduce next.

7.4.1 Bacterial quorum sensing

Cell-to-cell signalling is crucial to the development and proper functioning of all multi-cellular organisms. For bacterial cells, the need for intercellular communication is less critical, but these cells nevertheless use a multitude of such signals to monitor their environment. One well-studied example of bacterial cell-to-cell communication is *quorum sensing*—a mechanism by which bacterial cells measure the local density of their population. Bacteria use this information to enhance their survival. (One example is the formation of bacterial *biofilms* when cells reach sufficiently high density. Biofilms are protective layers of proteins and polysaccharides that are secreted from the cells.)

To implement quorum sensing, each cell communicates its presence by secreting a signalling molecule, called an *autoinducer*, into the local environment. These molecules are taken up by neighboring cells, and activate gene expression—including genes that lead to production of the autoinducer itself. This positive feedback results in a switch-like response (as in Section 7.2) to changes in the local population density.

Quorum sensing was first identified in the bioluminescent marine bacterium *Vibrio fischeri*. These cells live freely in seawater, but can also take up residence in specialized light organs of some squid and fish. In seawater, *V. fischeri* are usually found at low densities (less that 100 cells per mL), and produce only a small amount of light (less than 0.8 photons/cell/second). In light organs, the cells reach densities of more than 10^{10} cells per mL and increase their per-cell light output more than a thousandfold.

The quorum sensing mechanism that controls light output makes use of a signalling molecule called acyl-homoserine lactone (AHL). This autoinducer is a small non-polar molecule that diffuses freely across the cell membrane. As shown in Figure 7.24, production of AHL is catalysed by an enzyme called LuxI. Intracellular AHL (whether self-generated or imported from the environment) binds to the constitutively expressed protein LuxR. When complexed with AHL, LuxR binds to an operator called the lux box, enhancing production of LuxI. The light-producing protein—called *luciferase*—is coded in an operon with LuxI (along with enzymes needed to fuel its activity). Thus increased LuxI expression leads to increased light production.

LuxI and AHL form a positive feedback loop: expression of LuxI enhances AHL production, and so enhances LuxI expression. This system responds to external AHL with a steep switch-like response in LuxI expression—and in light production.

Sally James and her colleagues published a model of the *V. fischeri* quorum sensing mechanism in the year 2000 (James *et al.*, 2000). A simplified version of their model is the following:

$$\begin{aligned}
\frac{d}{dt}A(t) &= k_0 I(t) - r(A(t) - A_{\text{ext}}(t)) - 2k_1(A(t))^2(R_T - 2R^*(t))^2 + 2k_2 R^*(t) \\
\frac{d}{dt}R^*(t) &= k_1(A(t))^2(R_T - 2R^*(t))^2 - k_2 R^*(t) \\
\frac{d}{dt}I(t) &= a_0 + \frac{aR^*}{K_M + R^*(t)} - bI(t) \\
\frac{d}{dt}A_{\text{ext}}(t) &= pr(A(t) - A_{\text{ext}}(t)) - dA_{\text{ext}}(t).
\end{aligned} \tag{7.24}$$

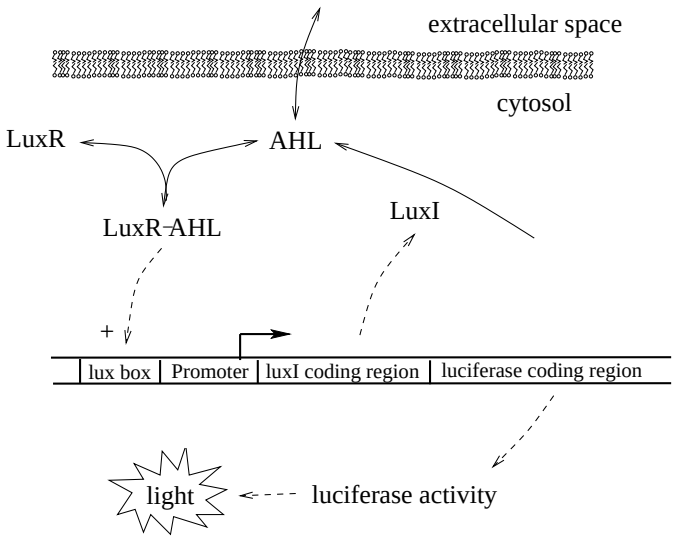

Figure 7.24: Quorum sensing in *Vibrio fischeri*. The autoinducer AHL diffuses freely across the cell membrane. Its production is catalysed by LuxI. AHL binds to the regulator LuxR, causing it to enhance transcription of LuxI and of the luciferase genes, whose protein products generate light. Adapted from Figure 18 of (Weiss *et al.*, 2003).

The state variable A is the (averaged) intracellular concentration of free autoinducer (AHL), R^* is the concentration of active LuxR-AHL complexes (each composed of a LuxR homodimer bound to two molecules of AHL), I is the concentration of LuxI, and A_{ext} is the extracellular concentration of autoinducer. The rate of diffusion of AHL across each cell membrane is given by $r(A(t) - A_{\text{ext}}(t))$. This results in diffusion into the extracellular environment at rate $pr(A(t) - A_{\text{out}}(t))$, where the parameter p accounts for the population density. The rate at which extracellular AHL diffuses away from the population (i.e. out of the system) is characterized by d. Parameter R_T is the total concentration of LuxR monomers (presumed fixed).

The solid curve in Figure 7.25 shows the model's response (the LuxI concentration, which is proportional to the rate of light production) as a function of population density p. At low cell density, AHL diffuses out of the system and there is no response in LuxI expression. As the density rises above a threshold value, the positive feedback causes a run-away increase in intracellular AHL and LuxI levels, culminating in maximal expression of LuxI (and luciferase). The figure also shows a hypothetical graded response in which the positive feedback is absent (dashed curve), corresponding to a modified system in which AHL production is not LuxI-dependent.

Exercise 7.4.1 In the model (7.24), the LuxR concentration is held fixed (corresponding to constitutive expression and decay). In fact, LuxR expression is activated by AHL. Considering the dose-response curve in Figure 7.25, would you expect this additional feedback on LuxR expression to make the response steeper or more shallow? □

7.4.2 Engineered cell-to-cell communication

In the year 2000, Ron Weiss and Tom Knight published a paper describing two engineered strains of *E. coli* that demonstrate cell-to-cell communication (Weiss and Knight, 2001). Signals could be passed from cells of the first strain, called 'sender cells,' to cells of the second strain, called 'receiver

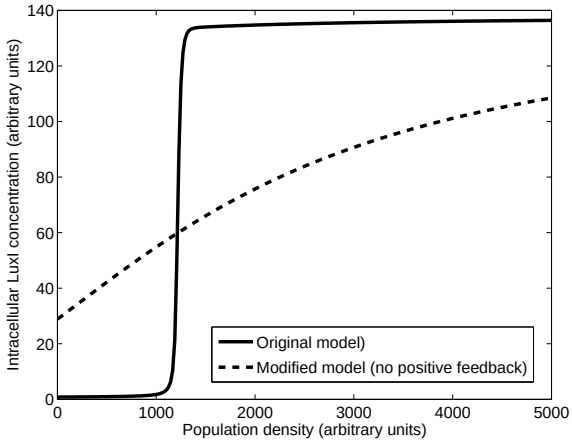

Figure 7.25: Dose-response curves for the model of quorum sensing in *V. fischeri* (solid curve). As the population density rises, switch-like activation of the quorum sensing mechanism occurs at a threshold value. This sigmoidal response is caused by the positive feedback loop involving LuxI and AHL. The dashed curve shows the dose-response of a model variant in which the AHL production rate is fixed. In this case the LuxI levels rise in a graded manner. Parameter values: $k_0 = 8 \times 10^{-4}$ (time^{-1}), $r = 0.6$ (time^{-1}), $R_T = 0.5$ (concentration), $k_1 = 0.5$ (time$^{-1} \cdot$ concentration^{-3}), $k_2 = 0.02$ (time$^{-1} \cdot$ concentration^{-3}), $a = 10$ (concentration $\cdot$ time^{-1}) $b = 0.07$ (time^{-1}), $K_M = 0.01$ (concentration), and $d = 1000$ (time^{-1}). In the modified model, the term $k_0 I(t)$ is replaced with $15k_0$, corresponding to a mid-range LuxI concentration. Units are arbitrary.

cells.' They used the *Vibrio* autoinducer AHL as the inter-cellular signalling molecule. The two strains were created by splitting the *V. fischeri* quorum sensing network into separate sending and receiving modules: the sender cells host the *LuxI* gene, and hence can produce AHL; the receiver cells contain the *LuxR* gene and so respond to the presence of AHL (Figure 7.26).

Weiss and Knight engineered the sender population so that AHL production could be controlled experimentally: they placed the *LuxI* gene under the control of a promoter that is repressed by TetR, and incorporated a constitutively expressed *tetR* gene in the cells. The addition of aTc (which inhibits TetR) induces expression of LuxI, and hence generates AHL. Activity of the receiver cells is monitored via a *gfp* gene controlled by the LuxR-sensitive promoter. (As in the original network, LuxR expression was constitutive).

Exercise 7.4.2 Modify the model of quorum-sensing cells in (7.24) to arrive at a model of Weiss's receiver cell population as in Figure 7.26. □

The Weiss group followed-up on this design with elaborations of the receiver cell network that result in spatio-temporal pattern formation. We next consider two of their constructions.

Pulse generation

As we saw in Section 6.3.1, the bacterial chemotaxis signalling network generates a transient response to a persistent stimulus. This behaviour, described as *pulse generation*, can be produced by a simple gene regulatory network called a *feedforward loop*, in which a gene's activity is activated on a fast time-scale and inhibited on a slower time-scale (Problem 7.8.16).

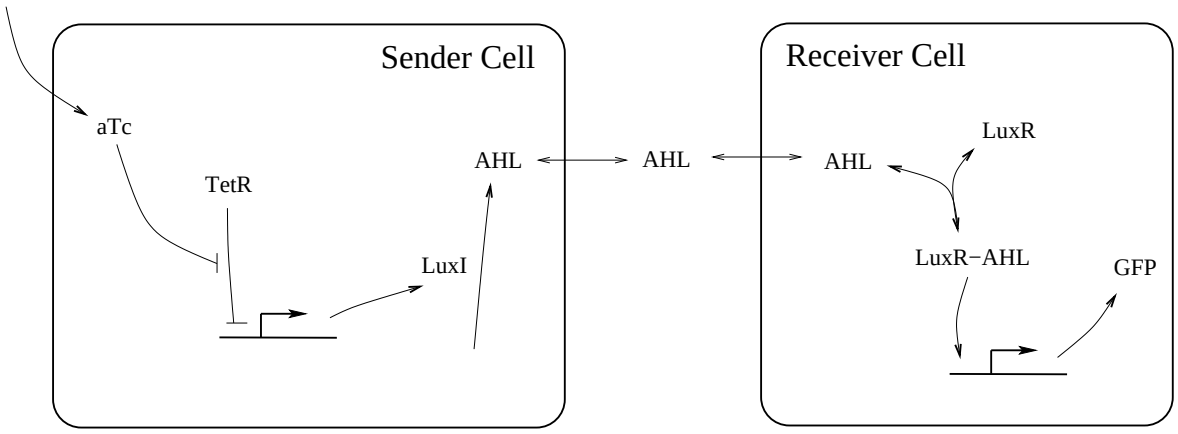

Figure 7.26: Engineered network for cell-to-cell communication. Addition of aTc to the sender cells induces expression of LuxI, and hence leads to production of AHL. This chemical signal diffuses to the receiver cells, where it activates LuxR, leading to GFP expression. Adapted from Figure 19 of (Weiss *et al.*, 2003).

Subhayu Basu and colleagues adapted Weiss's cell-to-cell communication system by engineering a new receiver population that responds to an AHL stimulus with a transient pulse of GFP expression (Basu *et al.*, 2004). The receiver cell network, shown in Figure 7.27, incorporates the *cI* gene from phage lambda into the original receiver cell design. In this network, both *cI* and *GFP* are activated by the LuxR-AHL complex, but GFP expression is also inhibited by cI. Exposure to AHL causes an initial increase in GFP and cI levels, but once cI levels are sufficiently high, GFP expression is repressed.

Basu and colleagues developed a model to explore the system's behaviour. A simplified version of the model for receiver cell activity is:

$$\begin{aligned}
\frac{d}{dt}R^*(t) &= k_1 A^2 (R_T - 2R^*(t))^2 - k_2 R^*(t) \\
\frac{d}{dt}C(t) &= \frac{a_C (R^*(t)/K_R)}{1 + (R^*(t)/K_R)} - b_C C(t) \\
\frac{d}{dt}G(t) &= \frac{a_G (R^*(t)/K_R)}{1 + (R^*(t)/K_R) + (C(t)/K_C)^2 + (R^*(t)/K_R)(C(t)/K_C)^2} - b_G G(t)
\end{aligned} \tag{7.25}$$

where R^*, C, and G are the concentrations of the AHL-LuxR complex, cI, and GFP, respectively. The AHL concentration A is taken as an input signal. Figure 7.28 shows the model behaviour. AHL is introduced at time zero, after which both cI and GFP levels rise. Once cI levels are sufficiently high, the GFP abundance drops.

Basu and co-workers used their model as an aid to design. They selected destabilized versions of cI and GFP, a specific ribosome binding site for cI, and tuned the sensitivity of the GFP promoter to cI by introducing point mutations. Experiments confirmed the network's pulse-generating behaviour.

Exercise 7.4.3 Verify that the GFP expression rate in equation (7.25) corresponds to the case that cI binds with strong cooperativity at two sites, LuxR-AHL binds at a single site, the binding events are independent, and expression occurs only when LuxR-AHL is bound and cI is not bound. □

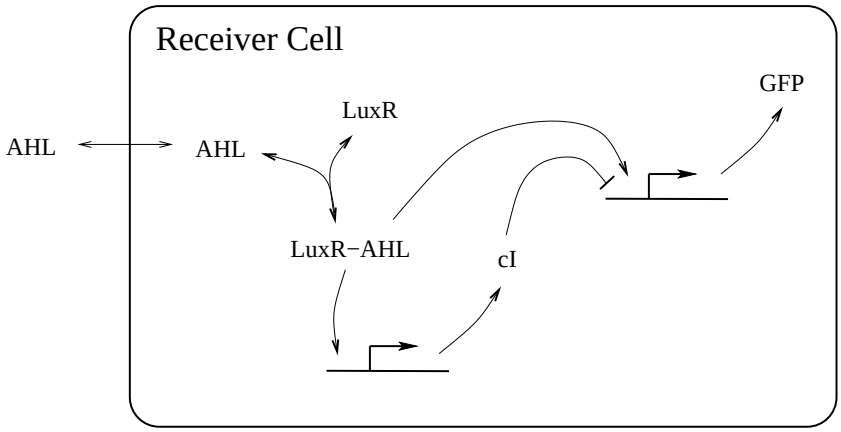

Figure 7.27: Engineered pulse generator. In this receiver cell, LuxR (constitutively expressed) binds AHL taken up from the environment. The LuxR-AHL complex activates expression of both cI and GFP. Production of GFP is repressed by cI, so only a transient pulse of fluorescence is produced in response to an AHL signal. Adapted from Figure 1 of (Basu *et al.*, 2004).

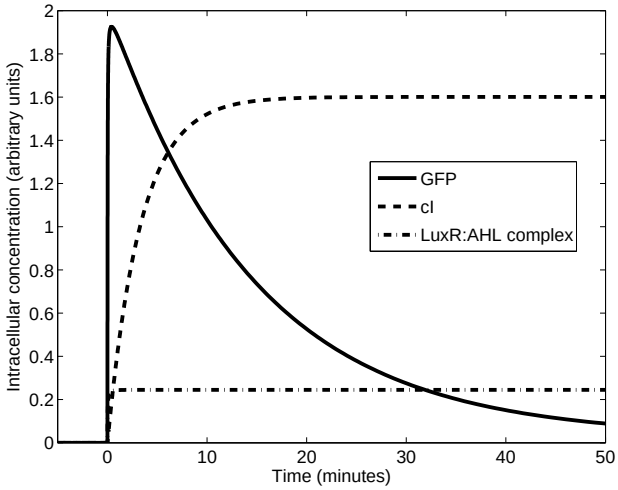

Figure 7.28: Pulse generation. At time zero the AHL concentration rises from 0 to 10, causing a sudden increase in the LuxR-AHL abundance. This leads to a rapid rise in GFP and a slower rise in cI. As the cI concentration increases, repression of GFP leads to a drop in GFP abundance. Parameter values: $k_1 = 0.5$ ($\text{min}^{-1} \cdot \text{concentration}^{-3}$), $k_2 = 0.02$ ($\text{min}^{-1} \cdot \text{concentration}^{-3}$), $R_T = 0.5$ (concentration), $a_C = 0.5$ (concentration $\cdot \text{min}^{-1}$) $K_R = 0.02$ (concentration), $b_C = 0.07$ (min^{-1}), $a_G = 80$ (concentration $\cdot \text{min}^{-1}$), $K_C = 0.008$ (concentration), $b_G = 0.07$ (min^{-1}). Concentration units are arbitrary.

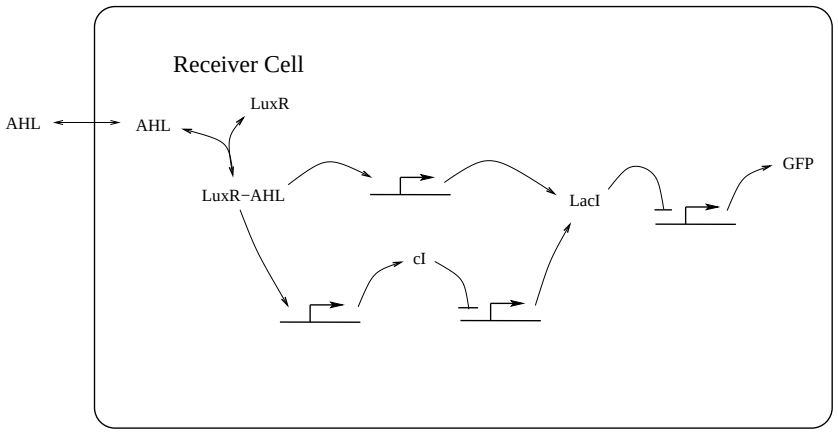

Figure 7.29: Engineered band detector. The AHL input binds LuxR, leading to expression of LacI and cI. LacI is also expressed from a separate cI-repressible promoter. GFP expression is repressed by LacI. At high and low levels of AHL, GFP expression is repressed. At intermediate AHL levels, a sufficiently low LacI level allows for GFP expression. Adapted from Figure 1 of (Basu *et al.*, 2005).

Spatial patterning

In addition to temporal patterns like pulses, cell-to-cell communication can also produce steady spatial patterns. In another project, Basu and colleagues developed an AHL-receiver strain that acts as a *band detector* (Basu *et al.*, 2005). These cells were engineered to respond only to a mid-range of inducer activity—no response is shown at low or high AHL concentrations. A population of these receiver cells surrounding a group of AHL-sender cells will then fluoresce in a 'bullseye' pattern.

The gene network in the band detector cells is sketched in Figure 7.29. The autoinducer AHL binds to LuxR, leading to expression of cI and the *lac* repressor, LacI. LacI is also expressed from a separate promoter that is repressed by cI. Finally, GFP expression is inhibited by LacI. The system's behaviour can be understood in terms of the dose-response curves shown in Figure 7.30. At high levels of AHL, the LuxR-induced levels of LacI are high, and GFP expression is repressed. At low AHL levels, cI is not expressed. Consequently, LacI is generated from the cI-repressible promoter and, again, GFP expression is repressed. At intermediate levels of AHL, moderate expression of cI and LacI occur. The system was tuned so that repression of LacI by cI is highly effective, while repression of GFP by LacI is not. Thus at these mid-range input levels, expression of LacI is sufficiently low that significant GFP expression occurs.

The curves shown in Figure 7.30 were generated from the following simple model of the band-detector network, which is a variant of the model developed by Basu and colleagues.

$$\begin{aligned}
\frac{d}{dt}R^*(t) &= k_1 A^2 (R_T - 2R^*(t))^2 - k_2 R^*(t) \\
\frac{d}{dt}L(t) &= \frac{a_{L1}}{1 + (C(t)/K_C)^2} + \frac{a_{L2} R^*(t)}{K_R + R^*(t)} - b_L L(t) \\
\frac{d}{dt}C(t) &= \frac{a_C R^*(t)}{K_R + R^*(t)} - b_C C(t) \\
\frac{d}{dt}G(t) &= \frac{a_G}{1 + (L(t)/K_L)^2} - b_G G(t)
\end{aligned} \tag{7.26}$$

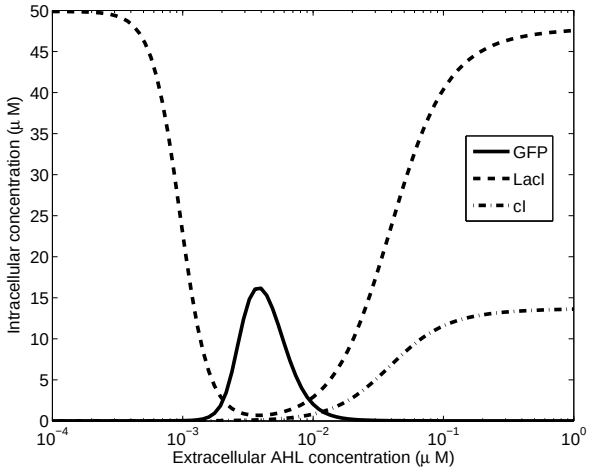

Figure 7.30: Dose-response curve for the band-detector circuit. The extracellular AHL concentration increases from left to right, so distance from the sender population increases from right to left. At high AHL levels there is strong expression of LacI from the LuxR-induced promoter. At low AHL levels, there is strong expression of LacI from the cI-repressible promoter. In the intermediate range, LacI levels are sufficiently low to allow significant GFP expression. Parameter values: $k_1 = 0.5$ min^{-1} μM^{-3}, $k_2 = 0.02$ min^{-1} μM^{-3}, $R_T = 0.5$ μM, $a_{L1} = 1$ μM min^{-1} $K_C = 0.008$ μM, $a_{L2} = 1$ μM min^{-1}, $K_R = 0.01$ μM, $b_L = 0.02$ min^{-1}, $a_C = 1$ μM min^{-1}, $b_C = 0.07$ min^{-1}, $a_G = 2$ μM min^{-1}, $b_G = 0.07$ min^{-1}, $K_L = 0.8$ μM. Adapted from Figure 26 of (Weiss *et al.*, 2003).

The state variables R^*, L, C, and G are the concentrations of the AHL-LuxR complex, LuxI, cI, and GFP, respectively. The AHL concentration A is taken as an input signal.

7.4.3 Synchronization of oscillating cells

Cell-to-cell communication allows intracellular oscillations to be synchronized across a population. This occurs in the circadian rhythm generators in animals. The engineered oscillatory networks discussed in Section 7.3.3 can generate population-wide oscillations when cells are able to communicate their states to one another.

Synchronization behaviour can be illustrated by a simple extension of the relaxation oscillator model of Section 7.3.3, as follows. Consider a pair of identical cells each hosting a relaxation oscillator. Suppose further that the activation signal X can diffuse across the cell membranes and so can be shared between the two cells. Using a subscript $i = 1, 2$ to indicate concentrations in each cell, we can model the pair of networks as:

$$\begin{aligned}
\frac{d}{dt}x_1(t) &= \frac{1 + x_1(t)^2 + \alpha\sigma x_1(t)^4}{(1 + x_1(t)^2 + \sigma x_1(t)^4)(1 + y_1(t)^4)} - \gamma_x x_1(t) + D(x_2 - x_1) \\
\frac{d}{dt}y_1(t) &= a_y \frac{1 + x_1(t)^2 + \alpha\sigma x_1(t)^4}{(1 + x_1(t)^2 + \sigma x_1(t)^4)(1 + y_1(t)^4)} - \gamma_y y_1(t), \\
\frac{d}{dt}x_2(t) &= \frac{1 + x_2(t)^2 + \alpha\sigma x_2(t)^4}{(1 + x_2(t)^2 + \sigma x_2(t)^4)(1 + y_2(t)^4)} - \gamma_x x_2(t) + D(x_1 - x_2) \\
\frac{d}{dt}y_2(t) &= a_y \frac{1 + x_2(t)^2 + \alpha\sigma x_2(t)^4}{(1 + x_2(t)^2 + \sigma x_2(t)^4)(1 + y_2(t)^4)} - \gamma_y y_2(t)
\end{aligned}$$

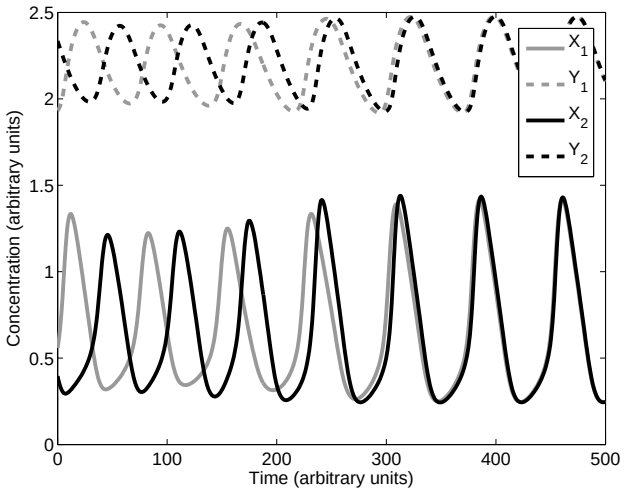

Figure 7.31: Synchronized relaxation oscillators. The cells each contain a relaxation oscillator. Initially, they are oscillating out of phase. The cells communicate their phase to one another through the shared activator; over time, this bring the cells into synchrony. Parameter values: $\alpha = 11$, $\sigma = 2$, $\gamma_x = 0.2$ (time^{-1}), $\gamma_y = 0.012$ (time^{-1}), $a_y = 0.2$ (concentration $\cdot$ time^{-1}), $D = 0.015$ (time^{-1}).

where D characterizes the rate at which activator X diffuses between the two cells. The behaviour of this simple model is illustrated in Figure 7.31, which shows the two cells beginning their oscillations out of phase, and then being drawn into synchrony by the shared activator.

The synchronization strategy employed in this model cannot be easily applied to the relaxation oscillator design of Stricker and colleagues, since the activator (araC) is a transcription factor protein (and so will not cross the cell membrane without a dedicated transporter). In 2010, Tal Danino and colleagues successfully demonstrated synchronization of intracellular relaxation oscillators; they employed a design in which AHL acts as the inter-cellular signal (Danino *et al.*, 2010). A synchronization scheme for the repressilator is addressed in Problem 7.8.19.

7.5 Computation by Gene Regulatory Networks

The initial discovery of gene regulatory networks prompted an analogy to the human-made technology of electrical circuits, and thus lead to the term 'genetic circuit.' This analogy can be made explicit by treating promoter/transcription-factor interactions (the building blocks of gene networks) as *logic gates* (the building blocks of computational electrical circuits). These ideas were reviewed in (Weiss *et al.*, 2003).

7.5.1 Promoters as logic gates

In digital electronics, a signal (e.g. voltage), is either considered HIGH (present) or LOW (absent), depending on whether a threshold has been passed. The same discretization process can be applied to the continuously varying concentrations of transcription factors in a gene network, as illustrated in Figure 7.32. This abstraction results in a binary description of gene activity: at a give time-point, each gene is either 'on' (expressing above threshold) or 'off' (expressing below threshold). Dynamic

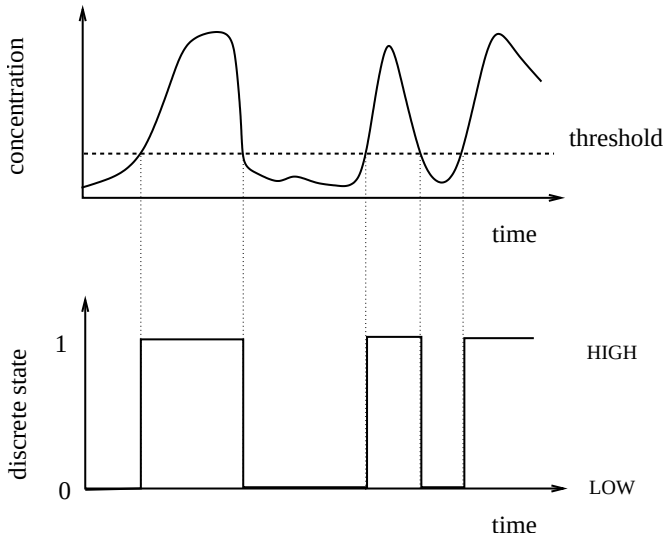

Figure 7.32: Discretization of gene activity. When the concentration of a gene's protein product is above a threshold, the gene is considered to be 'on,' and the protein concentration is assigned a value of 1 (HIGH). When the concentration drops below threshold, the gene is 'off,' and the protein concentration is assigned a value of 0 (LOW).

models that describe two-state (on/off) behaviours are called *Boolean* models. (Boolean models are often used to describe gene regulatory networks, and are particularly useful for addressing large networks. A review of this and other modeling approaches can be found in (De Jong *et al.*, 2002).)

Using the Boolean framework, all signals take either the value 1 (HIGH) or 0 (LOW). Applying this notion to the concentration of a transcription factor provides, as an example, an explicit comparison between repression of expression and a digital *inverter* (Figure 7.33). An inverter is a device that inverts a binary signal—a HIGH input yields a LOW output, while a LOW input yields a HIGH output. Figure 7.33 also includes the *truth table* for the inverter, which summarizes its input-output behaviour. The inverter is an example of a *logic gate*—a device that responds to a set of Boolean input variables (each equal to 0 or 1) and returns a Boolean output. The inverter is referred to as a NOT gate.

Promoters that are regulated by multiple transcription factors can be represented by multi-input logic gates. Figure 7.34 illustrates two promoters that are each regulated by two distinct activators. In Panel A, the binding of *either* promoter is sufficient to drive expression, so the promoter acts as an OR gate. Panel B shows the case in which binding of *both* activators is necessary to drive expression; this implements AND gate logic. Promoters that are regulated by two distinct repressors can be classified in a similar way: if either repressor suffices to inhibit repression, the promoter acts as a NOR (i.e. NOT-OR) gate, while if repression only occurs if both repressors are bound, then a NAND (i.e. NOT-AND) logic applies.

Exercise 7.5.1 Construct truth tables for the NOR and NAND logic gates. Verify that they can be constructed by connecting NOT gates downstream of the OR and AND gates, respectively. □

Exercise 7.5.2 For promoters that are regulated by both an activator and a repressor, different cases arise depending on the priority of the inputs. The corresponding digital elements, called IMPLIES gates, can be built by combining an inverter and one of the two-input gates already

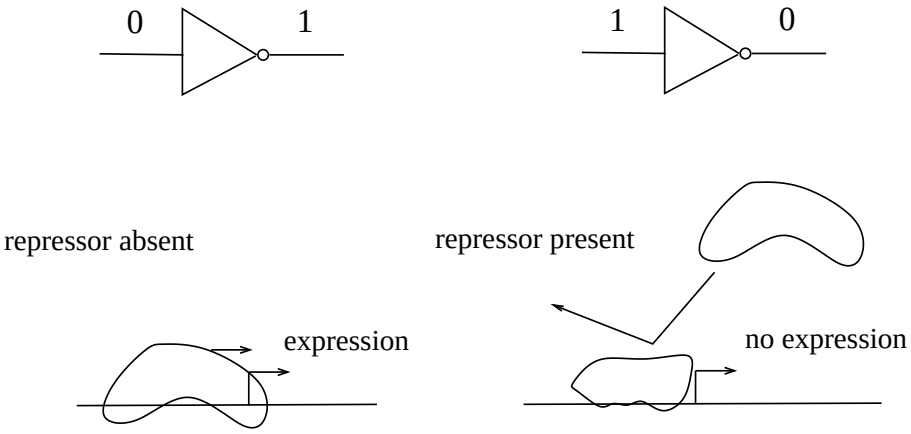

Inverter (NOT gate)	
input	output
0	1
1	0

Figure 7.33: Repression of gene expression as an inverter. When the repressor input is absent (LOW; value 0), expression proceeds (the output is HIGH; value 1). Alternatively, when repressor is present (HIGH; value 1), expression does not occur (LOW; value 0). The promoter thus "inverts" the input signal (repressor concentration) to determine the output signal (expression rate, and thus concentration of protein product). This same behaviour is exhibited by a digital inverter, or NOT gate, characterized by the truth table shown on the right. Adapted from Figure 1 of (Weiss *et al.*, 2003).

considered (e.g. AND or OR). Referring to Section 7.2.1, determine the truth table that describes *lac* operon expression, where the two inputs are the *lac* repressor and allolactose. Verify that the resulting IMPLIES logic can be constructed by an appropriate combination of a NOT gate and an OR gate.

□

7.5.2 Digital representations of gene circuits

In digital electronics, elementary logic gates provide a foundation for the construction of complex computational devices. The same notions can be applied to the design of gene regulatory networks.

Consider, as an example, the repressilator circuit described in Section 7.3.3. Because each promoter is repressed by the gene that precedes it in the loop, this device can be described as a set of three NOT gates strung together in a loop, as shown in Figure 7.35. This type of network is known in digital electronics as a ring oscillator, and is commonly used to generate periodic behaviour.

The dynamic behaviour of a ring oscillator can be simulated by supposing that all three of the elements update simultaneously at discrete time-steps. Although this rigid lock-step does not reflect the smooth variation of genetic processes, digital analogies often provide a useful abstraction of gene network behaviour.

The analogy between promoter activity and digital logic gates provides a useful framework for the design and analysis of gene regulatory networks. However, logic gates cannot provide a comprehensive description of gene circuit behaviour. In addition to the abstraction introduced by discretization, the Boolean framework is not well-suited to represent genes that exhibit multiple expression rates. This fact was vividly demonstrated in an experiment by Yaki Setty and colleagues, who mapped the response of the *lac* promoter to two inducers and found the resulting response to be a hybrid of OR and AND behaviours (Setty *et al.*, 2003).

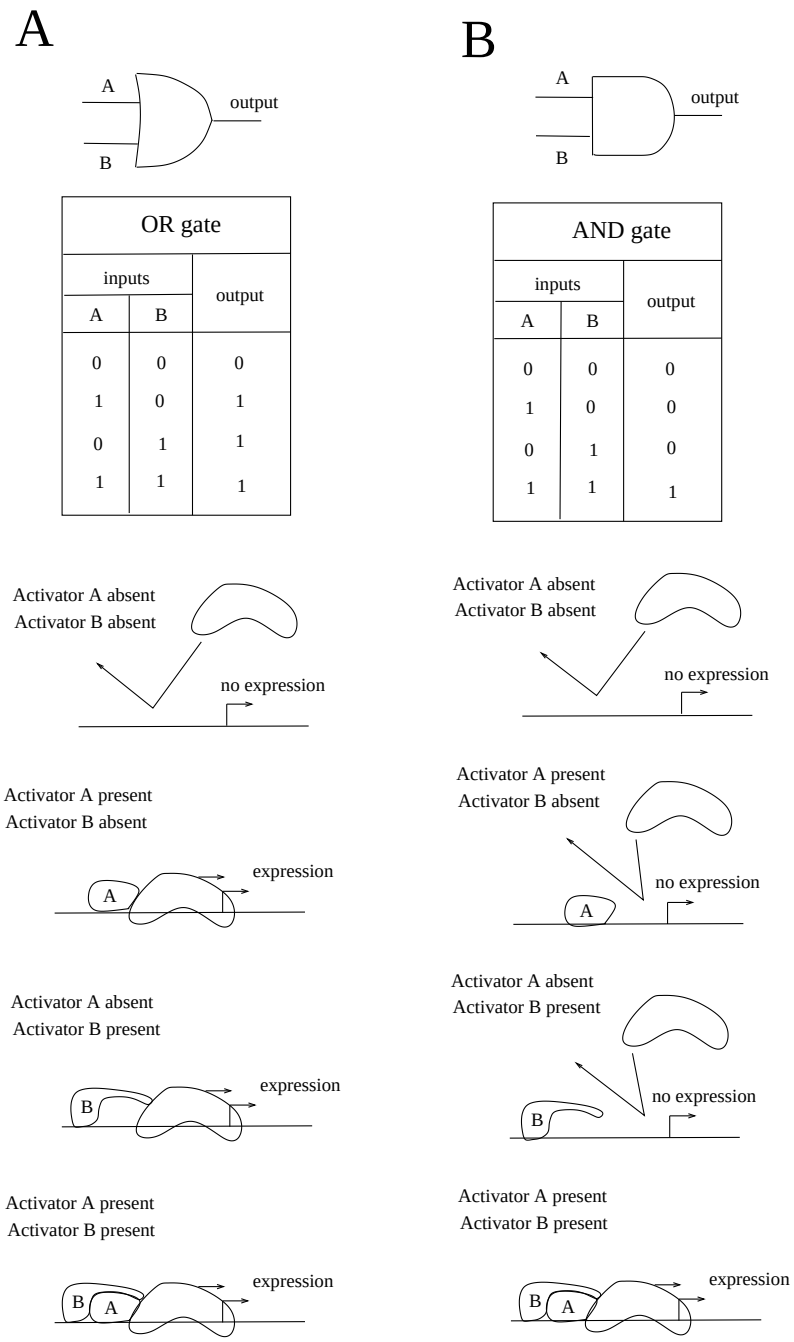

Figure 7.34: Dual-activator promoters as digital logic gates **A.** If either transcription factor suffices to activate expression, the promoter exhibits an OR gate logic. **B.** If expression only occurs when both activators are present, the promoter is represented by an AND gate.

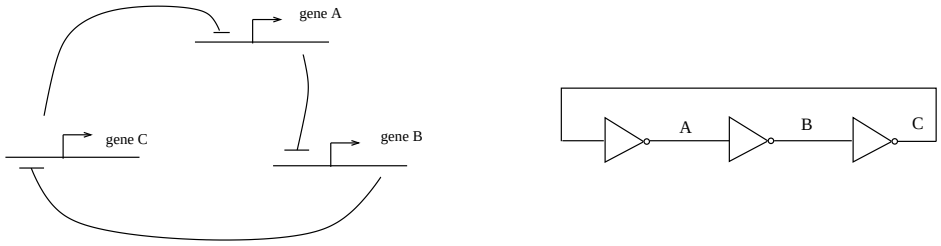

	t=0	t=1	t=2	t=3	t=4	t=5	t=6	t=7	
A	0	1	1	1	0	0	0	1	
B	1	1	0	0	0	1	1	1	• • •
C	0	0	0	1	1	1	0	0	

Figure 7.35: Digital representation of the repressilator circuit. A loop of three NOT gates forms a ring oscillator. In the simulation shown, the signals are simultaneously updated at each time-step. At time $t = 0$ the three signals have values A=0, B=1, C=0. At the next time-step ($t = 1$), the value of A is replaced with the new value NOT(C)=1, while B is updated as NOT(A)=1, and C takes the value NOT(B)=0. (Because the updates occur simultaneously, the values of the signals at the previous time-step are used in the update computation.) The behaviour is periodic: the state at the sixth time-step is identical to the initial state ($t = 0$). Adapted from Figure 9 of (Weiss *et al.*, 2003).

Another crucial distinction between electrical circuits and gene circuits is the manner in which the specificity of the interconnections is achieved. In an electrical circuit, all connections employ the same signal (flow of charge). Undesired connections (short-circuits) are avoided by maintaining spatial separation between signals. In contrast, the signal carriers for gene circuits (transcription factors) are mixed together in a single compartment. Unwanted interconnections are avoided through chemical specificity (of the protein-DNA binding surfaces). This reliance on chemical specificity allows complex networks to operate on tiny spatial scales, but it means that each time a connection is added to an existing network, a chemically distinct promoter-regulator interaction must be introduced.

7.5.3 Complex gene regulatory networks

The synthetic biology community is engaged in the design and construction of gene circuits of increasing complexity. Examples include a tunable version of a band detector, a gene cascade designed to display ultrasensitive responses, and a cellular 'counter' that is able to keep track of a sequence of input events (These projects were surveyed in the paper (Khalil and Collins, 2010), which also highlights applications of synthetic circuits to biosensing, bioremediation, biofuel production, and biomanufacturing and delivery of drugs.) A broad range of computational and signal-processing gene networks has been proposed by the iGEM community.* Nevertheless, current attempts at gene circuit design pale in comparison to the complexity found in natural gene networks.

*www.igem.org

Natural gene regulatory networks

Natural gene circuits can be roughly divided into two classes: sensory networks, which mount a response to a cell's current environmental conditions; and cell-fate decision (or developmental) networks, which cause cells to adopt persistent states.

Sensory networks enhance a cell's survival by tailoring its behaviour to suit the prevailing conditions. The *lac* operon of *E. coli* is a canonical example. Because they demand a timely response, sensory networks tend to be rather 'shallow'—they do not usually involve long cascades of gene regulation between input and output. (Such cascades would introduce significant gene expression lags.)

Cell-fate decision networks do not normally act under tight time-constraints; they often involve long cascades of interacting genes and complex feedback loops, particularly positive feedback loops that 'lock in' decisions. There are many known examples of bacterial cell-fate decision networks, such as the lysis-lysogeny switch in phage lambda (Section 7.2.2) and the sporulation decision network in *B. subtilis*. These bacterial networks are typically simpler than the gene networks responsible for the development of multicellular organisms. These developmental networks can involve dozens of individual genes, each typically regulated by several distinct transcription factors (reviewed in (Stathopoulos and Levine, 2005) and (Davidson, 2006)).

We conclude this section by introducing two well-studied examples of complex developmental gene networks.

The segmentation gene network in the fruit fly *Drosophila melanogaster*

During their growth, *Drosophila* embryos develop a segmented body-plan. This spatial patterning is derived from maternal genes whose mRNA transcripts are placed in different regions of the egg. The gene regulatory network responsible for the segmentation process is sketched in Figure 7.36. The temporal progression of activity in the network corresponds to the steps in the segmentation process as shown. Since segmentation is a spatio-temporal process, ordinary differential-equation based models are not directly applicable. An ODE model can be employed if one supposes a compartmental structure across the embryo, but a more natural modelling approach is to make use of partial differential equations, as introduced in Section 8.4. (An ODE model appears in (Jaeger *et al.*, 2004); a spatial model was presented in (Perkins *et al.*, 2006).)

The endomesoderm specification network in *Strongylocentrotus purpuratus*

Eric Davidson's lab has worked for many years on mapping the gene regulatory network that drives differentiation of cells in the early embryo of the sea urchin *Strongylocentrotus purpuratus* (Figure 7.37). The behaviour of this network begins with maternally-specified asymmetries in the egg, and leads to development of the endoderm (inside layer), skeletal, and mesoderm (middle layer) components of the embryo. A full kinetic characterization of the interactions in a network of this size is daunting, and so models are typically constructed using simpler methods, such as Boolean frameworks. (Appropriate modelling frameworks are reviewed in (Bolouri and Davidson, 2002).)

The study of complex gene regulatory networks has revealed an important insight into their structure: they often exhibit a *modular* architecture, meaning that the network is composed of subnetworks that play their role somewhat independently of one another. Modularity is a key aspect

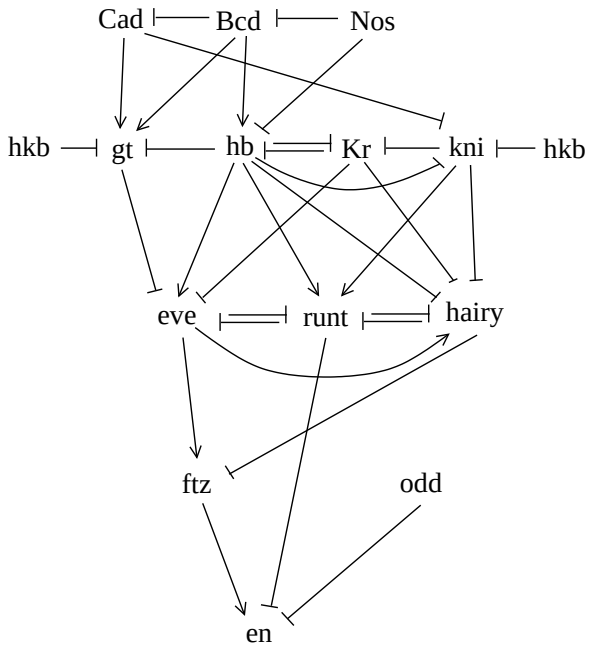

Figure 7.36: Segmentation gene network in *Drosophila*. Embryonic development is driven by spatial expression patterns of a number of genes, shown in the regulatory network that guides their behaviour. Adapted from Figure 3.5 of (Carroll *et al.*, 2005).

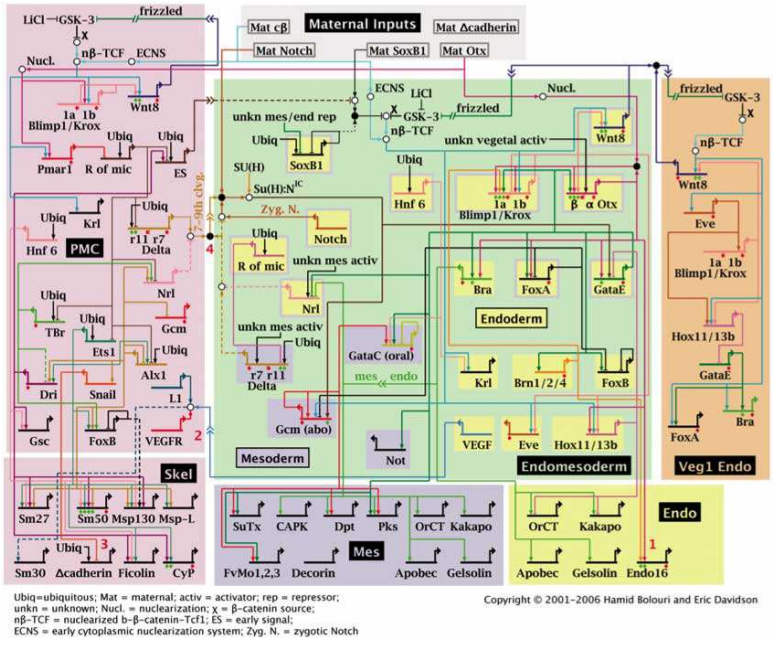

Figure 7.37: Endomesoderm specification network in the sea urchin *Strongylocentrotus purpuratus*. The genes are organized into boxes based on their function. Maternal inputs appear at the top; differentiation proteins are encoded by genes in the bottom boxes. The network describes events that occur in the 30 hours following fertilization. Reproduced, with permission, from (Davidson, 2006; Figure 4.2).

of human-engineered systems; it allows individual components to be designed, constructed and tested independently of the entire system. Moreover, modularity allows the re-use of components in multiple systems—a feature that is likely of use in evolutionary 'design'. (Modularity is reviewed in (Wagner *et al.*, 2007); the challenges and opportunities that modular design presents to synthetic biology are discussed in (Purnick and Weiss, 2009).)

7.6 *Stochastic Modelling of Biochemical and Genetic Networks

Chemical reactions result from collisions of individual molecules. Most molecular collisions do not cause reactions. On a molecular scale, reactions are thus rare events, and are difficult to predict. In many cellular processes, this molecular randomness is 'averaged out' over large numbers of reaction events, resulting in predictable system behaviour. In contrast, processes that depend on small numbers of molecules can be strongly affected by the randomness of biochemical events. Gene expression often involves molecular species that are present in low numbers, and so gene regulatory networks can be subject to this random variation. (The effects of noise on developmental gene networks reveals itself in differences between genetically identical organisms, from bacteria to humans. Stochasticity in gene expression is discussed in (Raj and van Oudenaarden, 2008).)

Random variation is often considered an inconvenience that must be overcome; the fact that this randomness is usually referred to as 'noise' suggests it is a nuisance. However, in some biological contexts, random behaviour can be exploited for improved performance. An example is provided by the phenomenon of bacterial *persistence*, in which a genetically identical population gives rise to a small number of so-called persistent cells that exhibit antibiotic resistance at the cost of a reduced growth rate. In the absence of antibiotics, slow-growing persistent cells are quickly out-competed, but the presence of a handful of these cells ensures the population's survival when antibiotics are applied.

At the cellular level, randomness can be partitioned into two categories: *extrinsic noise*, which refers to random variations that impact all processes in the cell equally, and *intrinsic noise*, which is driven by thermal fluctuations at the molecular level. In models of intracellular networks, extrinsic noise appears as randomness in the values of model parameters, and so can be directly incorporated into a differential equation-based framework. In contrast, treatment of intrinsic noise demands the adoption of a modelling framework that takes into account the randomness of the biochemical events that drive reaction dynamics.

A reaction network that comprises large numbers of reactant molecules will involve many simultaneous reaction events. In such cases, network behaviour corresponds to the average over these events, and is well described by deterministic differential equation models. Figure 7.38, which shows the behaviour of a decaying population of molecules, illustrates this averaging effect. The solid curve in each panel shows a simulation that incorporates randomness; the dashed curve shows a corresponding deterministic simulation. In Panel A, the initial population size is large. In this case, individual decay events have a negligible effect on the overall pool. Averaged over many events, the random timing of the reactions is smoothed out, so the deterministic model provides a good description of system behaviour. In panel B, the initial population consists of a smaller number of molecules, so the averaging effect is not as strong. Panel C shows a simulation that starts with just ten molecules. Each decay event has an appreciable effect on the overall abundance. In this case, the system's discrete, random behaviour is not well-described by the deterministic simulation.

In this section, we introduce a *stochastic* modeling framework that is suitable for describing

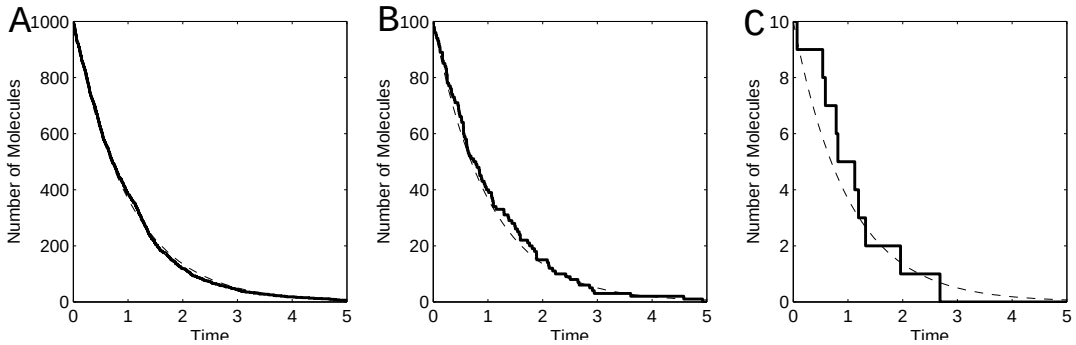

Figure 7.38: Simulations of constitutive decay. The solid curves show simulations that incorporate randomness (stochastic simulations). The dashed curves show the corresponding deterministic (differential equation-based) simulations. The initial pool sizes are 1000 (**A**), 100 (**B**) and 10 (**C**) molecules. For large pool size, the simulations coincide; as the molecule count decreases, random effects become more pronounced, and are not well-described by the deterministic model.

systems that involve small number of molecules. The term 'stochastic' means 'random'; it is used to describe dynamic processes that have some element of randomness in their progression. (Appendix B contains a brief introduction to some basic concepts from probability.)

7.6.1 A discrete modelling framework

In developing a stochastic modelling framework for chemical reactions networks, we will continue to assume spatial homogeneity, and a fixed volume. The abundance of each chemical species will be described by the *number* of molecules in the reaction volume. The state of the system is then the vector $\mathbf{N}$ of molecule counts. (Recall, in a differential equation-based model, the state is the vector $\mathbf{s}$ of species *concentrations*.) As the stochastic dynamics proceed, the molecule counts will change their values in discrete jumps (in contrast to the smooth changes in concentration values that occur in differential equation models).

We will characterize each reaction in the network by a *stoichiometry vector* $\mathbf{s}$, and a *propensity function* a. For each reaction, the stoichiometry vector indicates the identity and number of reactants and products in a reaction: the j-th component of this vector is the net number of molecules of species j produced or consumed in the reaction. The propensity is a description of reaction rate.

To illustrate these ideas, consider the network composed of the two reactions

$$R_1:\ A + B \xrightarrow{k_1} C \qquad\qquad R_2:\ C \xrightarrow{k_2}$$

The state of this system will be described by the numbers of molecules of species A, B, and C present at any given time. The stoichiometry vectors are

$$\mathbf{s}_1 = \begin{bmatrix} -1 \\ -1 \\ 1 \end{bmatrix} \begin{matrix} \leftarrow A \\ \leftarrow B \\ \leftarrow C \end{matrix} \qquad \text{and} \qquad \mathbf{s}_2 = \begin{bmatrix} 0 \\ 0 \\ -1 \end{bmatrix} \begin{matrix} \leftarrow A \\ \leftarrow B \\ \leftarrow C \end{matrix} .$$

When a reaction occurs, the state vector $\mathbf{N}$ is updated by addition of the corresponding stoichiometry vector. For example, suppose that at a given time the state is $\mathbf{N} = (N_A, N_B, N_C) = (12, 3, 4)$. If reaction R_1 were to occur, we would update the state by replacing $\mathbf{N}$ with $\mathbf{N} + \mathbf{s}_1 = (11, 2, 5)$.

The reaction propensities are functions of reactant abundance. We will assume that the probability of a reaction event is proportional to the product of the abundance of each reactant species (as in mass action). The propensities for this example are then

$$a_1(\mathbf{N}) = k_1 N_A N_B \qquad a_2(\mathbf{N}) = k_2 N_C$$

In general, reaction propensities take the same form as mass-action rate laws, but a difference appears when multiple copies of an individual reactant are involved.*

7.6.2 The chemical master equation

We will build a stochastic modelling framework on the assumption that there are small time increments dt for which:

- At most one reaction event can occur during any time interval of length dt.
- The probability that reaction R_k occurs in any time interval $[t, t+dt]$ is the product of the reaction propensity at time t and the length of the interval: $a_k(\mathbf{N}(t))\,dt$.

Under these assumptions, the probability that no reactions occur during a time interval $[t, t+dt]$ is $1 - \sum_k a_k(\mathbf{N}(t))dt$, where the sum is taken over all reactions in the system.

Let $P(\mathbf{N}, t)$ denote the probability that the system is in state $\mathbf{N}$ at time t. This is called the *probability distribution* of the state (and is dependent on the initial condition—it is a conditional probability distribution). If the distribution $P(\mathbf{N}, t)$ is known at time t, we can use the assumptions above to describe the distribution at time $t + dt$:

$$P(\mathbf{N}, t+dt) = P(\mathbf{N}, t) \cdot \underbrace{\left(1 - \sum_k a_k(\mathbf{N})\,dt\right)}_{\text{probability of no reactions firing}} + \sum_k \underbrace{P(\mathbf{N} - \mathbf{s}_k, t)\, a_k(\mathbf{N} - \mathbf{s}_k)\, dt.}_{\text{probability of reaction } R_k \text{ occurring while in state } \mathbf{N} - \mathbf{s}_k} \tag{7.27}$$

This equation is called a *probability balance*. The first term is the probability of being in state $\mathbf{N}$ at time t and remaining in that state until time $t + dt$ (because no reaction events occur). The second term is the sum of the probabilities of transitioning into state $\mathbf{N}$ from another state (because reaction R_k causes a transition from $\mathbf{N} - \mathbf{s}_k$ to $(\mathbf{N} - \mathbf{s}_k) + \mathbf{s}_k = \mathbf{N}$).

As an example, consider the simple reaction chain in which species A is produced at zeroth order and degrades at first order:

$$R_1: \xrightarrow{k_1} A \qquad\qquad R_2: A \xrightarrow{k_2}$$

The state of the system is the number of molecules of A, i.e. $N = N_A$. The reaction stoichiometries are $s_1 = [1]$, $s_2 = [-1]$. The reaction propensities are $a_1 = k_1$ and $a_2 = k_2 N_A$. The transitions between states follow the scheme in Figure 7.39.

*For instance, the propensity of the bimolecular reaction $A + A \xrightarrow{k} C$ is $kN_A(N_A - 1)/2$. This formula reflects the number of unique pairings of two A molecules.

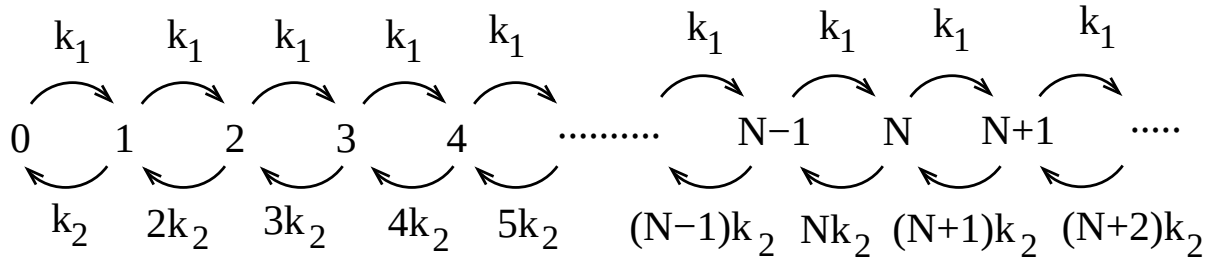

Figure 7.39: Transitions among states for the simple reaction chain $\stackrel{k_1}{\rightarrow} A \stackrel{k_2}{\rightarrow}$. The reaction propensities are indicated.

In this case, the probability balance reads:

$$\begin{aligned}
P(0,t+dt) &= P(0,t)\,[1-k_1 dt] + P(1,t)\cdot k_2\,dt \\
P(1,t+dt) &= P(1,t)\,[1-(k_1+k_2)dt] + P(0,t)\cdot k_1\,dt + P(2,t)\cdot 2k_2\,dt \\
P(2,t+dt) &= P(2,t)\,[1-(k_1+2k_2)dt] + P(1,t)\cdot k_1\,dt + P(3,t)\cdot 3k_2\,dt \\
P(3,t+dt) &= P(3,t)\,[1-(k_1+3k_2)dt] + P(2,t)\cdot k_1\,dt + P(4,t)\cdot 4k_2\,dt \\
&\vdots \\
P(N,t+dt) &= P(N,t)\,[1-(k_1+Nk_2)dt] + P(N-1,t)\cdot k_1\,dt + P(N+1,t)\cdot (N+1)k_2\,dt \\
&\vdots
\end{aligned}$$

Exercise 7.6.1 Verify that the probability balance for the scheme:

$$\begin{aligned}
R_1: &\quad \stackrel{k_1}{\longrightarrow} A \\
R_2: &\quad \stackrel{k_2}{\longrightarrow} B \\
R_3: &\quad A + B \stackrel{k_3}{\longrightarrow}
\end{aligned}$$

is

$$\begin{aligned}
P((N_A,N_B),t+dt) &= P((N_A,N_B),t)\,[1-(k_1+k_2+N_A N_B k_3)dt] \\
&\quad + P((N_A-1,N_B),t)\cdot k_1 dt + P((N_A,N_B-1),t)\cdot k_2 dt \\
&\quad + P((N_A+1,N_B+1),t)\cdot (N_A+1)(N_B+1)k_3 dt.
\end{aligned}$$

□

The probability balance (7.27) can be used to derive a differential equation describing the rate of change of the probability distribution, as follows. Subtracting $P(\mathbf{N},t)$ from each side of equation (7.27) gives

$$P(\mathbf{N},t+dt) - P(\mathbf{N},t) = -P(\mathbf{N},t)\left(\sum_k a_k(\mathbf{N})\,dt\right) + \sum_k P(\mathbf{N}-\mathbf{s}_k,t)\,a_k(\mathbf{N}-\mathbf{s}_k)\,dt.$$

Dividing both sides by dt and taking the limit as dt tends to zero results in

$$\begin{aligned}\frac{d}{dt}P(\mathbf{N},t) &= -P(\mathbf{N},t)\left(\sum_k a_k(\mathbf{N})\right) + \sum_k P(\mathbf{N}-\mathbf{s}_k,t)a_k(\mathbf{N}-\mathbf{s}_k) \\ &= \sum_k \left(\underbrace{-P(\mathbf{N},t)a_k(\mathbf{N})}_{\text{flow out of state } \mathbf{N}} + \underbrace{P(\mathbf{N}-\mathbf{s}_k,t)a_k(\mathbf{N}-\mathbf{s}_k)}_{\text{flow into state } \mathbf{N}} \right)\end{aligned}$$

This is called the *chemical master equation*. It is a system of differential equations describing the time-varying behaviour of the probability distribution. The terms on the right-hand-side account for probability flow out of, and into, the state $\mathbf{N}$ at time t. The master equation includes a differential equation for every state $\mathbf{N}$ that the system can adopt, and so typically involves an infinite number of equations.

For the simple reaction chain described above ($\stackrel{k_1}{\rightarrow} A \stackrel{k_2}{\rightarrow}$), the master equation is

$$\begin{aligned}\frac{d}{dt}P(0,t) &= -P(0,t)\,k_1 + P(1,t)\,k_2 \\ \frac{d}{dt}P(1,t) &= -P(1,t)\,(k_1+k_2) + P(0,t)k_1 + P(2,t)\,2k_2 \\ \frac{d}{dt}P(2,t) &= -P(2,t)\,(k_1+2k_2) + P(1,t)k_1 + P(3,t)\,3k_2 \\ &\vdots \\ \frac{d}{dt}P(N,t) &= -P(N,t)\,(k_1+Nk_2) + P(N-1,t)\,k_1 + P(N+1,t)\,(N+1)k_2 \\ &\vdots\end{aligned} \tag{7.28}$$

Exercise 7.6.2 Determine the chemical master equation for the system in Exercise 7.6.1 □

To illustrate the behaviour of solutions of the master equation, we consider the closed reaction network:

$$R_1:\ A \xrightarrow{k_1} B \qquad\qquad R_2:\ B \xrightarrow{k_2} A$$

To keep the analysis simple, we suppose that there are only two molecules present in the system. The system state $\mathbf{N} = (N_A, N_B)$ can then take only three possible values: $(2,0)$, $(1,1)$, or $(0,2)$. The master equation is a system of three differential equations:

$$\begin{aligned}\frac{d}{dt}P((2,0),t) &= -P((2,0),t)\,2k_1 + P((1,1),t)\,k_2 \\ \frac{d}{dt}P((1,1),t) &= -P((1,1),t)\,k_2 - P((1,1),t)\,k_1 + P((2,0),t)2k_1 + P((0,2),t)\,2k_2 \\ \frac{d}{dt}P((0,2),t) &= -P((0,2),t)\,2k_2 + P((1,1),t)\,k_1\end{aligned} \tag{7.29}$$

Note the right-hand-sides sum to zero, as dictated by conservation of probability.

A simulation of system (7.29) is illustrated in Figure 7.40, which shows plots of the probability distribution (histograms) at three time points.

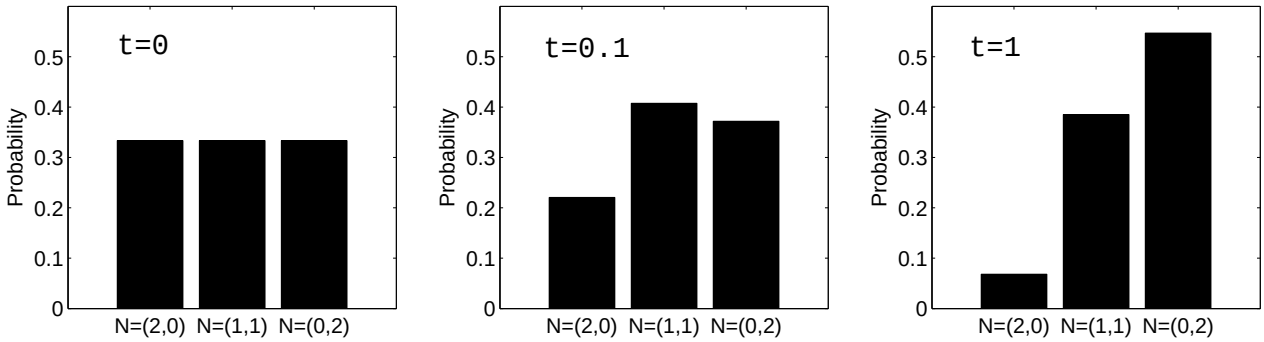

Figure 7.40: Evolution of probabilities for the closed reaction network (7.29). Probability distributions for $\mathbf{N} = (N_A, N_B)$ at times $t = 0$, $t = 0.1$, and $t = 1$ are shown. A uniform initial distribution is chosen, so that at time $t = 0$ all states are equally likely: $P((2,0),0) = P((1,1),0) = P((0,2),0) = 1/3$. Parameter values (in time^{-1}): $k_1 = 3$, $k_2 = 1$. Time units are arbitrary.

For this network, the steady-state distribution $P^{ss}(N_A, N_B)$ can be found by setting the time rates of change to zero:

$$\begin{aligned} 0 &= -P^{ss}(2,0)\,2k_1 + P^{ss}(1,1)\,k_2 \\ 0 &= -P^{ss}(1,1)\,k_2 - P^{ss}(1,1)\,k_1 + P^{ss}(2,0)\,2k_1 + P^{ss}(0,2)\,2k_2 \\ 0 &= -P^{ss}(0,2)\,2k_2 + P^{ss}(1,1)\,k_1 \end{aligned}$$

Solving these equations, along with the condition that probability is conserved ($P^{ss}(2,0)+P^{ss}(1,1)+P^{ss}(0,2) = 1$), yields the steady state probability distribution:

$$P^{ss}((2,0)) = \frac{k_2^2}{(k_1+k_2)^2}, \qquad P^{ss}((1,1)) = \frac{2k_1k_2}{(k_1+k_2)^2}, \qquad P^{ss}((0,2)) = \frac{k_1^2}{(k_1+k_2)^2}. \tag{7.30}$$

Exercise 7.6.3 Verify equations (7.30). Does the simulation in Figure 7.40 appear to have reached steady state by time $t = 1$? □

As the number of molecules in the system increases, the steady state distribution of probabilities becomes smoother and more tightly peaked. Figure 7.41 shows the steady-state probability distributions for N_B in system (7.29) when there are 2, 20, and 200 molecules present. As the molecule count increases, the distribution converges to a tight peak at which three-fourths of the total pool consists of molecules of B. The deterministic (mass-action based) description of the system corresponds to a histogram that is concentrated at this single point. The probabilistic solution thus converges to the deterministic description for large molecule counts.

Exercise 7.6.4 Verify that the mean (i.e. expected value) of N_A and N_B in the steady-state probability distribution (7.30) correspond to the deterministic (mass-action based) model of system (7.40). □

For most systems, chemical master equation is intractable. (Simulations typically need to incorporate an infinite number of equations!) Consequently, a number of methods have been developed to provide alternative descriptions of stochastic behaviour (reviewed in (Khammash, 2010)).

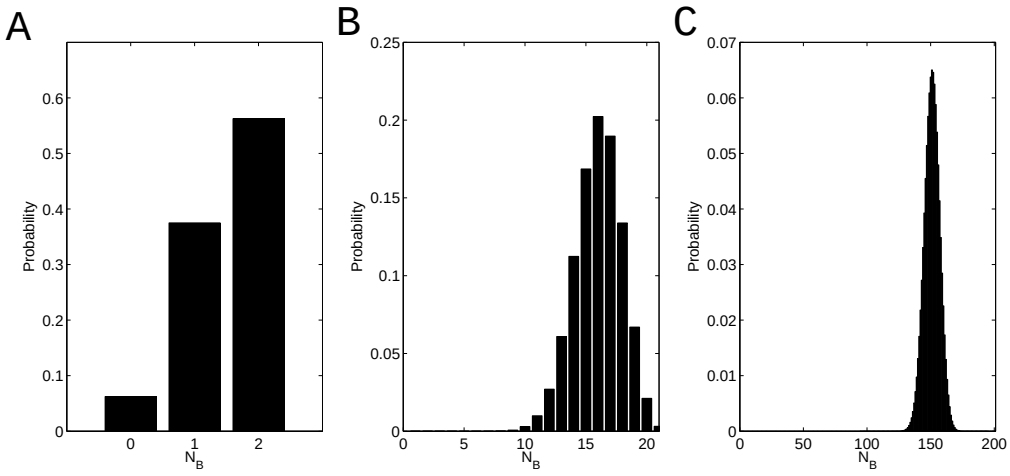

Figure 7.41: Steady-state probability distribution for N_B in reaction network (7.29) for a total molecule count of 2 (**A**), 20 (**B**), and 200 (**C**). As the molecule count grows, the distribution tends to a single peak for which $N_B = 3N_A$, which corresponds to the deterministic (mass-action) equilibrium.

These include the *linear noise approximation*, which generates differential equations whose solutions approximate the mean and variance of system behaviour; *moment closure methods*, which allow calculation of approximate statistics for the probability distribution; and the *finite state projection*, which approximates the chemical master equation by a finite system of differential equations.

Rather than address these analytic approaches, we next consider a numerical method for generating simulations of stochastic systems.

7.6.3 Gillespie's stochastic simulation algorithm

Numerical algorithms that incorporate stochastic effects (by calling on random number generators) are called *Monte Carlo* methods. In 1977, Dan Gillespie published a Monte Carlo method for simulating individual trajectories of chemical reaction networks characterized by the chemical master equation (reviewed in (Gillespie, 2007)). These trajectories, called *sample paths*, represent single elements drawn from a probability distribution generated by the system. Statistics of the trajectory distribution can be determined by generating a large collection of these sample paths (called an *ensemble*).

Gillespie's method, which he called the Stochastic Simulation Algorithm (SSA), tracks each individual reaction event. The simulation does not proceed over a fixed time-grid, but jumps forward in time from one reaction event to the next. After each reaction, the algorithm determines which reaction will occur next, and how much time will elapse before it occurs.

The simulation algorithm depends on the properties of two *random variables*: the time T to the firing of the next reaction, and the reaction R that will occur next. We next consider how these two random variables are determined.

Determining the next reaction

The probability that a particular reaction will occur is proportional to the propensity of the reaction. Consider a network that involves three reactions, R_1, R_2, and R_3, with propensities a_1, a_2, and

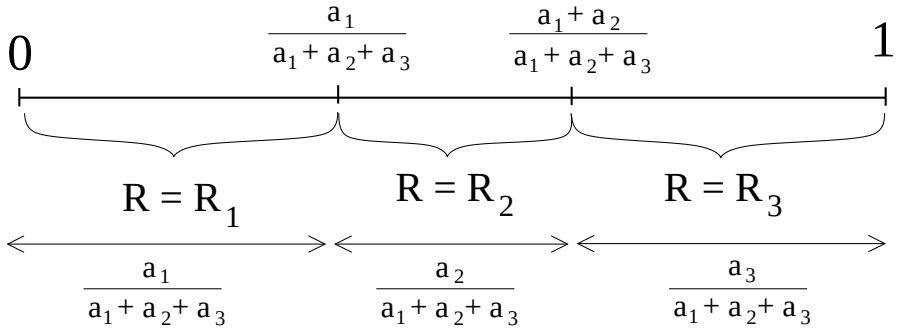

Figure 7.42: Selection of the next reaction. For a network with three reactions, the interval from zero to one is divided into three subintervals, whose lengths correspond to the probabilities of the reactions. A number sampled from the uniform zero-to-one distribution corresponds to a selection of the next reaction.

a_3. Let $P(R = R_i)$ denote the probability that R_i will be the next reaction to occur. Probability $P(R = R_i)$ is proportional to the propensity a_i of reaction R_i. Together, these probabilities sum to one. The probability distribution is:

$$\begin{aligned} P(R = R_1) &= \frac{a_1}{a_1 + a_2 + a_3} \\ P(R = R_2) &= \frac{a_2}{a_1 + a_2 + a_3} \\ P(R = R_3) &= \frac{a_3}{a_1 + a_2 + a_3} \end{aligned} \tag{7.31}$$

In order to implement a simulation of this network's behaviour, we need to sample from this probability distribution. Most numerical software packages have built-in functions that generate random numbers drawn uniformly between zero and one. Samples from this uniform distribution can be converted to samples from the distribution (7.31), as follows. We divide the zero-to-one interval into three subintervals—one for each reaction—as in Figure 7.42. The length of each subinterval is equal to the probability of the corresponding reaction. A number u that is drawn from the uniform distribution falls into one of these subintervals, and thus corresponds to a particular reaction. This procedure can be formalized as follows:

$$\begin{aligned} &\text{if} && 0 \leq && u && \leq \frac{a_1}{a_1 + a_2 + a_3}, && \text{then we set } R = R_1 \\ &\text{if} && \frac{a_1}{a_1 + a_2 + a_3} < && u && \leq \frac{a_1 + a_2}{a_1 + a_2 + a_3}, && \text{then we set } R = R_2 \\ &\text{if} && \frac{a_1 + a_2}{a_1 + a_2 + a_3} < && u && \leq \frac{a_1 + a_2 + a_3}{a_1 + a_2 + a_3} = 1, && \text{then we set } R = R_3. \end{aligned} \tag{7.32}$$

Figure 7.43 provides a visualization of this process. Here, the uniform random number u is assigned to the vertical axis. The height of the staircase graph corresponds to the cumulative probabilities as employed in algorithm (7.32). The next reaction is determined by selecting a number u from the uniform zero-to-one distribution and then extending a horizontal line to the staircase graph, as shown. This graph is called the *cumulative distribution function* for the random variable R.

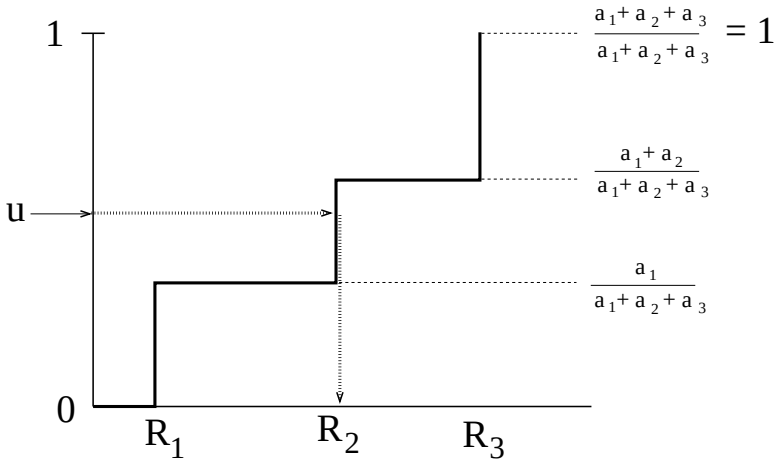

Figure 7.43: Cumulative distribution function for the random variable R. The height of the staircase graph corresponds to the cumulative probability as in algorithm (7.32). A reaction is chosen by selecting a number u from the uniform distribution on the horizontal axis and then extending a horizontal line to the staircase graph.

Determining the time to the next reaction

The time T that elapses between reactions is also a random variable. Unlike R, it does not have a discrete value-set, but can take any non-negative value. Since it can take infinitely many values, the probability of T having any particular value is vanishingly small. Thus, rather than frame our discussion in terms of point-wise probabilities, we will instead sample T directly from the cumulative distribution function, as we did for the random variable R in Figure 7.43. The cumulative distribution function for T is given by:

$$P(0 \leq T \leq t) = 1 - e^{-at}, \tag{7.33}$$

where a is the sum of the reaction propensities:

$$a = a_1 + a_2 + a_3.$$

Equation (7.33) characterizes T as an *exponential random variable.*

The cumulative distribution function for T is shown in Figure 7.44. Most often, samples u from the uniform zero-to-one distribution will correspond to short wait-times between reactions; only occasionally (when u is chosen near 1) will a long time be selected. The steepness of the curve depends on a, the sum of the propensities. If this sum is large (many highly probably reactions) then the curve rises steeply and waiting times are almost always short. If the sum is smaller, then the curve rises more slowly, and longer waiting times are more likely.

Gilliespie's algorithm can be summarized as follows:

Stochastic Simulation Algorithm (SSA)

1. Set the initial state $\mathbf{N}$. Initialize time t to zero.
2. Calculate the reaction propensities $a_k(\mathbf{N})$.
3. Draw a sample R_k from the random variable R (Figure 7.43).

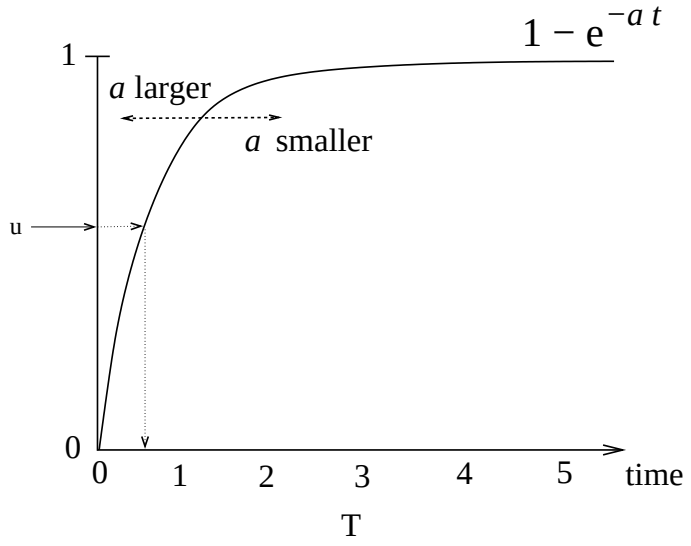

Figure 7.44: Cumulative distribution function for the waiting time T. The parameter a is the sum of the propensities. Waiting times T are determined by selecting numbers u from the uniform zero-to-one distribution and then extending a horizontal line to the graph, as shown. For large values of a, the curve rises sharply—most samples u correspond to short waiting times. For smaller a values, larger waiting times are more likely.

4. Draw a sample τ from the random variable T (Figure 7.44).
5. Increment the simulation time $t \to t + \tau$ to account for the elapsed time.
6. Update the state vector $\mathbf{N} \to \mathbf{N} + \mathbf{s}_k$ to reflect the fact that reaction R_k has occurred.
7. Return to step 2.

The algorithm is usually continued until the simulation time t reaches the end of a specified time interval.

7.6.4 Examples

We conclude by using Gillespie's stochastic simulation algorithm to explore the behaviour of some simple reaction networks.

Constitutive Decay

We begin by revisiting the decay reaction

$$A \xrightarrow{k}$$

The behaviour of this system was illustrated by the stochastic simulations in Figure 7.38, which showed that the trajectories are highly variable when the system consists of only a small number of molecules. Figure 7.45 shows ensembles of sample paths, each starting with only ten molecules. Three ensembles are shown, along with the average behaviour (solid line). Although the individual

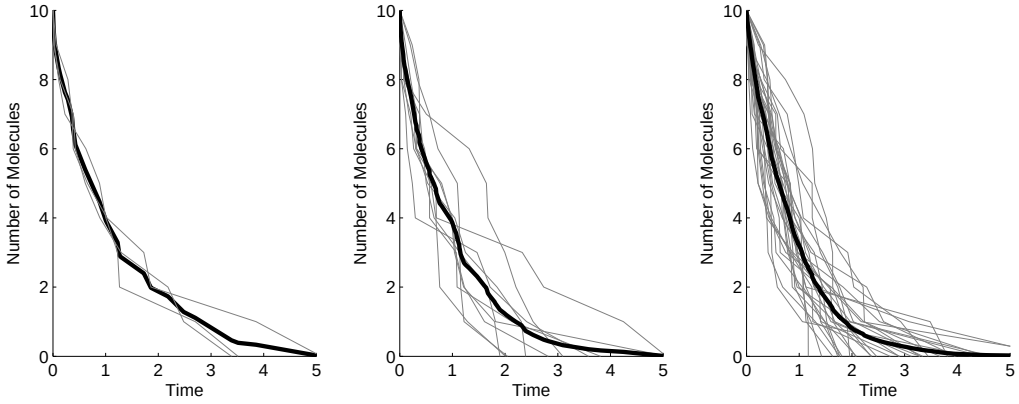

Figure 7.45: Ensembles of sample paths for the decay reaction. Each sample path begins with 10 molecules. Ensembles of 3 (**A**), 10 (**B**), and 30 (**C**) sample paths are shown (gray curves). The black lines shows the ensemble average. This averaged behaviour approaches the deterministic prediction (exponential decay) as the ensemble size grows. Parameter value: $k = 1$ (time^{-1}). Time units are arbitrary.

sample paths show significant variability, the average is more consistent. As the ensemble size increases, the averaged behaviour converges to the solution of the deterministic model. By generating a large ensemble, a complete description of system behaviour—including measures of the variability in the distribution of trajectories—can be reached (Problem 7.8.24).

In some cases, a very large number of sample paths is needed to guarantee confidence in these ensemble-derived results; generating a sufficiently large ensemble can be a time-consuming process. A number of refinements of the stochastic simulation algorithm have been proposed that aim to reduce the computational requirements for simulation (see Problem 7.8.25 for an example).

Constitutive gene expression

We next consider a simple model of unregulated gene expression, involving mRNA, M, and protein, P. The reaction network is:

$$\begin{array}{lll} R_1 : \text{(transcription)} & \longrightarrow M & \text{propensity: } k_r \\ R_2 : \text{(translation)} & \longrightarrow P & \text{propensity: } k_p N_M \\ R_3 : \text{(degradation)} & M \longrightarrow & \text{propensity: } \delta_r N_M \\ R_4 : \text{(degradation)} & P \longrightarrow & \text{propensity: } \delta_p N_P \end{array} \tag{7.34}$$

Sample paths from a Gillespie simulation are shown in Figure 7.46A. The mRNA traces are centered around an average of about 10 molecules. The protein count shows an average of about 60.

Experimental observations have revealed that transcription is sometimes a 'bursty' process in which each transcription event leads to the production of multiple copies of mRNA (reviewed in (Chubb and Liverpool, 2010).)

This model can be modified to describe bursty transcription by replacing reaction R_1 with

$$\tilde{R}_1 : \text{(bursty transcription)} \quad \longrightarrow \quad 5M \quad \text{propensity: } \frac{k_r}{5}$$

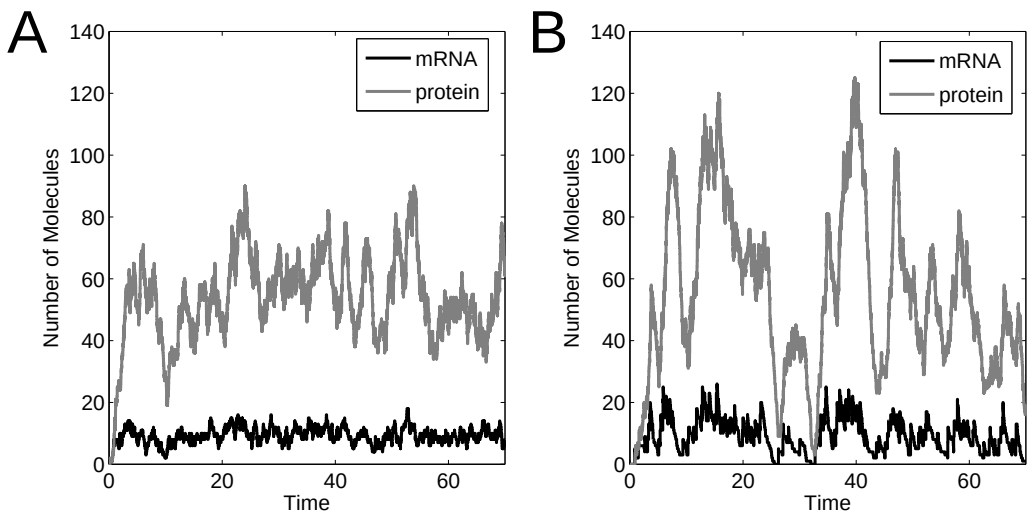

Figure 7.46: Stochastic simulations of constitutive gene expression. **A**. Each transcription event produces a single mRNA transcript. **B.** Transcription is modelled as 'bursty': each transcription events produces 5 mRNA molecules. The propensity of the transcription reaction has been reduced by a factor of 5 to give the same average as in panel A. Parameter values (in time^{-1}): $k_r = 10$, $k_p = 6$, $\delta_r = 1$, $\delta_p = 1$. Time units are arbitrary.

In this modified model, each transcription event produces 5 mRNA molecules. To allow direct comparison with the original model, the propensity of this bursty transcription reaction has been reduced by a factor of 5, so that the time-averaged mRNA production rate is unchanged. Figure 7.46B shows simulations of this modified model. Although the mRNA and protein averages are the same in both models, the modified model exhibits considerably more variability. This difference in behaviour could not be described by a mass action-based model: the deterministic versions of these two models are identical (in both cases, the transcription rate is k_r). Variability is an experimentally observable feature of system behaviour that can only be captured in a stochastic modelling framework.

The Brusselator

Our final example is a stochastic system that exhibit oscillatory behaviour. The *Brusselator* is a theoretical chemical system that exhibits sustained oscillations (Exercise 4.3.1). The reaction network is:

R_1 :	$\longrightarrow X$	propensity: k_1
R_2 :	$X \longrightarrow Y$	propensity: $k_2 N_X$
R_3 :	$2X + Y \longrightarrow 3X$	propensity: $\frac{k_3}{2} N_X (N_X - 1) N_Y$
R_4 :	$X \longrightarrow$	propensity: $k_4 N_X$

A sample path is shown in Figure 7.47, in both the time domain (panel A) and the phase space (panel B). The trajectories are somewhat jagged, but the oscillations are fairly regular. In contrast,

some oscillatory stochastic systems exhibit considerable variability in the timing and shape of the cycles (Problem 7.8.27).

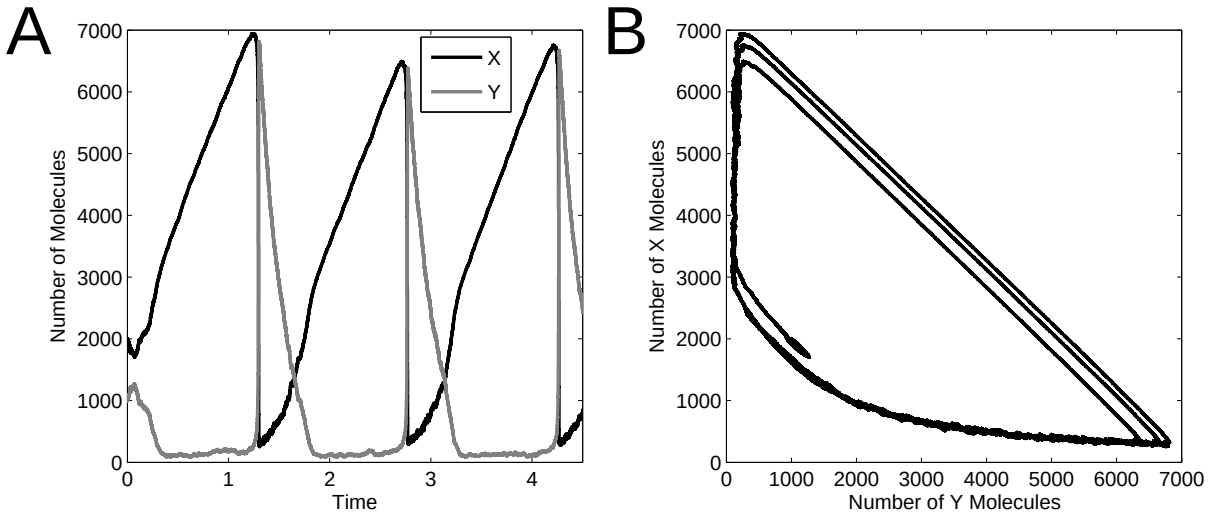

Figure 7.47: Stochastic simulation of the Brusselator. **A**. Oscillations are evident in the time-domain: a slow increase in Y is followed by a sudden crash when Y levels are sufficiently high. **B.** This phase-portrait shows the approximate limit cycle followed by the periodic trajectories. Initial conditions are $X = 1000$, $Y = 2000$. Parameter values (in time^{-1}): $k_1 = 5000$, $k_2 = 50$, $k_3 = 0.00005$ and $k_4 = 5$. Time units are arbitrary.

7.7 Suggestions for Further Reading

- **Modelling gene regulatory networks:** The book *An Introduction to Systems Biology* (Alon, 2007) surveys a number of results that employ models of gene regulatory networks. The text *Computational Modeling of Gene Regulatory Networks – a Primer* (Bolouri, 2008) addresses a wider range of modelling approaches than discussed in this chapter.

- **Phage Lambda:** The book *A Genetic Switch: Phage Lambda Revisited* (Ptashne, 2004) provides a detailed description of the molecular genetics of the decision switch, including an accessible account of the experiments that lead to these discoveries.

- **Synthetic gene circuits:** Discussions of modelling and design in synthetic biology are provided in the book chapter "Synthetic gene regulatory systems" (Weiss and Kaern, 2006) and in *Engineering Gene Circuits* (Myers, 2010). The non-technical book *Biology is Technology: The Promise, Peril, and New Business of Engineering Life* (Carlson, 2010) provides a thoughtful discussion of the potential impact of synthetic biology.

- **Stochastic modelling in systems biology:** An introduction to stochastic modelling techniques in systems biology is provided in the book chapter "Modeling and analysis of stochastic biochemical networks," (Khammash, 2010). The book *Stochastic Modelling for Systems Biology* (Wilkinson, 2006) provides a detailed treatment of stochastic approaches.

7.8 Problem Set

7.8.1 Response time of autoinhibitory genes. Consider expression from an unregulated gene as modelled in equation (7.2):

$$\frac{d}{dt}p(t) = \alpha_0 - \delta p(t) \tag{7.35}$$

For comparison, consider an autoinhibitory gene whose expression can be modelled as in equation (7.8):

$$\frac{d}{dt}p(t) \quad = \quad \alpha\frac{1}{1+p(t)/K} - \delta p(t), \tag{7.36}$$

a) Take $\delta = 1$ (time^{-1}) in models (7.35) and (7.36) and let $K = 1$ (concentration) for the autoinhibited gene. Verify that both genes generate the same steady-state protein concentration when $\alpha = \alpha_0(\alpha_0 + 1)$. (Hint: substitute $p^{ss} = \alpha_0$ into the autoinhibited model.)
b) Simulate the two models with $\alpha_0 = 5$ and $\alpha = 30$ (concentration $\cdot$ time^{-1}). Take the initial concentrations to be zero. Verify that, as a result of having a higher maximal expression rate, the autoinhibited gene reaches steady state more quickly than the unregulated gene.
c) How would you expect the response time to be affected by cooperative binding of multiple copies of the repressor? Verify your conjecture by comparing your results from part (b) with the model

$$\frac{d}{dt}p(t) \quad = \quad \alpha_2\frac{1}{1+(p(t)/K)^2} - \delta p(t).$$

Take $\alpha_2 = 130$ (concentration $\cdot$ time^{-1}).

7.8.2 Robustness of autoinhibitory genes.
a) Verify that the steady states of the unregulated and autoinhibitory models in Section 7.1 (equations (7.2) and (7.8)) are given by

$$p^{ss}_{\text{unreg}} = \frac{\alpha}{\delta_p} \qquad \text{and} \qquad p^{ss}_{\text{reg}} = \frac{-1+\sqrt{1+4\alpha/(K\delta_p)}}{2/K}$$

where the unregulated model has expression rate α.
b) Take derivatives with respect to α to verify the relative sensitivities:

$$\frac{\alpha}{p^{ss}_{\text{unreg}}}\frac{\partial p^{ss}_{\text{unreg}}}{\partial \alpha} = 1 \qquad \frac{\alpha}{p_{\text{reg}^{ss}}}\frac{\partial p^{ss}_{\text{reg}}}{\partial \alpha} = \frac{2\alpha/(K\delta_p)}{(\sqrt{1+4\alpha/(K\delta_p)})(-1+\sqrt{1+4\alpha/(K\delta_p)})}$$

c) Verify that the sensitivity of the autoinhibited protein is smaller than the sensitivity of the unregulated protein by showing that the expression for $\frac{a}{p^{ss}_{\text{reg}}}\frac{\partial p^{ss}_{\text{reg}}}{\partial a}$ is always less than one, regardless of the parameter values. Hint: the formula depends on the quotient $4\alpha/(K\delta_p)$. Letting $x = 4\alpha/(K\delta_p)$, it is required to show that

$$\frac{x/2}{(\sqrt{1+x})(-1+\sqrt{1+x})} < 1.$$

for any positive x value. You can convince yourself of this by plotting this function of x. For a mathematically rigorous proof, begin by expanding the denominator and multiplying by the conjugate $(1+x+\sqrt{1+x})$.

7.8.3 Alternative regulatory schemes. The models in this chapter focus on the regulation of transcriptional initiation (i.e. the binding of RNA polymerase to promoter regions). Other regulatory mechanisms include:
a) *Antisense mRNA.* Gene expression can be inhibited by the production of antisense RNA, which is complementary to a gene's mRNA. The antisense RNA binds tightly to its complementary partner (by base pairing), and so sequesters the mRNA away from the translation machinery. In this case the transcription of the gene is unaffected, but translation of the resulting mRNA is inhibited. Extend the model of gene expression in equation (7.1) to incorporate inhibition by antisense RNA.
b) *mRNA stability.* Protein production can be repressed by factors that target mRNA molecules for degradation. (An example is the protein β-tubulin, which destabilizes its own mRNA.) Develop a model of autoinhibition of protein expression in this manner.

7.8.4 Transcription factor multimerization. Many transcription factors function as multimers (e.g. dimers or tetramers). Consider a transcription factor P that dimerizes and binds an operator O. The reaction scheme is:

$$P + P \underset{k_2}{\overset{k_1}{\rightleftharpoons}} P_2 \qquad\qquad O + P_2 \underset{d}{\overset{a}{\rightleftharpoons}} OP_2$$

a) Letting $K_0 = k_2/k_1$ and $K_1 = d/a$, suppose that these binding events are in equilibrium and verify that the resulting promoter occupancy is:

$$\text{Fraction of bound operators:} \qquad \frac{[OP_2]}{[O]+[OP_2]} = \frac{[P]^2/K_0K_1}{1+[P]^2/K_0K_1},$$

This is the same Hill function we used in Section 7.1.2 to describe cooperativity in operator binding. However, when this function is used in a model of gene expression, additional nonlinearities appear.
b) Ignoring mRNA dynamics, a model of an autoactivating gene whose product acts as a dimer takes the form:

$$\begin{aligned}\frac{d}{dt}p(t) &= a\frac{p_2(t)/K}{1+p_2(t)/K} - 2k_1p^2(t) + 2k_2p_2(t) - \delta_1 p(t)\\ \frac{d}{dt}p_2(t) &= k_1p^2(t) - k_2p_2(t) - \delta_2 p_2(t)\end{aligned}$$

where p is the monomer concentration and p_2 is the dimer concentration. Verify that if $\delta_2 = 0$, then a quasi-steady-state approximation applied to p_2 to will result in a reduced model that is equivalent to the cooperative-binding autoinhibitor model (7.10) (with $N = 2$). Thus multimerization generates the same dynamics as cooperative DNA-binding if multimers are protected from degradation.

7.8.5 The *lac* operon: effect of leak. Consider the model of the *lac* operon presented in Section 7.2.1, with parameter values as in Figure 7.7. The dose-response curve in Figure 7.7B indicates that the system shows little response to external lactose levels below 55 μM. Modify the model by adding a small 'leak' rate of transcription from the operon: add a constant term a_0 to the mRNA production rate in equation (7.11). Set $a_0 = 0.01$ molecules/min. Run simulations to determine how this change affects the triggering threshold. Explain your result in terms of the system behavior. How does the system behave when $a_0 = 0.1$?

7.8.6 The *lac* operon: role of feedback. As presented in Section 7.2.1, the model of the *lac* operon can be modified to explore the hypothetical situation in which there is no positive feedback from lactose to operon expression. In that case, the tasks of lactose uptake and lactose-to-allolactose conversion would be carried out by proteins that are present at fixed quantities. The model in Section 7.2.1 can be modified to describe this hypothetical system by replacing equation (7.14) with

$$\frac{d}{dt}L(t) = \frac{4k_L E L_e}{K_{ML} + L_e} - \frac{k_g B(t) L(t)}{K_{Mg} + L(t)} - \frac{k_g E L(t)}{K_{Mg} + L(t)} - \delta_L L(t),$$

where E is fixed. (The factor 4 in the uptake rate has been included to preserve the ratio between the number of permease proteins and lactose-to-allolactose conversion enzymes.) In this scenario, β-galactosidase still metabolizes lactose, but it does not participate in the conversion of lactose to allolactose.

The dose-response curve for this modified model is shown in Figure 7.7B. The graded response of this feedback-free system may be inefficient, but this modified system nevertheless has some advantages. Take $E = 40$ molecules and simulate this modified system's response to an abrupt introduction of external lactose. Comparing with Figure 7.7A, comment on the speed of response for this hypothetical system. Explain why this modified system exhibits a faster response.

7.8.7 The *lac* operon: CAP. Consider the model of the *lac* operon presented in Section 7.2.1. With parameter values as in Figure 7.7, extend the model to include the transcription factor CAP, which represses expression from the *lac* operon whenever glucose levels are sufficiently high, regardless of the lactose level.

7.8.8 The Goodwin oscillator Recall the generic model of an oscillating autoregulatory gene proposed by Goodwin (equation (7.22)):

$$\begin{aligned}
\frac{d}{dt}x(t) &= \frac{a}{k^n + (z(t))^n} - bx(t) \\
\frac{d}{dt}y(t) &= \alpha x(t) - \beta y(t) \\
\frac{d}{dt}z(t) &= \gamma y(t) - \delta z(t)
\end{aligned}$$

This system exhibits limit-cycle oscillations provided the Hill coefficient n is sufficiently large. Unfortunately, for reasonable choices of the other parameter values, n has to be chosen very high (> 8) to ensure oscillatory behaviour. Modifications that generate oscillations with smaller Hill coefficients are as follows. (In exploring these models, make sure simulation runs sufficiently long for the asymptotic behaviour to be clear.)

a) Taking parameter values as in Figure 7.17, modify the model by adding a fourth step to the activation cascade. (Use dynamics identical to the third step.) Verify that the additional lag introduced by this fourth component allows the system to exhibit sustained oscillations with $n < 8$.

b) Replace the term for degradation of Z by a Michaelis-Menten term: $-\delta z/(K_M + z)$. Verify that this modified system oscillates with no cooperativity (i.e. with $n = 1$). Take $a = 150$, $k = 1$, $b = \alpha = \beta = \gamma = 0.2$, $\delta = 15$, and $K_M = 1$. (Units as in Figure 7.17.)

c) Consider a one-state model in which the time-delay caused by the cascade of molecular events is abstracted into an explicit time delay:

$$\frac{d}{dt}x(t) = \frac{a}{k^n + (x(t-\tau))^n} - bx(t).$$

Take parameter values $a = 10$, $k = 1$, $b = 0.5$ and $n = 4$. Verify that this one-dimensional model exhibits sustained oscillations when $\tau = 3$. Describe the effects of changing the delay by running simulations with $\tau = 2$, $\tau = 0.75$ and $\tau = 20$. (Units as in Figure 7.17.) Details on simulating delay equations can be found in Appendix C.

Increased loop length was explored by Goodwin in his original paper (Goodwin, 1965); explicit delay and nonlinear degradation were considered in (Bliss *et al.*, 1982).

7.8.9 Circadian rhythms: Goldbeter model. Recall Goldbeter's model of a circadian oscillator from Section 7.3.2.
a) Using the parameter values in Figure 7.19, run a simulation of the model and verify the system oscillates with a period of roughly 24 hrs.
b) The oscillatory behaviour of this model is crucially dependent on the level of cooperativity. Determine the minimum value of the Hill coefficient n for which this system exhibits oscillations. Does the period depend strongly on n?
c) Modify the model so that the two phosphorylation steps are replaced by an explicit delay. (Details on simulating delay equations can be found in Appendix C.) What size delay is required to recover circadian (24-hour) oscillations?
d) Returning to the original model formulation, verify Goldbeter's finding that the period can be shortened or lengthened by mutations to the *per* gene that affect the protein's degradation rate. Suggest an alternative effect of the mutation in the *per* gene that could also lead to changes in the period of the oscillation. Verify your conjecture by running simulations.

7.8.10 Circadian rhythms: TIM. In addition to the PER protein described by the model in Section 7.3.2, the circadian network in *Drosophila* also involves a protein called TIM (for 'timeless'), expressed from the gene *tim*. John Tyson and colleagues published a simple model that incorporates the interaction between PER and TIM (Tyson *et al.*, 1999). In their model, PER proteins form homodimers. These dimers then associate with two molecules of TIM into a PER_2-TIM_2 complex. These complexes migrate to the nucleus, where they inhibit expression of both PER and TIM. Degradation of both TIM and PER is constitutive, but PER is protected from degradation when in dimer form.
a) Draw an interaction diagram describing the mechanism.
b) Verify that this mechanism can explain the following experimental observations:
i) Cells that lack the *tim* gene do not exhibit oscillatory behaviour.
ii) Circadian oscillations can be entrained to follow 24 hour light-dark cycles. Exposure to light enhances degradation of TIM.
c) Develop a differential equation model of this system. Describe the features of your model that could enable oscillatory behaviour. You may want to make use of the following reasonable assumptions: (i) mRNA dynamics occur quickly; (ii) dimerization events occurs quickly; (iii) PER and TIM concentrations follow similar time-courses and so the two species can be lumped into a single protein pool. As verified by Tyson and colleagues, a satisfactory model can involve as few as three dynamic variables.

7.8.11 Repressilator: ring size. Recall the model of the repressilator in Section 7.3.3.
a) Taking parameter values as in Figure 7.21, verify the oscillatory behaviour of the system. Change the value of the Hill coefficient so that $n = 1.5$. Verify that the system does not oscillate in this case. Next, model an expanded network in which five genes participate in a ring of sequential repression. Using the same symmetric model framework and parameter values, verify that this expanded model can produce oscillations when the Hill coefficient is 1.5. Provide an explanation in terms of the lag in the negative feedback loop.
b) Why is it that a ring of four sequential repressors would not be expected to oscillate?

7.8.12 Repressilator: effect of leak. Recall the model of the repressilator in Section 7.3.3.
a) Taking parameter values as in Figure 7.21, verify that when the leak α_0 is increased to 2 (molecules per cell min^{-1}) the system no longer exhibits oscillations. Provide an intuitive interpretation of this finding: why does a persistent leak dampen the system's oscillatory behaviour?
b) With $\alpha_0 = 2$, can the oscillations be rescued by increasing the degree of cooperativity n? If so, how much of an increase in n is required?

7.8.13 Repressilator: IPTG arrest. Recall the model of the repressilator in Section 7.3.3.
a) Modify the model to incorporate the effect of IPTG—an allolactose mimic—on the circuit. (Recall, allolactose deactivates the *lac* repressor, LacI, which is one of the three repressors in the loop.)
b) Take parameter values as in Figure 7.21, and choose parameter values for your model extension. Simulate the system's response to an extended pulse of IPTG. Your simulation should show the oscillations stopping when IPTG is introduced, and resuming after it is removed. Comment on the protein concentrations in the arrested steady-state.

7.8.14 Atkinson oscillator. In 2003, Mariette Atkinson and colleagues described a synthetic genetic relaxation oscillator (Atkinson *et al.*, 2003). Like the Stricker oscillator presented in Section 7.3.3, Atkinson's circuit involves two genes and their protein products: a repressor and an activator. The activator induces expression of both genes (as in the Stricker oscillator) but the repressor only represses the activator. Model 7.23 can be modified to describe the Atkinson oscillator by removing the term $(1+y(t)^4)$ from the denominator of the expression rate for Y (the repressor). Take parameter values as in Figure 7.23, but with $\gamma_y = 1$, and verify that the resulting model displays damped oscillations, as were observed by Atkinson and her coworkers. Next, decrease a_y until the system exhibits sustained oscillations. Suggest a design feature that would provide control over the value of parameter a_y.

7.8.15 NF-κB signalling. The transcription factor NF-κB is involved in a range of signalling pathways in eukaryotic cells (Section 1.6.2). A simple model of NF-κB activation, which captures the oscillations observed during signalling, was published in 2006 by Sandeep Krishna, Mogens Jensen, and Kim Sneppen (Krishna *et al.*, 2006). Their model lumps the NF-κB inhibitors into a single pool, IκB, whose expression is activated by NF-κB. The network is shown in Figure 7.48.

The model describes three state variables: nuclear NF-κB (concentration: N_n), IκB mRNA (I_m), and cytosolic IκB (I). The concentration scale is chosen so that the total NF-κB concentration

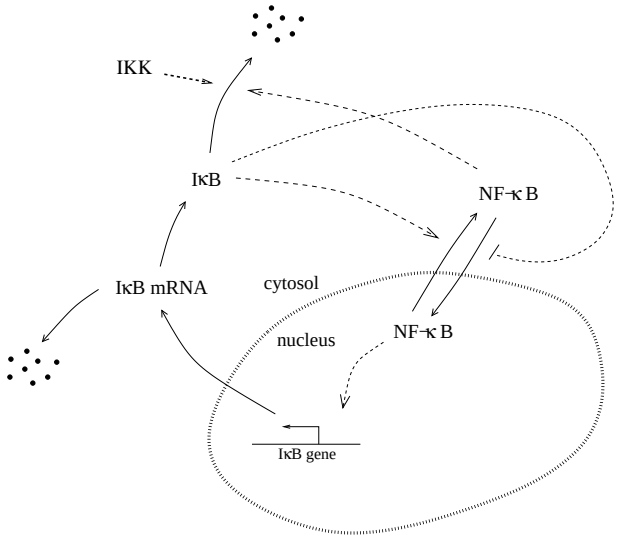

Figure 7.48: NFkB signalling network for Problem 7.8.15. Adapted from Figure 1 of (Krishna *et al.*, 2006).

is 1. Because NF-κB is conserved, the cytosolic NF-κB concentration is then $1 - N_n$. The model equations are

$$\begin{aligned}
\frac{d}{dt}N_n(t) &= A\frac{1-N_n}{\varepsilon + I(t)} - B\frac{I(t)N_n(t)}{\delta + N_n(t)} \\
\frac{d}{dt}I_m(t) &= N_n(t)^2 - I_m(t) \\
\frac{d}{dt}I(t) &= I_m(t) - IKK(t)\frac{(1-N_n(t))I(t)}{\varepsilon + I(t)}
\end{aligned}$$

The input is the level of IκB kinase IKK. The units of time and concentration have been rescaled to reduce the number of model parameters.

a) Take parameter values (scaled to be dimensionless) $A = 0.007$, $B = 954.5$, $\delta = 0.029$, $\varepsilon = 0.00005$ and $IKK = 0.035$. Verify that the concentration of nuclear NF-κB (N_n) exhibits spike-like oscillations.

b) The model time-units were scaled by the degradation rate of IκB mRNA, which is 0.017 min^{-1}. (That is, the model is expressed in time-units of $\frac{1}{0.017}$ minutes.) What is the period of the oscillations in NF-κB?

c) Krishna and colleagues confirmed that the spiky oscillations in NF-κB are quite robust to variation in the parameter values. However, they observed that when IKK levels are increased, the oscillations become smoother. Confirm this result by running a simulation in which the IKK concentration is tripled.

d) Recall from Section 1.6.2 that there are three isoforms of IκB (IκBα, IκBβ, and IκBε), and that production of IκBβ and IκBε is not inhibited by NF-κB. These uninhibited isoforms can be included in the model by adding a constant production term for IκB mRNA (so that $dI_m/dt = c_0 + N_n^2 - I_m$). Verify that when $c_0 = 0.005$ the system exhibits sustained oscillations, but the amplitude of the spikes in nuclear NF-κB (N_n) is diminished. How does the system behave when c_0 is increased to 0.02?

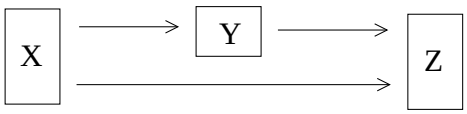

Figure 7.49: Coherent feedforward loop (Problem 7.8.16).

7.8.16 Feed-forward loops. Uri Alon has investigated the behaviour of a three-gene network that is a common component of natural gene regulatory systems (Alon, 2007). The network, shown in Figure 7.49, is activated at a single gene (X), which activates both the pathway target (Z) and an intermediary (Y). The intermediary co-regulates the target. The network is called a *feedforward loop*. If Z is activated by both X and Y, it is called *coherent*. (Alternatively, if Y represses Z, the loop is called *incoherent*; the pulse generator discussed in Section 7.4.2 is an incoherent feedforward loop.)

Consider a coherent feedforward loop in which expression of Z requires activation by both X and Y (the Z promoter implements AND logic, as in Section 7.5.1). This network provides signalling from X to Z that is robust to input noise, in the sense that brief input pulses will not lead to activation of the target gene Z.

a) Using the formulation in Section 7.1.2 for expression from promoters activated by single or multiple transcription factors, construct a differential equation model of a coherent feedforward loop with AND logic. (Take protein X as an input to the pathway. You'll need to develop differential equations describing the dynamics of protein products Y and Z. Treat mRNA dynamics in quasi-steady state.)

b) Choose parameter values and simulate the response of your system to an abrupt increase in X. You should observe an increase in Y, followed by a later increase in Z.

c) Next simulate the response of your system to a brief pulse in X (in which X jumps to a non-zero value for a short time, and then jumps back to zero). Verify that for short pulses, no significant expression of Z is observed (compared to the direct response in Y). Provide an intuitive explanation of this behaviour in terms of the network structure.

d) Explain why a coherent feedforward loop that implements an OR logic at the Z promoter would not exhibit the robustness property observed in part (c).

7.8.17 Band detector: sensitivity. Referring to the band-detector construction in Section 7.4.2, Basu and colleagues used their model to determine that, compared to the other kinetic parameters in the model, the rate constant for LacI decay (b_L) had the most significant impact on the shape of the GFP band. Investigate the effects of perturbation in γ_L and at least three other kinetic parameters. Do your findings agree with Basu's conclusion?

7.8.18 Band detector: design variants. Referring to the band-detector circuit described in Section 7.4.2, Basu and coworkers constructed variants of their design: one in which the LuxR concentration was reduced (by the use of a low-copy plasmid); and one in which the LuxR-DNA binding affinity was enhanced (by mutation). How would you expect these variations in LuxR activity to impact the system behaviour? Implement changes in model (7.26) to mimic these variants, and run simulations to confirm your conjectures.

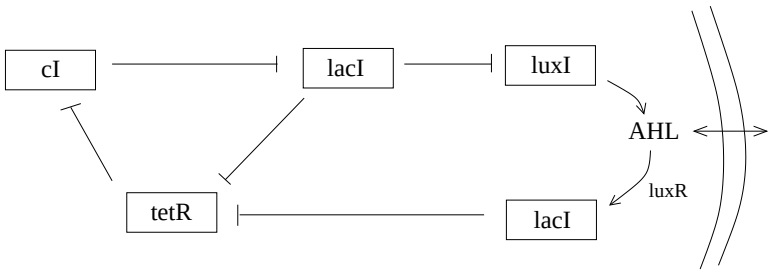

Figure 7.50: Extended repressilator circuit for synchronization (Problem 7.8.19). Adapted from Figure 1 of (Garcia-Ojalvo *et al.*, 2004).

7.8.19 Synchronized Repressilators. In a 2004 paper, Jordi Garcia-Ojalvo, Michael Elowitz, and Steven Strogatz proposed an extension of the repressilator circuit (Section 7.3.3) that could synchronize oscillations in a population of cells (Garcia-Ojalvo *et al.*, 2004). In their proposed circuit, the *LuxI* gene, whose protein product catalyses production of AHL (Section 7.4.2) is placed under the control of the *lac* promoter. Additionally, a second copy of the *LacI* gene is introduced, under the control of the AHL-LuxR sensitive promoter from *V. fischeri*. Finally, a constitutively expressed copy of *LuxR* is added. The network is shown in Figure 7.50.

To explore the behaviour of this circuit, consider a pair of identical cells, each hosting the network. AHL diffuses between the two cells, and so can bring the two oscillators into synchrony. Garcia-Ojalvo and colleagues modelled the network as follows. The three repressilator genes (*tetR*, *cI*, and *LacI*, with mRNA concentrations a, b, and c) and their protein products (concentrations A, B, and C) are modelled as in the repressilator, except for an additional source of LuxI, which is induced by intracellular AHL (denoted S):

$$\frac{d}{dt}a_i(t) = \frac{\alpha}{1+C_i(t)^n} - a_i(t) \qquad \frac{d}{dt}A_i(t) = \beta(a_i(t) - A_i(t))$$

$$\frac{d}{dt}b_i(t) = \frac{\alpha}{1+A_i(t)^n} - b_i(t) \qquad \frac{d}{dt}B_i(t) = \beta(b_i(t) - B_i(t))$$

$$\frac{d}{dt}c_i(t) = \frac{\alpha}{1+B_i(t)^n} + \frac{\kappa S_i}{1+S_i} - c_i(t) \qquad \frac{d}{dt}C_i(t) = \beta(c_i(t) - C_i(t))$$

where the subscripts indicate concentrations in the two cells ($i = 1, 2$). The dynamics of LuxI are assumed to be identical to TetR, so the concentration of intracellular AHL can be described by

$$\frac{d}{dt}S_i(t) = k_{s1}A_i(t) - k_{s0}S_i(t) - \eta(S_i(t) - S_e(t)).$$

The first term in this equation describes LuxI-dependent production, the second term describes degradation/dilution, and the final term is transport, where S_e is the external AHL concentration. A simple formulation for the external AHL concentration is:

$$S_e(t) = Q\,\frac{S_1(t) + S_2(t)}{2},$$

where the parameter Q characterizes diffusion of AHL away from the cells.

a) Using parameter values $\alpha = 216$, $n = 2$, $\beta = 1$, $\kappa = 20$, $k_{s0} = 1$, $k_{s1} = 0.01$, $\eta = 2$ and $Q = 0.9$, simulate the system from an initial condition in which $A = 10$ in cell 1, $B = 10$ in cell 2, and all

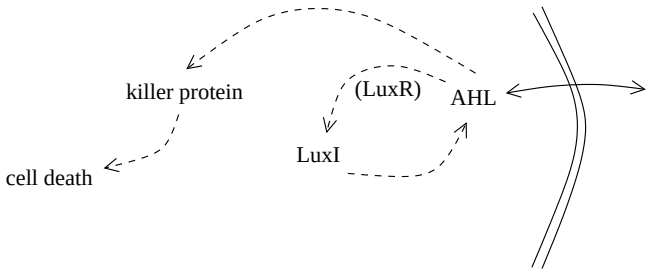

Figure 7.51: Population control network for Problem 7.8.20(a). Adapted from Figure 1 of (You *et al.*, 2004).

other concentrations start at zero. Confirm that the two cells synchronize after about 100 time units.
b) What condition is described by setting $\kappa = 0$? Simulate the system under this condition, and provide a justification for the system behaviour.
c) With $\kappa = 20$, explore the effect of reducing Q. As Q decreases, AHL diffuses more quickly away from the cells. Do the cells synchronize when $Q = 0.2$? What is the effect on the synchronization speed? What about when $Q = 0.02$?

7.8.20 Population control. In a 2004 paper, Lingchong You and colleagues described a synthetic gene regulatory network that uses the *Vibrio fischeri* quorum sensing mechanism (Section 7.4.1) to control the density of a population of *E. coli* cells (You *et al.*, 2004). The quorum-sensing network drives expression of a 'killer' gene whose protein product causes cell death (Figure 7.51).
a) You and colleagues used a simple model to describe a population of cells containing this circuit. The model describes the cell density (N) and the averaged intracellular concentrations of killer protein (E) and AHL (A):

$$\begin{aligned}
\frac{d}{dt}N(t) &= kN(t)(1 - N(t)/N_m) - d_N E(t)N(t) \\
\frac{d}{dt}E(t) &= k_E A(t) - d_E E(t) \\
\frac{d}{dt}A(t) &= v_A N(t) - d_A A(t)
\end{aligned}$$

The population growth rate is $k(1 - N/N_m)$, which diminishes to zero as the population tends to N_m. The parameter N_m is called the *carrying capacity* of the environment. (This is a *logistic* growth model.)

i) Take parameter values of $d_N = 0.004$ nM^{-1} h^{-1}, $k_E = 5$ h^{-1}, $d_E = 2$ h^{-1}, $v_A = 4.8 \times 10^{-7}$ nM ml h^{-1}, $k = 0.97$ h^{-1}, $N_m = 1.24 \times 10^9$ CFU ml^{-1}, and $d_A = 0.639$ h^{-1}. (Note: colony-forming units (CFU) is a standard measure of abundance of viable cells.) Simulate the model from initial condition $(N, E, A) = (1, 1, 1)$. Next, modify the model to mimic the control case in which no killer protein is produced, and compare the steady-state population densities (N) in the two cases.

ii) Verify that the steady-state population size can be tuned by the value of k_E. Describe an intervention or design change that would alter this parameter value. What value of k_E would result in the population reaching half of the (no killer protein) control size?

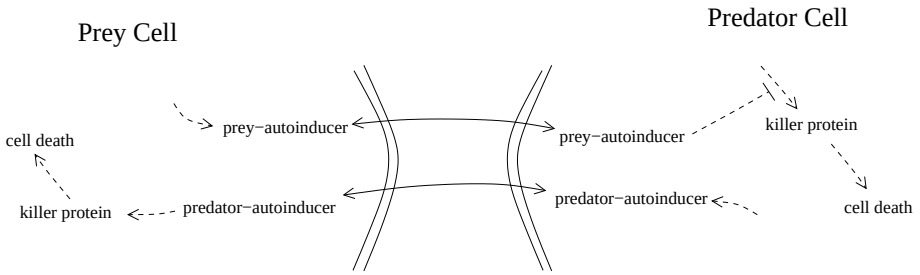

Figure 7.52: Predator-prey system for Problem 7.8.20(b). Adapted from Box 1 of (Balagaddé *et al.*, 2008).

b) In a follow-up study, Frederick Balagaddé and co-workers constructed a two-species ecosystem employing the density-dependent killing mechanism of part (a) (Balagaddé *et al.*, 2008). Their system involves two separate engineered strains of *E. coli*: a 'prey' strain and a 'predator' strain. The prey strain uses the *V. fischeri* quorum-sensing mechanism to signal its population density. The predator strain uses an analogous quorum-sensing mechanism from another bacterial species. Predation is mimicked by the prey's response to the predator-specific autoinducer—it activates expression of the killer protein in prey cells. The predator population is controlled by expression of killer protein, which is repressed by the prey-specific autoinducer (thus mimicking survival of predators when prey are abundant). The network is shown in Figure 7.52.

Balagaddé and colleagues developed a model that describes the densities of predator (c_1) and prey (c_2), and the strain-specific autoinducer concentrations (a_1 and a_2, respectively):

$$\begin{aligned}
\frac{d}{dt}c_1(t) &= k_1 c_1(t)\left(1-\frac{c_1(t)+c_2(t)}{c_m}\right) - d_1 c_1(t)\frac{K_1}{K_1+a_2^\beta} - Dc_1(t) \\
\frac{d}{dt}c_2(t) &= k_2 c_2(t)\left(1-\frac{c_1(t)+c_2(t)}{c_m}\right) - d_2 c_2(t)\frac{a_1^\beta}{K_2+a_1^\beta} - Dc_2(t) \\
\frac{d}{dt}a_1(t) &= \gamma_1 c_1(t) - (\delta_1 + D)a_1(t) \\
\frac{d}{dt}a_2(t) &= \gamma_2 c_2(t) - (\delta_2 + D)a_2(t)
\end{aligned}$$

As in part (a), a logistic growth model is used (with carrying capacity c_m). The killer protein abundance is in quasi-steady-state, so growth inhibition is directly dependent on the autoinducer levels. For each autoinducer, the intracellular and extracellular concentrations are presumed identical. The parameters δ_1 and δ_2 are decay rates for the two autoinducers; the parameter D characterizes dilution of all species.

i) Take parameter values $k_2 = 0.4$ hr^{-1}, $c_m = 10^5$ cells per nL, $\beta = 2$, $d_1 = 1$ hr^{-1}, $d_2 = 0.3$ hr^{-1}, $K_1 = K_2 = 10$ nM, $\gamma_1 = \gamma_2 = 0.1$ nM ml hr^{-1}, $\delta_1 = 0.017$ hr^{-1}, $\delta_2 = 0.11$ hr^{-1}, and $D = 0.2$ hr^{-1}. Simulate the system for three cases: $k_1 = 0.2$, 0.8, and 1.4 hr^{-1}. Verify that in the first and last case, one population dominates over the other, while for $k_1 = 0.8$ hr^{-1}, the populations tend to a persistent oscillatory pattern. Explain the long-time system behaviour in each case.

ii) Using this model, Balagaddé and coworkers discovered that the system is more likely to exhibit oscillations when the predator death rate (d_1) is sufficiently large. They thus engineered a modified killer protein to reach a higher death rate. Confirm their finding by exploring the range of k_1 values over which the system oscillates at low ($d_1 = 0.2$) and high ($d_1 = 1$) predator death rates.

7.8.21 Genetic logic gate design.
a) Develop a differential equation model of a regulated promoter that implements an OR logic gate, as discussed in Section 7.5.1. Hint: recall the expression rates for regulated promoters in Section 7.1.2.
b) Using genes that implement only OR, AND, and NOT gates, design a genetic circuit that implements an XOR (exclusive OR) gate. The output from an XOR gate is 'on' when exactly one of its two inputs is 'on.' Develop a differential equation model of your circuit.

7.8.22 *Chemical master equation: closed system. Consider the reaction network

$$A \xrightarrow{k_1} B + C \qquad\qquad B + C \xrightarrow{k_{-1}} A.$$

a) Suppose that the system starts with two molecules of A, one molecule of B, and no molecules of C, that is $(N_A, N_B, N_C) = (2, 1, 0)$. Determine the set of possible states the system can adopt and write the chemical master equation that describes the corresponding probability distribution.
b) Take $k_1 = 1$ (time^{-1}) and $k_{-1} = 1$ (time^{-1}), and solve for the steady-state probability distribution.

7.8.23 Chemical master equation: open system. Consider the open system

$$\xrightarrow{k_1} A \xrightarrow{k_2}$$

a) Take $k_1 = 1$ (concentration$\cdot$time^{-1}) and $k_2 = 1$ (time^{-1}). Referring to the corresponding master equation (7.28), verify that in steady state the probabilities satisfy

$$P(N_A = n) = \frac{1}{n} P(N_A = n - 1).$$

b) Use the fact that $\sum_{n=0}^{\infty} \frac{1}{n!} = e$, (where the factorial $n! = n(n-1)(n-2)\cdots 3 \cdot 2 \cdot 1$ and e is Euler's number $e \approx 2.71828$), to derive the steady-state probability distribution:

$$P(N_A = n) = \frac{1/e}{n!},$$

for each $n = 0, 1, 2, \ldots$ (By convention $0! = 1$.)

7.8.24 *Statistics of an ensemble of sample paths. Consider the simple model of unregulated gene expression in Section 7.6.4:

R_1 : (transcription)	$\longrightarrow M$	propensity: k_r
R_2 : (translation)	$\longrightarrow P$	propensity: $k_p N_M$
R_3 : (degradation/dilution)	$M \longrightarrow$	propensity: $\delta_r N_M$
R_4 : (degradation/dilution)	$P \longrightarrow$	propensity: $\delta_p N_P$

Take parameter values as in Figure 7.46A. Simulate sample paths using the stochastic simulation algorithm. Analyse the statistics of your ensemble to verify that in steady state (so called *stationary* behaviour) the coefficient of variation (standard deviation divided by mean) for each species is

$$\text{mRNA: } C_r = \left(\frac{\delta_r}{k_r}\right)^{1/2}, \qquad \text{protein: } C_p = \left(\frac{\delta_r \delta_p}{k_r k_p}\right)^{1/2} \left(1 + \frac{k_p}{\delta_r + \delta_p}\right)^{1/2}.$$

(For a derivation of these formulas, see (Khammash, 2010).) Note: statistics can be gathered from an ensemble of sample paths or a single long simulation. XPPAUT users will have to `write` the data from the simulation and calculate the mean and variance using another program (e.g. a spreadsheet).

7.8.25 *Stochastic simulation: the first-reaction method. An alternative to the stochastic simulation algorithm presented in Section 7.6.3 is the *first-reaction method*, which also involves stepping from reaction event to reaction event. However, rather than sample the next reaction and the waiting time separately (as in the SSA), the first-reaction algorithm samples a waiting time for each reaction in the network, and then selects the shortest of these times; this selection specifies the identity of the next reaction and the elapsed time. Because these waiting times can often be re-used from one time-step to the next, this algorithm can be significantly more efficient than the SSA. (An implementation of the first-reaction method was presented in (Gibson and Bruck, 2000).)

Recall that the waiting time $T = T_{\text{wait}}$ in the SSA has a cumulative distribution function given by $P(0 \le T_{\text{wait}} \le t) = 1 - e^{-at}$, where a is the sum of the propensities for all of the reactions in the network. In the first-reaction algorithm, the waiting time T_{first} is the minimum of a collection of reaction-specific waiting times T_i, each of which is characterized by $P(0 \le T_i \le t) = 1 - e^{-a_i t}$, where a_i is the reaction propensity. Confirm that the cumulative distribution function for the first-reaction waiting time ($T_{\text{first}} = \min(T_1, T_2, \ldots, T_m)$) agrees with the distribution of $T = T_{\text{wait}}$ in the SSA. Hint: Verify that $P(T_{\text{wait}} > t) = e^{-at}$ and $P(T_i > t) = e^{-a_i t}$. Then use the fact that $P(T_{\text{first}} > t) = P((T_1 > t) \text{ and } (T_2 > t) \cdots \text{and } (T_m > t))$ where the T_i are independent of one another.

7.8.26 *Noisy toggle switch. Stochastic systems can exhibit a range of bistable-like behaviours, ranging from 'true' bistability to frequent noise-induced transitions between two nominally stable states. To explore this behaviour, consider a stochastic system that recapitulates the bistable toggle switch discussed in Section 7.2.3:

R_1 : (synthesis)	$\longrightarrow P_1$	propensity: $\frac{\alpha}{1+N_2^\beta}$
R_2 : (synthesis)	$\longrightarrow P_2$	propensity: $\frac{\alpha}{1+N_1^\beta}$
R_3 : (decay)	$P_1 \longrightarrow$	propensity: δN_1
R_4 : (decay)	$P_2 \longrightarrow$	propensity: δN_2

Here N_1 and N_2 are the molecular counts for the two repressors. The Hill-type propensities for the synthesis reactions are not well justified at the molecular level, but these expressions nevertheless provide a simple formulation of a bistable stochastic system. Take parameter values $\delta = 1$ and $\beta = 4$. The corresponding deterministic system (i.e. $dp_i/dt = \alpha/(1 + p_j^4) - p_i$) is bistable for any

$\alpha > 1$. Run simulations of the stochastic system for $\alpha = 5$, 50, 500, and 5000. Be sure to run the simulations sufficiently long so that the steady trend is clear (i.e. at least 10,000 reaction steps). Verify that for $\alpha = 5000$ the system exhibits bistability (with about 5000 molecules of the dominant species, in the long term). In contrast, verify that with $\alpha = 5$, noise dominates and the system shows no signs of bistability. What about at $\alpha = 50$ and 500? Comment on how the steady-state molecule abundance affects system behaviour. (Note: it may be necessary to run multiple simulations to confirm your findings.)

7.8.27 *Noise-induced oscillations. Stochastic systems can exhibit a range of oscillatory behaviours, ranging from near-perfect periodicity to erratic cycles. To explore this behaviour, consider a stochastic relaxation oscillator studied by José Vilar and colleagues (Vilar *et al.*, 2002). The system involves an activator and a repressor. The activator enhances expression of both proteins. The repressor acts by binding the activator, forming an inert complex. A simple model of the system is

R_1 : (activator synthesis)	$\longrightarrow b_A A$	propensity: $\frac{\gamma_A}{b_A}\frac{\alpha_0+N_A/K_A}{1+N_A/K_A}$
R_2 : (repressor synthesis)	$\longrightarrow b_R R$	propensity: $\frac{\gamma_R}{b_R}\frac{N_A/K_R}{1+N_A/K_R}$
R_3 : (activator decay)	$A \longrightarrow$	propensity: $\delta_A N_A$
R_4 : (repressor decay)	$R \longrightarrow$	propensity: $\delta_R N_R$
R_5 : (association)	$A + R \longrightarrow C$	propensity: $k_C N_A N_R$
R_6 : (dissociation and decay)	$C \longrightarrow R$	propensity: $\delta_A N_C$

Here N_A, N_R and N_C are the molecular counts for the activator, repressor, and activator-repressor complex. The parameter b_A and b_R characterize the expression burst size. The Hill-type propensities for the synthesis reactions are not well justified at the molecular level, but these expressions nevertheless provide a simple formulation of a stochastic relaxation oscillator.
a) Take parameter values $\gamma_A = 250$, $b_A = 5$, $K_A = 0.5$, $\alpha_0 = 0.1$, $\delta_A = 1$, $\gamma_R = 50$, $b_R = 10$, $K_R = 1$, $k_C = 200$, and $\delta_R = 0.1$. Run simulations of this model and verify its quasi-periodic behaviour.
b) The deterministic version of this model is

$$\begin{aligned}
\frac{d}{dt}a(t) &= \gamma_A \frac{\alpha_0 + a(t)/K_A}{1 + a(t)/K_A} - k_C a(t) r(t) - \delta_A a(t) \\
\frac{d}{dt}r(t) &= \gamma_R \frac{a(t)/K_R}{1 + a(t)/K_R} - k_C a(t) r(t) + \delta_A c(t) - \delta_R r(t) \\
\frac{d}{dt}C(t) &= k_C a(t) r(t) - \delta_A c(t),
\end{aligned}$$

where a, r, and c are the concentrations of activator, repressor, and complex. Run a simulation with the same parameter values as in part (a). Does the system exhibit oscillations? How is the behaviour different if you set $\delta_R = 0.2$?
c) The contrast between the behaviour of the models in parts (a) and (b), for $\delta_R = 0.1$, can be explained by the excitability of this relaxation oscillator. Run two simulations of the deterministic model ($\delta_R = 0.1$), one from from initial conditions $(a, r, c) = (0, 10, 35)$ and another from initial

conditions $(a, r, c) = (5, 10, 35)$. Verify that in the first case, the activator is quenched by the repressor, and the system remains at a low-activator steady state, while in the second case, this small quantity of activator is able to break free from the repressor and invoke a (single) spike in expression. Explain how noise in the activator abundance could cause repeated excitations by allowing the activator abundance to regularly cross this threshold. This is referred to as *noise-induced oscillation*.